

35

Studies of the Soluble Methane Monooxygenase:
Heterologous Expression and Reactions with Nitric Oxide

by

David E. Coufal

B.Sc., California Institute of Technology (1991)

Submitted to the Department of Chemistry in
Partial Fulfillment of the Requirements for the Degree of

Doctor of Philosophy

at the

Massachusetts Institute of Technology

September, 1998

[February 1999]

© 1998 Massachusetts Institute of Technology
All Rights Reserved

Signature of Author _____

Department of Chemistry
September 21, 1998

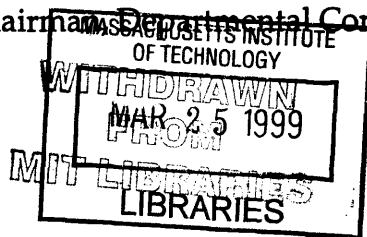
Certified by _____

Professor Stephen J. Lippard
Thesis Supervisor

Accepted by _____

Professor Dietmar Seyferth

Chairman, Departmental Committee on Graduate Students



Science

This doctoral thesis has been examined by a Committee of the Department of Chemistry as follows:

JoAnne Stubbe

Novartis Professor of Chemistry and Professor of Biology

Committee Chair

Stephen J. Lippard

Arthur Amos Noyes Chair and Professor of Chemistry

Thesis Advisor

Jun Liu

Assistant Professor of Biology and Chemistry

Studies of the Soluble Methane Monooxygenase:
Heterologous Expression and Reactions with Nitric Oxide

by

David Ernest Coufal

Submitted to the Department of Chemistry on September 21, 1998 in partial fulfillment of the requirements for the Degree of Doctor of Philosophy in Chemistry

ABSTRACT

In the first chapter, the determination of the correct sequence of the hydroxylase genes from the *M. capsulatus* soluble methane monooxygenase (sMMO) system is reported. This data was used in a comparison of all the sequenced members of the sMMO system family of proteins. Sequence alignments of the α subunits reveal absolutely conserved residues in the active site region that act as iron ligands, participate in a hydrogen bonding network and provide a source of protons in the largely hydrophobic substrate binding region. Further examination of the rest of the conserved residues in the α and β subunits reveal a possible binding site for protein B, two possible binding sites for the reductase and several regions of intersubunit contact. Possible models for the effects of interaction between all the sMMO proteins are suggested based on the alignment data.

The second chapter describes methodologies used in attempting to express the sMMO hydroxylase. This protein forms insoluble, intractable inclusion bodies upon expression in *E. coli*. The insoluble material was collected and subjected to refolding procedures while varying temperature, reduction potential, thiol concentration, protein concentration, and the identity of the denaturant. Production of the inclusion bodies could not be averted via changing the nature of the expression system by changing media conditions, *E. coli* strains, and expression vector. Conclusions about the folding pathway of the sMMO hydroxylase are drawn from the data collected. Possible future courses of action to express the sMMO hydroxylase are suggested.

The third and final chapter describes the reaction of nitric oxide (NO) with the reduced iron center in the sMMO hydroxylase. The majority of the iron centers react with NO to form a dinitrosyl adduct, termed $H_{\text{dinitrosyl}}$ that models the H_{peroxo} intermediate in the reaction of O_2 with the reduced sMMO hydroxylase. This reaction is characterized by Mössbauer, EPR and optical spectroscopies using both continuous and discontinuous kinetic techniques. The $H_{\text{dinitrosyl}}$ intermediate

forms whether protein B is present or not, in contrast to the H_{peroxo} intermediate which forms in detectable amounts only in the presence of protein B. This is interpreted in terms of changes in the open coordination sites in the reduced sMMO diiron site upon protein B binding. The $H_{\text{dinitrosyl}}$ species decays to form a complex mixture of products, including further reaction with NO to form $\text{Fe}(\text{NO})_2$ units and reductive coupling of bound NO molecules to form N_2O and oxidized sMMO hydroxylase. The effects of protein B, methane and fluoride ion on these reactions are investigated. In addition to formation of $H_{\text{dinitrosyl}}$, NO reacts with a small percentage of sMMO hydroxylase sites that are depleted in one iron to form an $S=3/2$ mononuclear iron-nitrosyl species.

Thesis Supervisor: Stephen J. Lippard

Title: Arthur Amos Noyes Professor of Chemistry

Acknowledgements

It has been a great privilege to work with many talented and helpful individuals without whom this thesis wouldn't exist. I must first thank Stephen Lippard for his advice and support during my stay in his laboratory. His enthusiasm for science and dedication to his laboratory are remarkable, and I was grateful to be a part of his group.

Thanks also to the many members of the Lippard Lab that I've had the opportunity to interact with over my stay. My two UROPs, Holly Imlach and Carisa Elise, were terrific. I appreciate the hard work both of them invested in the lab and in their projects. In my early days in the Bio Bay, the Joyce Whitehead/Megan McA'Nulty/Laura Pence triumvirate provided indispensable help and support. The lab's color-level dropped by an order of magnitude after they left. The MMO subgroup was always a great source of inspiration and fun. In particular, Sonja Komar-Panicucci, George Gassner, Ann Valentine, Jessica Blazyk and Young Douglas Whittington were a big help. Andrew Feig suggested that we look into the reactions of NO with the sMMO system; I have him to blame/thank for chapter three. The entire platinum family was valued for their biochemistry expertise. I especially thank Deb Zamble, Drew Gelasco, Uta Ohndorf, Karen Sandman and Betsy Redding for their help. I must also express my appreciation to the Martini Crew: Jon Wilker, Maria Bautista, Dan LeCloux and Tricia Takahara. It was both pleasure and privilege to raise one to Dean, Frank and Sammy with you folks.

Lots of other folks at MIT have been of great help. Prof. Lawrence Stern, Prof. Jonathan King, Prof. JoAnne Stubbe and Prof. William Orme-Johnson all provided useful advice and guidance along the way. Pam Riggs-Gelasco was invaluable in teaching me how to use the Stubbe Lab RFQ apparatus. I'd like to thank members of the basement crew '92-'93, especially Subhendu Joardar, Normand Cloutier, Jeremy Selengut, Patti Christie and Sherri Oslick. They were supportive of me during a difficult period in my graduate career. I've been a giant thorn in Susan Brighton's side, so I thank her for her infinite patience with my lack of competence with the MIT registration process. Mike Drooker was a great help in setting up and maintaining our SGI cluster in the early days. Colette Laurentcôt's competence and sense of humor have saved many a day from being a total loss for me.

Many folks outside MIT (I'm pretty sure such a place exists) were crucial as well. Prof. Brian Hoffman and Dave Tierney at Northwestern were helpful with EPR advice. Prof. Keith Hodgson, Dr. Britt Hedman, Matthew "Mortimer" Latimer and Jennifer DuBois at Stanford and SSRL were helpful in running EXAFS samples for us. Prof. Vincent Huynh, Prof. Dale Edmundson, Carsten Krebs, Pedro Tavares and Alice Periera at Emory University provided indispensable Mössbauer spectroscopy and rapid freeze quench kinetics help.

I'd thank my cat Friday, but she'd probably like one of those little jangly mice toys better.

My cousin Ronnie Graham read the first books in C.S. Lewis's Narnia series aloud to me when I was young, and gave me a copy of the septology to finish myself. This, along with a copy of "The Hobbit" by J.R.R. Tolkien from my aunt Rose Boyle, was the beginning of a lifelong love of reading and learning. My aunt Sharon Estes encouraged my grade school interest in science and technology with subscriptions to astronomy magazines and frequent loans of Apple II computers for me to fool around with. I thank all three of them for their support during my childhood.

Finally, my dad Gerry, mother Shirley and sister Kim are the greatest family one could have hoped for. I love them all very much.

*Dedicated to my family,
and to the memory of my grandfather
Earl Graham
and my grandmother
Rachel Coufal.*

Table of Contents

Abstract.....	3
Acknowledgments.....	5
Dedication.....	6
Table of Contents.....	7
List of Tables.....	10
List of Figures.....	11
Overview of the Soluble Methane Monooxygenase System.....	15
Chapter One: Sequencing and Analysis of the <i>Methylococcus capsulatus</i> (Bath) Soluble Methane Monooxygenase Genes.....	19
Introduction.....	19
Materials and Methods.....	23
DNA Sequencing.....	23
Sequence Analysis.....	24
Results.....	25
Corrections to the sMMO Gene Sequences.....	25
Roles for Genes from the sMMO Family Operons.....	27
Comparisons between the sMMO Family Protein Sequences.....	28
Search for OrfY Analogues.....	29
The sMMOH α Analogues.....	29
The sMMOH β Analogues.....	32
The Coupling Protein Analogues.....	32
The Reductase Analogues.....	33
Discussion.....	33
Implications of the Corrected <i>M. capsulatus</i> (Bath) DNA Sequence.....	33
Sequence Alignment of sMMO Family Proteins.....	34
Active Site of the Hydroxylase.....	34
Understanding Protein-Protein Interactions in sMMO.....	35
References.....	37
Chapter Two: Heterologous Expression of the <i>Methylococcus capsulatus</i> (Bath) Soluble Methane Monooxygenase Hydroxylase.....	100
Introduction.....	100
Materials and Methods.....	108
Low Pressure Chromatography sMMOH Purification Procedure.....	108
Production of MMOH Polyclonal Antibodies.....	108
ELISA Assays.....	109
Western Blots.....	110
Genomic DNA Sample Preparation.....	111
Purification of PCR Primers for pDEC002.....	112

PCR Conditions for pDEC002.....	113
Construction of pDEC002.....	113
Sequencing of pDEC002	115
Expression of MMOH by using the pDEC002 System	116
MMOH Inclusion Purification	116
Post-Expression Refolding Procedures	117
Dialysis Reconstitution of Native MMO Hydroxylase	
Isolated from <i>M. capsulatus</i> (Bath).....	117
Dialysis Reconstitution of Insoluble Expressed Hydroxylase	
Isolated from <i>E. coli</i>	117
Anaerobic Fe(II) Dialysis Reconstitution of Insoluble	
Expressed Hydroxylase Isolated from <i>E. coli</i>	118
Sarcosyl Lysis Growth	118
Detergent Lysis Screening	119
Sarcosyl Pellet Solubilization.....	119
Alteration of Expression Conditions	120
Low Temperature Induction Growth	120
<i>E. coli</i> Strain Screening	120
Variation of Media Content.....	120
Expression System Screening (pDEC010)	120
Individual Subunit Expression	121
Construction of pDEC05x.....	121
Construction of pDEC060	121
Construction of pDEC070	122
Simple MMOH Subunit Expression – pDEC05x	122
Periplasmic Expression of sMMOH α - pDEC060.....	123
Thioredoxin-sMMOH α Subunit Expression.....	123
Purification of sMMOH α	124
EPR Mixed-Valent Sample Preparation.....	124
EPR Reduced Sample Preparation	125
Results	125
Discussion and Conclusions	129
References	132

Chapter Three: Reactions of Nitric Oxide with the Reduced Non-Heme Iron Center of the Soluble Methane Monooxygenase Hydroxylase..... 180

Introduction	180
Materials and Methods	183
Preparation and Purification of sMMO Hydroxylase (H) and	
Protein B.....	183
Preparation of Diiron(II) sMMO Hydroxylase (H _{red}).....	183
Addition of NO Gas.....	183
Addition of NO via NONOates	184
Stopped Flow Spectrophotometry.....	184
Rapid Freeze Quench Mössbauer Sample Preparation	185

Rapid Freeze Quench EPR Sample Preparation.....	186
EPR Measurements.....	186
Mössbauer Measurements.....	186
Nitrous Oxide Detection via Gas Chromatography.....	187
Results.....	187
Preparation of NO Complexes of H_{red} and $H_{red}+2B$	187
Optical Absorption Spectra.....	188
Mössbauer Analysis of $H_{red}+NO$ and $H_{red}+2B+NO$ Samples.....	188
EPR Analysis of $H_{red}+NO$ and $H_{red}+2B+NO$ Samples.....	189
Stopped Flow Analysis of the $H_{red}+NO$ and $H_{red}+2B+NO$ Reaction	189
Rapid Freeze-Quench EPR Characterization of $H_{red}+NO$ Reaction Species.....	191
Mössbauer Characterization of $H_{red}+NO$ Reaction Species.....	191
Decay of $H_{dinitrosyl}$ to N_2O	192
Discussion.....	193
Reaction of Reduced Hydroxylase with NO to form a Diiron Dinitrosyl Species.....	193
A Mononuclear $\{Fe(NO)\}^7$ Minority Species in the $H_{red}+NO$ Reaction.....	194
Effects of Protein B on Mononuclear $\{Fe(NO)\}^7$	195
Comparison of the Reactions of the sMMO Hydroxylase with O_2 versus NO.....	195
Buildup of $H_{dinitrosyl}$	197
Decay of $H_{dinitrosyl}$	200
Comparison with the NO Reactions of the Reduced Ribonucleotide Reductase R2 Subunit and Hemerythrin.....	201
References.....	203
Biographical Note.....	232

List of Tables

Chapter One

Table 1-1: sMMO Hydroxylase Sequencing Primer Names and Binding Locations	41
Table 1-2: Electrospray-Ionization Mass Spectrometric Results from Buzy et al.....	43

Chapter Three

Table 1: Spectroscopic Properties of Non-Heme Carboxylate-Bridges Diiron Nitrosyl Complexes.....	206
Table 2: Mössbauer Properties of Species Observed in Reactions of the Reduced sMMO Hydroxylase with Nitric Oxide	207
Table 3: Time-Dependant Changes in the Mössbauer Spectra of Rapid Freeze Quench Time Points of the Reaction of Nitric Oxide with Reduced sMMO Hydroxylase.....	208
Table 4: Activation Parameters from Eyring Plots of the Reaction of the Reduced Hydroxylase with Nitric Oxide	209

List of Figures

Overview

The MMO Diiron Center in its Fe(II) Fe(II) Oxidation State.....	15
The Catalytic Cycle of the sMMO System.....	17

Chapter One

Figure 1-1: Structure of the <i>Methylococcus capsulatus</i> (Bath) sMMO Hydroxylase.....	45
Figure 1-2: Organization of the sMMO Operons from Three Different Organisms.....	47
Figure 1-3: Organization of other sMMO Family Multicomponent Monooxygenase Operons.....	49
Figure 1-4: Binding Locations of Primers Used in Sequencing the <i>M. capsulatus</i> sMMO Hydroxylase Genes.....	51
Figure 1-5 DNA Sequences and Deduced Peptide Sequences of the <i>M. capsulatus</i> sMMO Genes.....	53
Figure 1-6: Mistakes in the Published Hydroxylase Gene Sequences and Their Corrections.....	68
Figure 1-7: Mistakes in the Published DNA Sequence for the sMMO Genes <i>mmoB</i> and <i>mmoC</i>	70
Figure 1-8: Relationships between the Genes and Proteins of the sMMO Multicomponent Monooxygenase Family.....	72
Figure 1-9: Identity Statistics between the Closely Related Proteins of the sMMO Multicomponent Monooxygenase Family.....	76
Figure 1-10: Sequence Alignments of the Peptides Corresponding to the α Subunit of the Hydroxylase.....	72
Figure 1-11: Sequence Alignments of the Peptides Corresponding to the β Subunit of the Hydroxylase.....	76
Figure 1-12: Sequence Alignments of the Peptides Corresponding to Protein B.....	83
Figure 1-13: Sequence Alignments of the Peptides Corresponding to the Reductase.....	85
Figure 1-14: View of the Absolutely Conserved α Subunit Residues Near the Active Site of the <i>M. capsulatus</i> (Bath) sMMO Hydroxylase.....	88
Figure 1-15: Schematic of the Hydrogen Bonding Network in the Absolutely Conserved Residues Near the Active Site.....	90
Figure 1-16: View of the Absolutely Conserved α Subunit Residues Not Near the Active Site.....	92
Figure 1-17: View of the Absolutely Conserved β Subunit Residues in the <i>M. capsulatus</i> (Bath) sMMO Hydroxylase.....	94

Figure 1-18: View of the Conserved Residues in the <i>P. pudita</i> CF600 Phenol Hydroxylase P2 Protein	92
Figure 1-19: Cartoon of Two Possible sMMO Family Interprotein Interactions.....	94

Chapter Two

Figure 2-1: Methylotrophs in the Carbon Cycle.....	136
Figure 2-2: Metabolism of Methane in <i>M. capsulatus</i> (Bath).....	138
Figure 2-3: Native sMMOH PAGE.....	140
Figure 2-4: Sample Western Blot	142
Figure 2-5: PCR of the sMMOH Genes	144
Figure 2-6: Construction of pDEC002	146
Figure 2-7: Structure of pDEC002	148
Figure 2-8: Expression of sMMOH Genes in <i>E. coli</i> results in Inclusion Bodies	150
Figure 2-9: Attempted Refolding of Expressed, Insoluble sMMOH Under a Variety of Conditions	152
Figure 2-10: Expression of sMMOH from pDEC002 by using a Sarcosyl Lysis Procedure	154
Figure 2-11: Attempted Reconstitution of the Expressed, Insoluble sMMOH by using Detergents.....	156
Figure 2-12: Attempted Reconstitution of the Expressed, Insoluble sMMOH by using Sarcosyl Detergent	158
Figure 2-13: Expression by using the pDEC010 Plasmid in <i>E. coli</i>	160
Figure 2-14: Construction of pDEC050 and pDEC055.....	162
Figure 2-15: Structure of pDEC050 and pDEC055	164
Figure 2-16: Construction of pDEC060 and pDEC070.....	166
Figure 2-17: Structure of pDEC060 and pDEC070	168
Figure 2-18: Expression of sMMOH Genes from pDEC050 and pDEC055	170
Figure 2-19: Periplasmic Expression of the sMMOH α from pDEC060 ...	172
Figure 2-20: Expression of the Thioredoxin-sMMOH α Subunit Fusion Protein from pDEC070	174
Figure 2-21: Purification of the Thioredoxin-sMMOH α Subunit Fusion Protein	176
Figure 2-22: EPR Spectrum of Putatively Diiron(II) Thioredoxin-sMMOH α Subunit Fusion Protein.....	178

Chapter Three

Figure 3-1: Optical Spectra of the Nitrosyl Adducts of the Reduced sMMO Hydroxylase in 25 mM MOPS pH 7.0 and the Dinitrosyl Adduct of [Fe ₂ (μ -XDK)(μ -O ₂ CPh)(ImH) ₂ (O ₂ CPh)(MeOH)] in THF	210
Figure 3-2: Mössbauer Spectra of ⁵⁷ Fe-Enriched H _{red} and H _{red} +2B Reacted with NO for 45 min	212

Figure 3-3: EPR Spectra of $H_{red}+NO$ Adducts	214
Figure 3-4: Buildup of Optical Species Associated with Reaction of NO with H_{red} as Observed by using Stopped Flow Spectroscopy.....	216
Figure 3-5: Eyring Plots of the $H_{red}+NO$ and $H_{red}+2B+NO$ Reactions.....	218
Figure 3-6: Time-Dependent EPR Spectra following the Reaction of NO with the Reduced sMMO Hydroxylase.....	220
Figure 3-7: Time-Dependent Mössbauer Spectra following the Reaction of H_{red} with NO	222
Figure 3-8: Simulation of the $H_{dinitrosyl}$ Formation and Decay Reactions...	224
Figure 3-9: Proposed Reaction Mechanism for the Reactions of NO with H_{red} and Iron-Depleted H_{red}	226
Figure 3-10: Active Site Structure of the Reduced sMMO Hydroxylase .	228
Figure 3-11: Proposal for Ligand Movements in the Active Site of the Reduced sMMO Hydroxylase Induced by Binding of Protein B	230

"Qvid me anxivs svm?"

Overview of the Soluble Methane Monooxygenase System

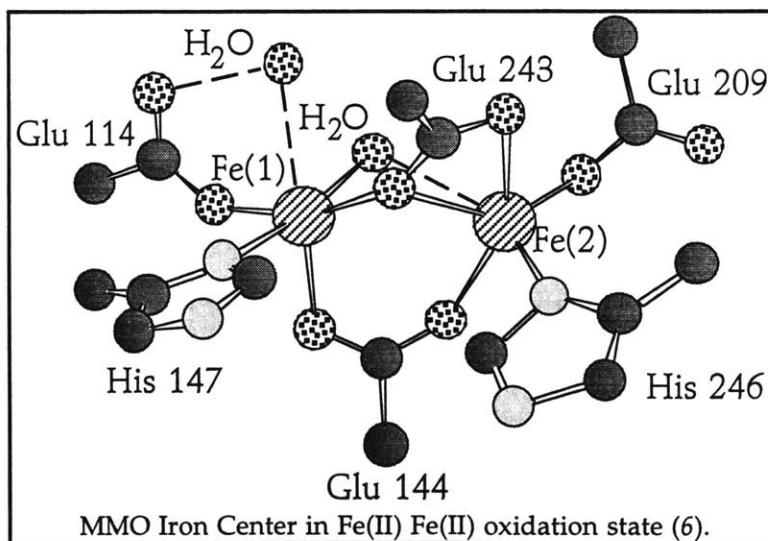
The soluble methane monooxygenase (sMMO) is a multicomponent enzyme system that catalyzes the conversion of methane gas to liquid methanol, utilizing oxygen as an oxidant and producing water as a byproduct, as depicted in eq. 1 (1-3). The reaction takes place at a carboxylate-bridged non-heme diiron center located in the MMO protein core.



This enzyme is one of a number of metalloproteins that perform biologically essential transformations of small molecules, including nitrogenase (which reduces nitrogen to ammonia) (4) and photosystem II (photosynthesis) (5). These types of reactions are of tremendous current interest, due to both their novel and interesting chemistry and our desire to replicate these reactions in inexpensive small molecule mimics for industrial purposes.

Utility of the sMMO System

The methane to methanol reaction is currently done industrially by using a variety of catalysts at high temperatures and pressures in the gas phase. MMO can catalyze this reaction at room temperature and pressure in water. It would be useful to use the method nature has devised, as methane gas is



dangerous and expensive to transport to the refinery sites where the catalytic transformation usually takes place. One can imagine small, easily transportable biocatalyst plants set up at natural gas mines. At those plants, liquid methanol would be produced and transported for further processing or distribution as fuel.

The MMO system also has other uses, as it is capable of oxidizing a wide variety of other molecules. Trichloroethylene (TCE), a common ground water pollutant and potent carcinogen, is rendered harmless by oxidation by MMO. TCE was used extensively by both industry and the government as a degreasing solvent. Used solvent was often left in waste containers that eventually developed leaks, or was simply dumped in the ground. The pollutant has found its way into the ground water drinking supply in several locations throughout the U.S., and cleanup via traditional "pump-and-treat" techniques is very expensive. It is possible that either biocatalysts based on the MMO system or microorganisms genetically engineered to produce the MMO enzymes could be used to clean up TCE spills cheaply, as well as other organic pollutants.

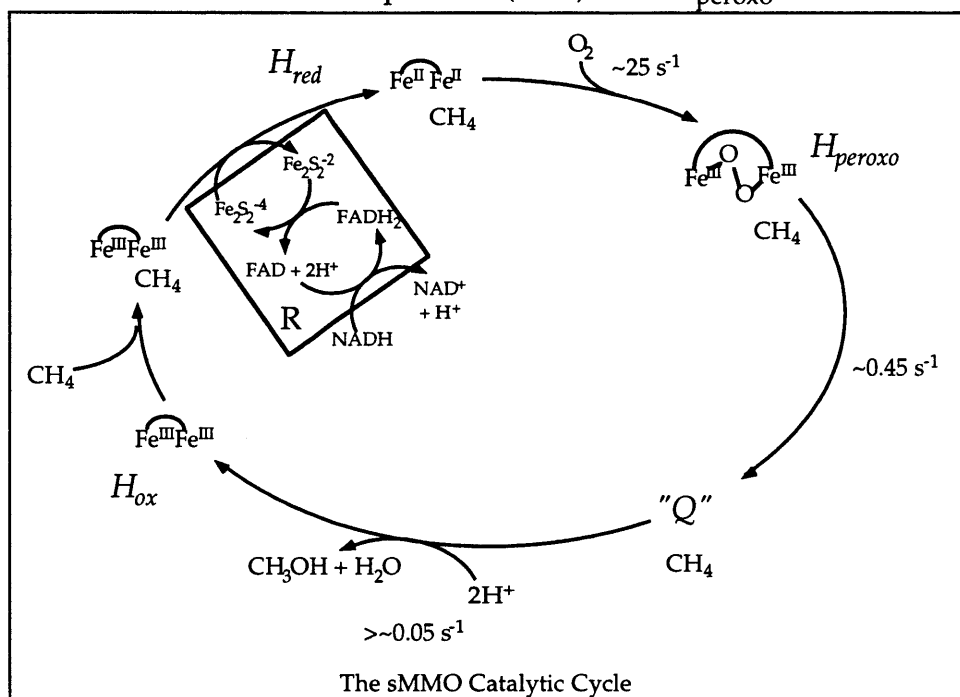
The sMMO Protein Components

The sMMO system consists of three proteins. The hydroxylase (H) contains two copies each of three subunits, α , β and γ . The α subunit is the location of the non-heme diiron active site that is the site of dioxygen activation and of methane hydroxylation. The reductase (R) contains a FAD, an [2Fe-2S] center and a NADH binding site, and is responsible for accepting electrons from NADH and transferring them to the hydroxylase. The third member of the sMMO system, the coupling protein or protein B (B), is presumably a regulatory protein and modulates the activity of the system depending upon the ratio of B to H.

The sMMO Catalytic Cycle

The catalytic cycle as it is currently understood is as follows. The H_{ox} (diiron(III)) resting state of the hydroxylase is reduced to the diiron(II) (H_{red}) oxidation level. Reaction with dioxygen produces the first well characterized intermediate, H_{peroxo} (7, 8). This intermediate is assigned as a (μ -1,2-peroxo)diiron(III) species through spectroscopic comparison with crystallographically characterized model compounds (9-11). The H_{peroxo} intermediate

spontaneously transforms into intermediate Q (8, 12), which has been assigned a di(μ -oxo)diiron(IV) structure based on EXAFS evidence (13), although other



interpretations of

the data are possible (1). Intermediate Q is widely assumed to be the active oxidant that reacts with alkyl substrates to form hydroxylated products. Upon reaction, the iron center returns to its resting, diferric state designated H_{ox} .

The sMMO system catalyzes a kinetically difficult reaction that would be of tremendous use to industry. A complete understanding of its structure and function is not yet achieved. This thesis reports progress towards this goal.

References

1. Valentine, A. M., and Lippard, S. J. (1997) *J. Chem. Soc., Dalton Trans.* 21, 3925-3931.
2. Wallar, B. J., and Lipscomb, J. D. (1996) *Chem. Rev.* 96, 2625-2657.
3. Lipscomb, J. D. (1994) *Annu. Rev. Microbiol.* 48, 371-399.
4. Howard, J. B., and Rees, D. C. (1996) *Chem. Rev.* 96, 2965-2997.
5. Yachandra, V. K., Sauer, K., and Klein, M. P. (1996) *Chem Rev.* 96, 2927-2959.
6. Rosenzweig, A. C., Nordlund, P., Takahara, P. M., Frederick, C. A., and Lippard, S. J. (1995) *Chemistry & Biology* 2, 409-418.
7. Liu, K. E., Valentine, A. M., Qiu, D., Edmondson, D. E., Appelman, E. H., Spiro, T. G., and Lippard, S. J. (1995) *J. Am. Chem. Soc.* 117, 4997-4998.
8. Lee, S.-K., Nesheim, J. C., and Lipscomb, J. D. (1993) *J. Biol. Chem.* 268, 21569-21577.
9. Kim, K., and Lippard, S. J. (1996) *J. Am. Chem. Soc.* 118, 4914-4915.
10. Dong, Y., Yan, S., Young, V. G., and Que, L. (1996) *Angew. Chem. Int. Ed. Engl.* 35, 618-620.
11. Ookubo, T., Sugimoto, H., Nagayama, T., Masuda, H., Sato, T., Tanaka, K., Maeda, Y., Okawa, H., Hayashi, Y., Uehara, A., and Suzuki, M. (1996) *J. Am. Chem. Soc.* 118, 701-702.
12. Liu, K. E., Valentine, A. M., Wang, D., Huynh, B. H., Edmondson, D. E., Salifoglou, A., and Lippard, S. J. (1995) *J. Am. Chem. Soc.* 117, 10174-10185.
13. Shu, L., Nesheim, J. C., Kauffmann, K., Münck, E., Lipscomb, J. D., and Que, L. (1997) *Science* 275, 515-517.

Chapter One

Sequencing and Analysis of the *Methylococcus capsulatus* (Bath)

Soluble Methane Monooxygenase Genes

Introduction

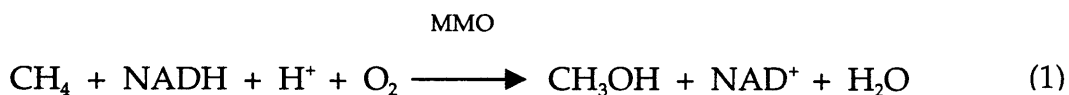
Non-heme carboxylate-bridged diiron centers have emerged as widespread and chemically diverse units in proteins (1-5). The prototypical members of this family of proteins are hemerythrin, ribonucleotide reductase R2 subunit (R2) and the soluble methane monooxygenase (sMMO) hydroxylase. A hallmark of these cofactors is their reactivity with dioxygen. For example, hemerythrin is a dioxygen transport protein, utilizing its iron center to reversibly bind O₂. The R2 subunit uses its iron center and one O₂ molecule to generate a tyrosine-based radical, which is subsequently used catalytically by the ribonucleotide reductase R1 subunit to reduce ribonucleotides to deoxyribonucleotides.

A common chemistry catalyzed by carboxylate-bridged diiron centers is monooxygenase activity. This function is exemplified by the soluble methane monooxygenase enzyme system (sMMO), the best studied member of this subclass (3, 6-8). It catalyzes the oxidation of methane to methanol, utilizing NADH as an electron source and releasing water as a byproduct. There are three known proteins in the sMMO system. The hydroxylase (H) contains two copies each of three subunits, α , β and γ , with the α subunits housing the diiron active sites. The reductase (R) contains a FAD, an [2Fe-2S] center and a NADH binding site, and is responsible for accepting electrons from NADH and transferring them to the hydroxylase. The third member of the sMMO system, the coupling

protein or protein B (B), is presumably a regulatory protein and modulates the activity of the system depending upon the B:H (vide infra). The sMMO systems from three different methylotrophs, *Methylococcus capsulatus* (Bath), *Methylosinus trichosporium* OB3b OB3B and *Methylocystis* sp. strain M have been characterized, and the proteins from the first two organisms are best understood. The structure of the sMMO hydroxylase from *M. capsulatus* (Bath) as determined by X-ray crystallography is shown in Figure 1-1, together with a schematic of the active site residues (9-11). The most striking element of the tertiary structure is a large canyon located in the center of the molecule formed by the α and β subunits.

The genes for the five polypeptides making up the three sMMO proteins are arranged in one operon, along with an open reading frame, designated *orfY*, for a heretofore unknown and unisolated protein (12-15). Figure 1-2 shows the sMMO operon organization for all three organisms.

The role of the two ancillary proteins is of current interest, for the chemistry (eq. 1) that takes place at the hydroxylase protein does not occur



without them. The reductase supplies electrons to the hydroxylase.

Characterizing the interactions between the reductase and the hydroxylase is important to the general understanding of the system and may be of use in designing industrially useful variants of the sMMOH. Protein B also plays an important role. Without the presence of protein B, the hydroxylase reduces dioxygen to water or hydrogen peroxide without concomitant oxidation of substrate (16, 17). As the protein B:hydroxylase ratio is increased, the coupling of dioxygen to substrate consumption increases. At a 1:1 ratio of protein

B:hydroxylase, the system is fully coupled, and activity is optimal. Protein B has an inhibitory effect when this ratio rises above 1. Understanding the effects of protein B on the active site of the hydroxylase is crucial to the elucidation of the mechanism; the structural consequences of B binding are unknown at this time.

The sMMO genes from all three organisms have been sequenced, but several mistakes were made in the gene sequence of both the *M. capsulatus* (Bath) and *M. trichosporium* OB3b operons. A base insertion that caused a frame shift was found at the end of the *M. capsulatus* (Bath) *mmoY* during X-ray crystallographic work on the enzyme (9). More recently, mass spectrometric studies of the hydroxylase from *M. capsulatus* (Bath) disagreed with the molecular mass predicted by the gene sequence (18). Many mistakes were found in the *M. trichosporium* OB3b hydroxylase peptide sequence as a result of X-ray crystallographic work (19).

There are several other monooxygenases that are quite similar to the methane monooxygenases. The toluene monooxygenases (toluene-2-monooxygenase (20), toluene-3-monooxygenase (21, 22) and toluene-4-monooxygenase (23-26)) are capable of specifically hydroxylating toluene to the corresponding *o*-, *m*- or *p*-cresol. Phenol hydroxylase (PH) from *Pseudomonas* sp. CF600 catalyzes the hydroxylation of phenol and certain methyl-substituted derivatives of phenol to catechol (27-30). The alkene monooxygenases (AMO) are capable of epoxidizing various alkenes and alkynes, a reaction that the sMMOs can also perform (31-34). All of these proteins have core similarities. They all contain a hydroxylase protein with three subunits and a non-heme carboxylate-bridged diiron center, a reductase and a coupling protein. They also catalyze hydroxylation or epoxidation reactions by using dioxygen as an oxidant. The operons for the phenol hydroxylase and toluene monooxygenase systems are shown in Figure 1-3.

Sequence analysis can be a useful tool in identifying residues that are important in structure and function, especially when combined with crystallographic information about the enzymes in question. There have been several sequence analyses of the MMO proteins in the literature. One of the first was a comparison of the protein sequence of the sMMOH, the structure of which was then unknown, with that of the structurally characterized R2 subunit (35). This remarkably prescient paper correctly deduced much of the detail of the diiron active site of sMMO by comparison with R2. A second report compares protein sequence data from several Δ -9 desaturases with those from several ribonucleotide reductases and the soluble methane monooxygenase (36). This alignment established that the desaturases were members of a carboxylate-bridged diiron center family of proteins distinct from both the sMMO family of monooxygenases and the ribonucleotide reductase R2 family. Homology between the hydroxylase alpha subunits from the toluene-4-monooxygenase, toluene-3-monooxygenase, toluene-2-monooxygenase, phenol hydroxylase, alkene monooxygenase and sMMO systems has been helpful to establish that all these proteins contain carboxylate-bridged diiron centers (21, 23, 37).

The reductase sequence from the sMMO family has been analyzed extensively. It is a member of the FNR family of oxidoreductases, which include ferredoxin-NADP⁺ reductase (38) and phthalate dioxygenase reductase (39). Sequence comparisons of the reductase proteins can be found in several places in the literature (24, 40, 41). The coupling proteins have also been compared (42).

The sequence analyses thus far reported focus mainly on the diiron center, its ligands, and the substrate binding region. No comparisons of the entire protein sequences have appeared. Such a comparison of all of the proteins of the multicomponent sMMO monooxygenase family would be of value in determining which areas of the protein are essential for activity. Similarities

between these proteins could provide important clues about structure, function and relationships for this subclass of enzymes, including areas contributing to interactions between the components. The docking site for protein B would be of particular interest as a first step to understanding its ability to affect on the iron active site.

Before the sequences can be compared, it is necessary to know that they are correct. Crystallographic work on the hydroxylase indicated that the published gene sequence was inaccurate.

This chapter reports the determination of the correct sequence of the *M. capsulatus* (Bath) soluble methane monooxygenase hydroxylase and sequence comparisons between the methane monooxygenases, alkene monooxygenases, toluene monooxygenases and phenol hydroxylase. Possible roles for several of the universally conserved residues are suggested based upon their locations in the *M. capsulatus* (Bath) sMMOH structure.

Materials and Methods

DNA Sequencing. Sequenase 2.0 kits and enzymes were purchased from United States Biochemicals. TEMED and 29:1 acrylamide:bis were purchased from Biorad. Long Ranger™ acrylamide was purchased from J. T. Baker and α [³²P]dATP and α [³⁵S]dATP from DuPont-NEN. All other chemicals were of the highest quality available.

Oligonucleotide primers were either synthesized on a Cruachem or Expedite DNA synthesizer or purchased from the MIT Biopolymers lab. All oligonucleotides were PAGE-purified according to the Cruachem manufacturer's instructions. Primer sequences are shown in Table 1-1, and the binding locations of those primers relative to the sMMO operon genes are given in Figure 1-4.

Plasmid DNA was purified by using Qiagen purification kits. Plasmid pCH4, which contains a genomic clone of the sMMO operon from *M. capsulatus* (Bath), was a gift from Prof. J. Colin Murrell (Warwick).

Plasmid DNA was sequenced by using the suggested protocol for double-stranded DNA from USB, except that the sequence extension steps were carried out at 45 °C. Both α [³²P]dATP and α [³⁵S]dATP were used in the sequencing reactions; 8% 29:1 acrylamide:bis and 5% Long Ranger™ gels were used in these experiments.

Sequence Analysis. The Wisconsin GCG sequence analysis package (version 7.3) was used to perform most of the sequence analysis (43). Initial sequence alignment was made by using the GCG PileUp program with a gap weight of 3 and a gap length weight of 0.1. Maligned (44) and BoxShade (45) were used to generate protein homology plots. The *M. capsulatus* (Bath) sMMOH oxidized Form I crystal structure was analyzed by using a combination of Quanta97 (46) and MolScript 2.02 (47). A search profile of an alignment of the three sMMO OrfY peptides was prepared by using the GCG ProfileMake program. Both the GenEMBL (peptide-translated) and SwissProt databases (release 107.0 with updates as of 7/20/98) were searched with the OrfY profile with a gap weight of 4.5 and gap length weight of 0.05.

The DNA sequences used in this chapter were obtained from the GenEMBL database on 7/20/98, through either the GCG Fetch program or the world wide web *Entrez* interface at the National Center for Biotechnology Information <<http://www.ncbi.nlm.nih.gov/Entrez/nucleotide.html>>. The sequences and accession numbers used are as follows: *Methylococcus capsulatus* (Bath) soluble methane monooxygenase (13, 14) (accession numbers M90050 and M32314, NID g149833, EC 1.14.13.25), *Methylosinus trichosporium* OB3b OB3b soluble methane monooxygenase (12) (accession number X55394, NID g44613,

EC 1.14.13.25), *Methylocystis* sp. strain M soluble methane monooxygenase (15) (accession number U81594, NID g2098694, EC 1.14.13.25), *Pseudomonas* sp. strain CF600 phenol hydroxylase (EC official name phenol-2-monooxygenase) (27) (accession numbers M60276, M37764, M37775 and M57564, NID g151449, EC 1.14.13.7), *Xanthobacter* sp. strain Py2 alkene monooxygenase (48) (accession number AJ006979, NID g3250923), *Nocardia corallina* B-276 alkene monooxygenase (32) (accession number D37875, NID g529091), *Pseudomonas mendocina* KR1 toluene-4-monooxygenase (23, 24) (accession numbers M65106 and M95045, NID's g151590 and g151596), *Pseudomonas pickettii* PKO1 toluene-3-monooxygenase (21) (accession number U04052, NID g1590790), and *Pseudomonas* sp. strain JS150 toluene/benzene-2-monooxygenase (20) (accession number L40033, NID g1008895). Note that the sequences for the two AMO systems are incomplete at this time. Only the α and β epoxygenase subunits, reductase and coupling sequences are known for the *N. corallina* AMO; only the epoxygenase α subunit sequence from *Xanthobacter* AMO has been reported. Corrections to the *M. trichosporium* OB3b sMMO hydroxylase amino acid sequence were applied as described (19). Corrections to the *M. capsulatus* (Bath) sMMO protein sequences were applied as reported herein.

Results

Corrections to the sMMO gene sequences. The DNA sequences of the six genes in the sMMO operon are shown in Figure 1-5, including the changes found as a result of the sequencing described in this chapter. The errors found in the published sequence are shown in Figure 1-6. Change A is a simple base pair switch that alters residue Val84 of the α subunit to Glu. Change B is a double frame shift that inserts a G at base pair 423 of *mmoY* and deletes a G at base pair

434. The net result in the β peptide sequence is that four residues are altered. Change C is a frame shift caused by the deletion of C at position 1086. This frame shift alters the last 27 residues of the β subunit. Change D is a base pair inversion in the *mmoZ* gene, changing residue H21 to Q and residue V22 to L.

An additional two changes to the *M. capsulatus* (Bath) sMMO operon have been determined. An error in the sequence of protein B was discovered by amino terminal sequencing, altering residue F12 to I (49). Electrospray mass spectrometry (50), MALDI mass spectrometry (51) and DNA sequencing (52) have confirmed this change, and that the protein sequence is otherwise correct. An error in the *mmoC* gene was found recently by DNA sequencing (52). Both of these errors are shown in Figure 1-7. Corrected DNA sequences for all of the sMMO genes have been submitted to the GenEMBL gene database.

Changes to the *M. trichosporium* OB3b gene sequence as suggested by the crystallographically determined electron density of the hydroxylase have also been incorporated as part of the sequence alignment in this chapter (19). One of the changes, D209E, is quite clearly correct from both a crystallographic and a sequence alignment viewpoint, as that position is a glutamic acid in every other sMMO family monooxygenase. Forty amino acid changes are made to the *M. trichosporium* OB3b sequence, including a 26-residue stretch at the end of the β subunit. Twenty of those alterations change the residue to its corresponding residue in the *M. capsulatus* (Bath) sequence. The *M. capsulatus* (Bath) structure was used as a starting model for the *M. trichosporium* OB3b enzyme structure determination, due to problems encountered obtaining the phases. The possibility therefore exists that the *M. trichosporium* OB3b model is biased. The changes reported in the literature unfortunately were not confirmed by DNA sequencing. For the purposes of this chapter, all of the changes made to the *M. trichosporium* OB3b hydroxylase sequence are taken as correct, and many of them

probably are, but it is impossible to determine which are correct and which are artifacts. Clearly, confirmation of the *M. trichosporium* OB3b sequence is needed.

Roles for genes from the sMMO family operons. The relationships between the genes and gene products of the nine proteins examined in this chapter, *M. capsulatus* (Bath) sMMO, *M. trichosporium* OB3b sMMO, *M. sp.* strain M sMMO, *P. mendocina* toluene-4-monooxygenase (T4M), *P. pickettii* PKO1 toluene-3-monooxygenase (T3M), *P. sp.* toluene-2-monooxygenase (T2M), *P. pudita* phenol hydroxylase (PH), *N. corallina* alkene monooxygenase (AMO) and *Xanthobacter sp.* Py2 alkene monooxygenase, are shown in Figure 1-8. All of these systems contain a hydroxylase that comprises three subunits. The homologies between the sMMOH α analogues are all very high, and it is clear which genes correspond to this important subunit. The same is true of the reductase and coupling protein analogues. Although the sMMO β analogues all have homology to each other, in some cases (*dmpL*, *tbmB*, *tbuA2* and *tmoE*), they have higher homologies to the *mmoX* genes of sMMO (20, 21). With knowledge of the crystal structure of the sMMO hydroxylase, this is understandable. Although the β subunit of the *M. capsulatus* (Bath) hydroxylase is not homologous to the α subunit, they have similar folding topologies (9). It is possible that a protein with sequence homologous to sMMOH α might have a tertiary structure like that of the sMMO β subunit, and would fulfill its function in the quaternary structure of the hydroxylase. It seems likely that the β subunit is evolutionarily related to the α subunit, and has retained structural aspects from its precursor. Note that the iron binding ligands are not present in any of the β subunit analogues. The identity of the γ subunit in each hydroxylase is not clear from homology in many of the cases. Because the P4 peptide of the phenol hydroxylase has been identified as the γ subunit in the hydroxylase of that system (28), and because its gene, *dmpO*, is homologous to *tbmE* of the T2M system (35.3% identity between the two) (20),

we can assign that role to those two proteins. Amino-terminal sequencing of the purified hydroxylase from T4M indicates that the TmoB peptide is its third subunit (25), and its homology with *tbuU* from T3M (38.8% identity) (20) completes the set of known γ analogues. The T3M and T4M systems both contain a ferredoxin (TbuB and TmoC) with a Rieske-type [2Fe-2S] center, which is necessary for turnover in the T4M system along with the reductase (25). This ferredoxin is not present in the other systems. Finally, there is a gene of unknown function in many of the systems: *orfY* in the sMMOs, *dmpK* in PH and *tbmA* in T2M. There is homology between the *orfY*s in the sMMOs, and between *dmpK* and *tbmA*. Interestingly, although the PH system is fully functional *in vitro* without the *dmpK* gene product (P0), it is necessary *in vivo* for growth on phenol (30). Note that the alkene monooxygenase operons are only partially sequenced. The assignment of the AMO genes to functions in the AMO system is clear from homology. Only the sMMOH α , sMMOH β , sMMOB and sMMOR homologies are high enough to align the peptide sequences from all nine proteins.

Comparisons between the sMMO family protein sequences. Percent identity and percent dissimilarity between MMOH α , MMOH β , MMOB and MMOR analogues are shown in Figure 1-9. The proteins can be divided into three groups that appear related: the sMMO systems, the T3M and T4M systems and the PH and T2M systems. The *N. corallina* AMO hydroxylase is quite similar to the sMMOH, but the reductase and coupling protein from that system are much different from any of the other systems. Surprisingly, the *Xanthobacter* AMO hydroxylase α subunit is very different from its homologues.

Sequence alignments for the α and β subunits of the hydroxylases/epoxidases, coupling proteins and reductases from the nine enzyme systems are shown in Figures 1-10 through 1-13 respectively.

Search for OrfY analogues. The three OrfY putative protein sequences from the sMMO systems were aligned, and a search profile based on the consensus sequence was prepared. Both a peptide-translated GenEMBL database and the SwissProt protein database were searched by using this profile. The top candidates were a putative RNA polymerase σ factor in the *Streptomyces coelicolor* rpoX operon, the E6 DNA-binding zinc-finger protein from Human Papillomavirus type 30, insertion element IS402 from *Pseudomonas cepacia* and *Rattus norvegicus* cortexin. None of these proteins exhibited significant homology with the OrfY sequences.

The sMMOH α analogues. The sequence alignment of the MMOH α analogues is shown in Figure 1-10. Clearly, the MMOH α subunit has the most homology to its counterparts in the other monooxygenases. The α subunit is mostly comprised of α -helices. It is apparent that many of the identical residues are spaced every 3-4 residues, indicating conservation of one side of an α -helix.

The MMOH α residues that are conserved absolutely between all the proteins can be divided into four groups. The first group is a series of residues in and around the active site of the enzyme. A view of the active site showing the residues discussed here is shown in Figure 1-14. The iron ligands (E114, E144, H147, E209, E243 and H246) are, of course, absolutely conserved. The iron ligand residue sequence pattern E•••EX₂H has been noted to be a hallmark of proteins containing carboxylate-bridged non-heme diiron centers (53), and is in fact the only sequence that is conserved all across the sMMO, R2 and stearyl-ACP desaturase families (36).

The active site can be divided into two regions. The first lies above the iron atoms as depicted in Figure 1-14, where there are few conserved residues. The top side of the active site might be where substrates bind, and where the monooxygenase chemistry takes place. This hypothesis is supported by a

number of observations. In the R2 family, a closely related set of enzymes, this side of the active site is where the tyrosine radical is located (54-56). The iron ligands on this side of the iron site are quite mobile (10, 11); such lability might indicate that this location is where dioxygen binds. Finally, the lack of conserved residues in this area is to be expected if it is the site of substrate binding. A phenol binding pocket is likely to be very different in size and shape from a methane binding pocket. The only two conserved residues in this area are both protic, T213 and N214. Threonine 213 is in a position homologous to a serine residue in the R2 subunit thought to be responsible for proton flux into the active site (57). Either one of these residues might assist in the delivery of protons during the hydroxylation reaction.

The bottom half of the active site is, by contrast, quite well conserved. A set of residues involved in hydrogen bonding between the F and C helices (D143, R146, S238, D242 and R245) are absolutely conserved among all sMMO family proteins. A schematic showing residues within hydrogen bonding distance of one another is presented in Figure 1-15. These residues might be part of a framework to hold the iron center in place, or possibly to deliver protons to the active site. There are also two residues that are conserved for clear steric reasons. Both A117 and G250 are located in positions where the packing is very tight, and a larger residue would not fit. Glycine 250 in particular is located where helices E and F come very close to one another. Finally, there is a triad of surface accessible residues, comprising A224, G228 and D229, located at the turn between helices E and F. It is possible that they form a "handle" on one end of the E/F helix half of the active site. One of the ancillary proteins might interact with the "handle", causing the E/F helices to shift, thereby altering the coordination environment at the iron center.

The conserved residues in other parts of the α subunit are shown in Figure 1-16. A group of aromatic residues located at the top of the hydroxylase (Y292, W371, Y376) in close proximity to each other are shown in Figure 1-16 in red. Along with those aromatics, a proline (P377) is absolutely conserved and may be important structurally. This entire cluster of residues may be some kind of docking site for another protein, or part of an electron transfer path. It has been suggested that this area of the hydroxylase is the site where the reductase binds (58).

Another set of residues is located in the second domain of the hydroxylase, shown in white in Figure 1-16. They comprise residues P424, G443, P461 and Y464. They are located slightly beneath the surface of the protein, near the γ subunit interface. No function for these residues is obvious. It is possible that they are involved in interactions with the γ subunit.

The fourth and final set of residues is located on the surface of the protein in the “canyon” area, above the active site. This residue group comprises Y67, K74, L321, G325, and P329, which can be seen in yellow in Figure 1-16. It has been hypothesized that the canyon is a docking site for some other protein, possibly protein B (9). These residues may be important in mediating the interactions between the two proteins. In particular, K74 and Y67 are very close to the surface and are located in the canyon. Combined with the E/F helix “handle” described above, these residues might be key interaction points between the coupling protein and the hydroxylase.

There are a number of residues that show up in the alignment that are probably artifacts of the alignment algorithm, due to proximity to gaps and isolation from other conserved residues. These residues are Y292, H344 and G492.

The sMMOH β analogues. There is less identity in the MMOH β subunit analogues than for the MMOH α subunit. It is therefore difficult to guess at the function of any of the conserved residues, which for MMOH β are shown in white in Figure 1-17. They can be divided into three general areas. The first is at the interface between the α and β subunits, and consists of D100, P101 and E185. These residues might be important in intersubunit interactions, although there are no conserved hydrogen bonding or salt bridge partners in the α subunit. A second group of residues can be found under the surface of the β subunit, comprising W218, R228 and A331. The third group of residues, D240, E243, Q313 and W320, is very near the surface and consists of mostly polar residues. Lack of knowledge about the function of the β subunit precludes making conclusions about the functions of these residues. They might be involved in protein folding, interactions with other ancillary proteins, or in electron transfer. Cross-linking experiments in the *M. trichosporium* OB3b sMMO system indicate that the reductase has a binding site on the β subunit (59). One or more of the conserved areas listed above may be part of a reductase binding site.

The coupling protein analogues. There is little identity between the coupling proteins from the sMMO family. The five absolutely conserved residues (V38, E53, I79, G97, G144) are mapped in white onto the NMR structure of the P2 protein (42) from the phenol hydroxylase system in Figure 1-18. There are also a number of closely homologous residues of interest near these absolutely conserved residues, including I/V52, I/L85, D/E94, R/K98 and I/V107, shown in yellow in Figure 1-18. The charged residues in this group might have partners in the charged surface residues in the hydroxylase canyon. This idea is consistent with cross-linking studies of the *M. trichosporium* OB3b sMMO system, where protein B was shown to have a binding site on the α subunit of the hydroxylase (59).

The reductase analogues. Conserved residues in the reductase have been discussed previously, as the sMMOR is a member of the FNR family of oxidoreductases, which contain well-characterized [2Fe-2S] and FAD cofactor sites and pockets for binding NADH (24, 38, 40). No reductase from a sMMO-family multicomponent monooxygenase has yet been characterized crystallographically. The T3M and T4M systems have electron delivery systems that are different from the other seven. They contain ferredoxins that are necessary for multiple turnover. Presumably, these ferredoxins ferry electrons from the reductase to the hydroxylase, but such a function has not been shown conclusively. If so, then identification of the reductase-hydroxylase interaction region from this alignment is problematic, since the site does not exist in two of the proteins.

Discussion

Proteins housing carboxylate-bridged non-heme diiron centers can be divided into two structurally distinct classes, the hemerythrin-like class and R2/sMMO-like class (36). The latter can be further divided into families of proteins, including the R2, stearoyl-ACP desaturase and sMMO families. The sMMO family has a number of distinguishing characteristics, including the ability to catalyze hydroxylation/epoxidation chemistry, the presence of a three-subunit hydroxylase that houses diiron centers in its α subunits, and the presence of a coupling protein that is necessary for optimal activity. This chapter compares the sequences of known members of this family in an effort to determine which areas of the protein are important for its unique features.

Implications of the corrected M. capsulatus (Bath) DNA sequence. The corrected sequence of the sMMO operon from *M. capsulatus* (Bath) presented

here is consistent with the crystallographically-determined electron density for the sMMO hydroxylase. All errors in the reported sequence can be easily attributed to gel-reading errors or typographical mistakes. It can also explain recent electrospray-ionization (ESI) mass spectrometric results (18), which were clearly not consistent with the published sequence. The unexplained ESI data obtained are listed in Table 1-2. Based on the mass spectrometric data obtained, the authors correctly deduced the actual sequence of the β and γ subunit, although they could not distinguish between isoleucine and leucine. Due to apparent misinterpretation of MS/MS sequencing of the α subunit peptides (data not shown in the published MS work), however, they misidentified L82 as T82, Q83 as R83 and failed to correct V84 to D84. These sequence changes, if correct, would require several changes to the DNA sequence of the *mmoX* gene, and these changes would be difficult to imagine as typographical errors. The sequence as reported in Figure 1-6, however, is consistent with the electrospray mass spectrometric data, clear from the cDNA sequencing and easy to imagine as a simple typographical TA base inversion at base 251 of *mmoX*. Although mass spectrometry is a useful tool, it is best used in concert with other complementary techniques to obtain meaningful, clear results.

Sequence alignment of sMMO family proteins. Comparison of the α and β hydroxylase subunits, coupling proteins and reductases from the known sMMO family proteins has revealed an interesting set of conserved residues. Much of the data can be interpreted in light of what is known about the sMMO function and structure.

Active site of the hydroxylase. A set of conserved residues corresponding to the immediate area of the active site was identified in the sMMOH α subunit. The residues comprised the iron ligands, a network of hydrogen bonds, a possible proton delivery site, and sterically necessary conservations. The conserved

residues were restricted to the area “below” the active site as it is usually drawn, which is not surprising, given that the substrate is thought to bind “above” the active site, and the proteins examined have very different substrates.

Understanding protein-protein interactions in sMMO. The structural and functional effects of binding of the ancillary sMMO proteins, protein B and the reductase, to the hydroxylase are important for understanding the mechanism of methane oxidation. Determining how and where the reductase binds is crucial to identifying the electron transfer pathway from the [2Fe-2S] site to the diiron active site. Characterizing the effects of protein B is also critical. The hydroxylation reaction does not occur without protein B, yet at high levels, protein B inhibits the reaction. The binding of protein B must have a major effect on the active site of the enzyme, without knowledge of which, an understanding of the sMMO systems cannot be complete.

A possible protein B binding site was identified on the surface of the hydroxylase canyon region. It is located just above the active site and could have a direct effect on the four helix bundle that surrounds the diiron center. Part of this binding site might include the residues A224, G228 and D229, which are located at the bend where helix E and helix F meet, as depicted in Figure 1-14. Crystallography reveals residues E209 and E243 to be the most mobile of all the iron ligands, and they are located on helices E and F, respectively. Protein B could affect the coordination of the active site irons through use of the E/F helix turn as a “handle.” Additionally, a set of residues that may be part of a binding site at or near the surface of the canyon was identified as depicted in Figure 1-16.

A set of aromatic residues where the electron transfer pathway might begin was also identified at the top of the hydroxylase molecule. The location of these residues is consistent with a model placing the reductase binding site on the top of the α subunit. Another possible binding site for the reductase was

located on the surface of the β subunit. Two possible models of the binding sites of the ancillary sMMO proteins are shown in Figure 1-19.

The sequence alignments described in this chapter provide information about functionally essential areas of the sMMO proteins. These areas are obvious targets for mutagenesis. The proposed binding sites for the reductase and coupling proteins are particularly attractive in this regard. Initial studies in this vein might involve mutating individual residues in the proposed binding sites and measuring the effects on protein-protein interactions, electron transfer or hydroxylase activity.

Many of the areas that are well conserved in the sMMO family have obscure functionality. Perhaps as more is learned about the structure and function of these interesting and useful protein systems, the functions of these residues will be understood.

References:

1. Lippard, S. J., and Berg, J. M. (1994) *Principles of Bioinorganic Chemistry*, 1st ed., University Science Books, Mill Valley, California.
2. Feig, A. L., and Lippard, S. J. (1994) *Chem. Rev.* 94, 759-805.
3. Wallar, B. J., and Lipscomb, J. D. (1996) *Chem. Rev.* 96, 2625-2657.
4. Kurtz, D. M. (1990) *Chem. Rev.* 90, 585-606.
5. Vincent, J. B., Olivier-Lilley, G. L., and Averill, B. A. (1990) *Chem. Rev.* 90, 1447-1467.
6. Valentine, A. M., and Lippard, S. J. (1997) *J. Chem. Soc., Dalton Trans.*, 3925-3931.
7. Liu, K. E., and Lippard, S. J. (1995) in *Adv. Inorg. Chem.* (Sykes, A. G., Ed.) pp 263-289, Academic Press, San Diego.
8. Lipscomb, J. D. (1994) *Annu. Rev. Microbiol.* 48, 371-399.
9. Rosenzweig, A. C., Frederick, C. A., Lippard, S. J., and Nordlund, P. (1993) *Nature* 366, 537-543.
10. Rosenzweig, A. C., Nordlund, P., Takahara, P. M., Frederick, C. A., and Lippard, S. J. (1995) *Chemistry & Biology* 2, 409-418.
11. Rosenzweig, A. C., Frederick, C. A., and Lippard, S. J. (1996) in *Microbial Growth on C1 Compounds* (Lidstrom, M. E., and Tabita, F. R., Eds.) pp 141-149, Kluwer Academic Publishers, Dordrecht.
12. Cardy, D. L. N., Laidler, V., Salmond, G. P. C., and Murrell, J. C. (1991) *Molec. Microbiol.* 5, 335-342.
13. Stainthorpe, A. C., Murrell, J. C., Salmond, G. P. C., Dalton, H., and Lees, V. (1989) *Arch. Microbiol.* 152, 154-159.

14. Stainthorpe, A. C., Lees, V., Salmond, G. P. C., Dalton, H., and Murrell, J. C. (1990) *Gene* 91, 27-34.
15. McDonald, I. R., Uchiyama, H., Kambe, S., Yagi, O., and Murrell, J. C. (1997) *App. Env. Microbiol.* 63, 1898-1904.
16. Green, J., and Dalton, H. (1985) *J. Biol. Chem.* 260, 15795-15801.
17. Gassner, G., and Lippard, S. J. (1998) *Manuscript in Preparation.*
18. Buzy, A., Millar, A. L., Legros, V., Wilkins, P. C., Dalton, H., and Jennings, K. R. (1998) *Eur. J. Biochem.* 254, 602-609.
19. Elango, N., Radhakrishnan, R., Froland, W., Wallar, B. J., Earhart, C. A., Lipscomb, J. D., and Ohlendorf, D. H. (1997) *Protein Science* 6, 556-568.
20. Johnson, G. R., and Olsen, R. H. (1995) *App. Env. Microbiol.* 61, 3336-3346.
21. Byrne, A. M., Kukor, J. J., and Olsen, R. H. (1995) *J. Bact.* 178, 65-70.
22. Olsen, R. H., Kukor, J. J., and Kaphammer, B. (1994) *J. Bact.* 176, 3749-3756.
23. Yen, K.-M., Karl, M. R., Blatt, L. M., Simon, M. J., Winter, R. B., Fausset, P. R., Lu, H. S., Harcourt, A. A., and Chen, K. K. (1991) *J. Bact.* 173, 5315-5327.
24. Yen, K.-M., and Karl, M. R. (1992) *J. Bact.* 174, 7253-7261.
25. Pikus, J. D., Studts, J. M., Achim, C., Kauffmann, K. E., Münck, E., Steffan, R. J., McClay, K., and Fox, B. G. (1996) *Biochemistry* 35, 9106-9119.
26. Whited, G. M., and Gibson, D. T. (1991) *J. Bact.* 173, 3010-3016.
27. Nordlund, I., Powlowski, J., and Shingler, V. (1990) *J. Bact.* 172, 6826-6833.
28. Nordlund, I., Powlowski, J., Hagström, Å., and Shingler, V. (1993) *J. Gen. Microbiol.* 139, 2695-2703.
29. Shingler, V., Franklin, F. C. H., Tsuda, M., Holroyd, D., and Bagdasarian, M. (1989) *Journal of General Microbiology* 135, 1083-1092.
30. Powlowski, J., and Shingler, V. (1990) *J. Bact.*, 6834-6840.
31. Gallagher, S. C., Cammack, R., and Dalton, H. (1997) *Eur. J. Biochem.* 247, 635-641.

32. Saeki, H., and Furuhashi, K. (1994) *J. Ferment. Bioeng.* 78, 399-406.
33. Miura, A., and Dalton, H. (1995) *Biosci. Biotech. Biochem.* 263, 853-859.
34. Small, F. J., and Ensign, S. A. (1997) *J. Biol. Chem.* 272, 24913-24920.
35. Nordlund, P., Dalton, H., and Eklund, H. (1992) *FEBS Lett.* 307, 257-262.
36. Fox, B. G., Shanklin, J., Ai, J., Loehr, T. M., and Sanders-Loehr, J. (1994) *Biochemistry* 33, 12776-12786.
37. Gallagher, S. C., George, A., and Dalton, H. (1998) *Eur. J. Biochem.* 254, 480-489.
38. Karplus, P. A., Daniels, M. J., and Herriot, J. R. (1991) *Science* 251, 60-66.
39. Correll, C. C., Batie, C. J., Ballou, D. P., and Ludwig, M. L. (1992) *Science* 258, 1604-1610.
40. Andrews, S. C., Shipley, D., Keen, J. N., Findlay, J. B. C., Harrison, P. M., and Guest, J. R. (1992) *FEBS Letters* 302, 247-252.
41. Neidle, E. L., Hartnett, C., Ornston, L. N., Bairoch, A., Rekik, M., and Harayama, S. (1991) *J. Bact.* 173, 5385-5395.
42. Qian, H., Edlund, U., Powlowski, J., Shingler, V., and Sethson, I. (1997) *Biochemistry* 36, 495-504.
43. Genetics Computer Group (1991) , The Wisconsin Package, Madison, Wisc.
44. Clark, S. (1991) Maligned.
45. Hofmann, K., and Baron, M. D. (1998) BoxShade , Pirbright, Surrey UK.
46. Molecular Simulations, Inc. (1997) Quanta97 , Molecular Simulations, Inc., San Diego, CA.
47. Kraulis, P. J. (1991) *J. Appl. Cryst.* 24, 946-950.
48. Zhou, N., Jenkins, A., Chion, C. C. K., and Leak, D. J. (1998) *Submitted for Publication.*
49. Wu, W., Rosenzweig, A., and Lippard, S. J. (1989) *Unpublished Results.*

50. Brandstetter, H., and Lippard, S. J. (1997) *Unpublished Results*.
51. Coufal, D., Wolf, S., Biemann, K., and Lippard, S. J. (1998) *Unpublished Results*.
52. Blazyk, J., and Lippard, S. J. (1998) *Unpublished Results*.
53. Nordlund, P., Sjöberg, B.-M., and Eklund, H. (1990) *Nature* 345, 593-598.
54. Nordlund, P., Åberg, A., Uhlin, U., and Eklund, H. (1993) *Biochem. Soc. Trans.* 21, 735-738.
55. Nordlund, P., and Eklund, H. (1993) *J. Mol. Biol.* 232, 123-164.
56. Kauppi, B., Nielsen, B. B., Ramaswamy, S., Larsen, I. K., Thelander, M., Thelander, L., and Eklund, H. (1996) *J. Mol. Biol.* 262, 706-720.
57. Regnström, K., Åberg, A., Ormö, M., Sahlin, M., and Sjöberg, B.-M. (1994) *J. Biol. Chem.* 269, 6355-6361.
58. Rosenzweig, A. C., Brandstetter, H., Whittington, D. A., Nordlund, P., Lippard, S. J., and Frederick, C. A. (1997) *Proteins* 29, 141-152.
59. Fox, B. G., Liu, Y., Dege, J. E., and Lipscomb, J. D. (1991) *J. Biol. Chem.* 266, 540-550.

Table 1-1. sMMO Hydroxylase Sequencing Primer Names and Binding Locations.

Primer Name	Direction	BaseLocation
D12344	sense	mmoX 236-255
D12345	antisense	mmoX 1304-1323
D12346	antisense	mmoX 1126-1145
D12347	antisense	mmoX 1018-1037
D12348	antisense	mmoX 552-571
D12351	sense	mmoX 722-741
D123453	sense	mmoX 497-516
D12354	antisense	mmoX 737-756
D12355	sense	mmoX 1014-1033
seq01	sense	mmoY 351-370
seq02	sense	mmoY 701-720
seq03	antisense	mmoY 781-800
seq04	antisense	mmoY 431-450
seq05	sense	mmoZ 251-270
seq06	antisense	mmoZ 251-270
seq07	antisense	mmoX 236-255
seq08	sense	mmoX 1304-1323
seq09	sense	mmoX 1505-1524
seq10	antisense	mmoY 41-60
seq11	antisense	mmoY 190-209
seq12	sense	mmoY 421-480
seq14	sense	mmoY 1116-1135
seq15	antisense	mmoZ 26-45
seq16	sense	mmoZ 461-480
seq19	sense	mmoZ 434-453
seq20	antisense	mmoY 912-931

Table 1-1

Table 1-2. Electrospray-Ionization Mass Spectrometric Results. Taken from Buzy et al. (18). Only selected results that exhibited differences from the expected, published sequence are shown. The amino-terminal methionine was cleaved off in all cases. All results can be explained by the revised sequence as described herein. The α' refers to α subunit that is cleaved between T7 and K8, and the α'' refers to α subunit cleaved between A9 and A10. The α T3a, β T2, β CB8 and γ T4 peptides are cyanogen bromide/trypsin cleavage products; the parenthetical numbers identify the residue range that they cover. These peptides cover the areas of the sMMOH peptides that were not consistent with the published sequence.

Sample	Molecular Mass (Daltons)				
	Measured	Expected Average Mass from Published Sequence	Δ (measured - expected)	Expected Average Mass from Corrected Sequence	Δ (measured - expected)
α	60518.3 \pm 5.8	60499.42	18.88	60515.38	2.92
α'	59973.9 \pm 8.4	59954.81	19.09	59970.77	3.13
α''	59774.9 \pm 6.0	59755.56	19.34	59771.52	3.38
α T3a (77-87)	1235.2 \pm 0.3	1219.41	15.79	1235.36	-0.16
β	45001.7 \pm 2.1	44590.18	411.52	45001.73	-0.03
β T2 (141-146)	792.4 \pm 0.2	666.71	125.69	792.85	-0.45
β CB8 (337-end)	5913.7 \pm 0.3	5628.31	285.39	5913.73	-0.03
γ	19715.6 \pm 0.9	19710.52	5.08	19715.54	0.06
γ T4 (18-26)	1029.5 \pm 0.5	1024.19	5.31	1029.20	0.30

Table 1-2

Figure 1-1. *Methylococcus capsulatus* (Bath) sMMO Hydroxylase Structure. a. Structure of the *Methylococcus capsulatus* (Bath) sMMO hydroxylase (crystal form I, diferric state) (9). The α -subunits are shown in purple, the β -subunits are in aqua, and the γ -subunits are in green. The iron atoms are colored green, and one of the two protomers is partially transparent to emphasize the location of the iron center within the α subunit. The canyon is visible between the two α subunits. This Figure was prepared by using MolScript (47). b. Structure of the active site, showing all ligands, including protein residues, a hydroxide bridge, a terminal water and an exogenous acetate bridge.

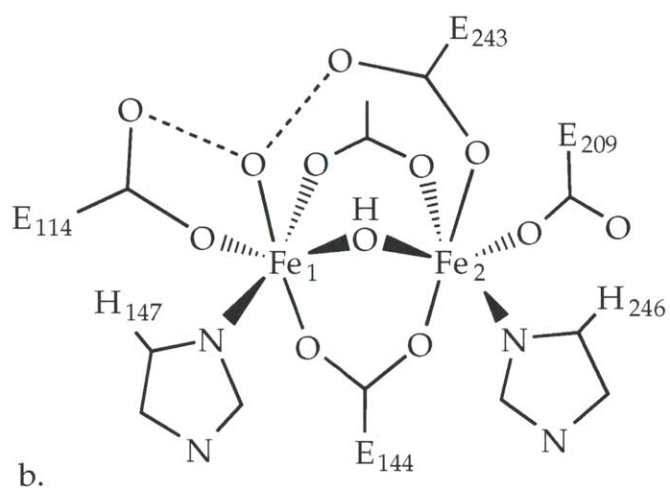
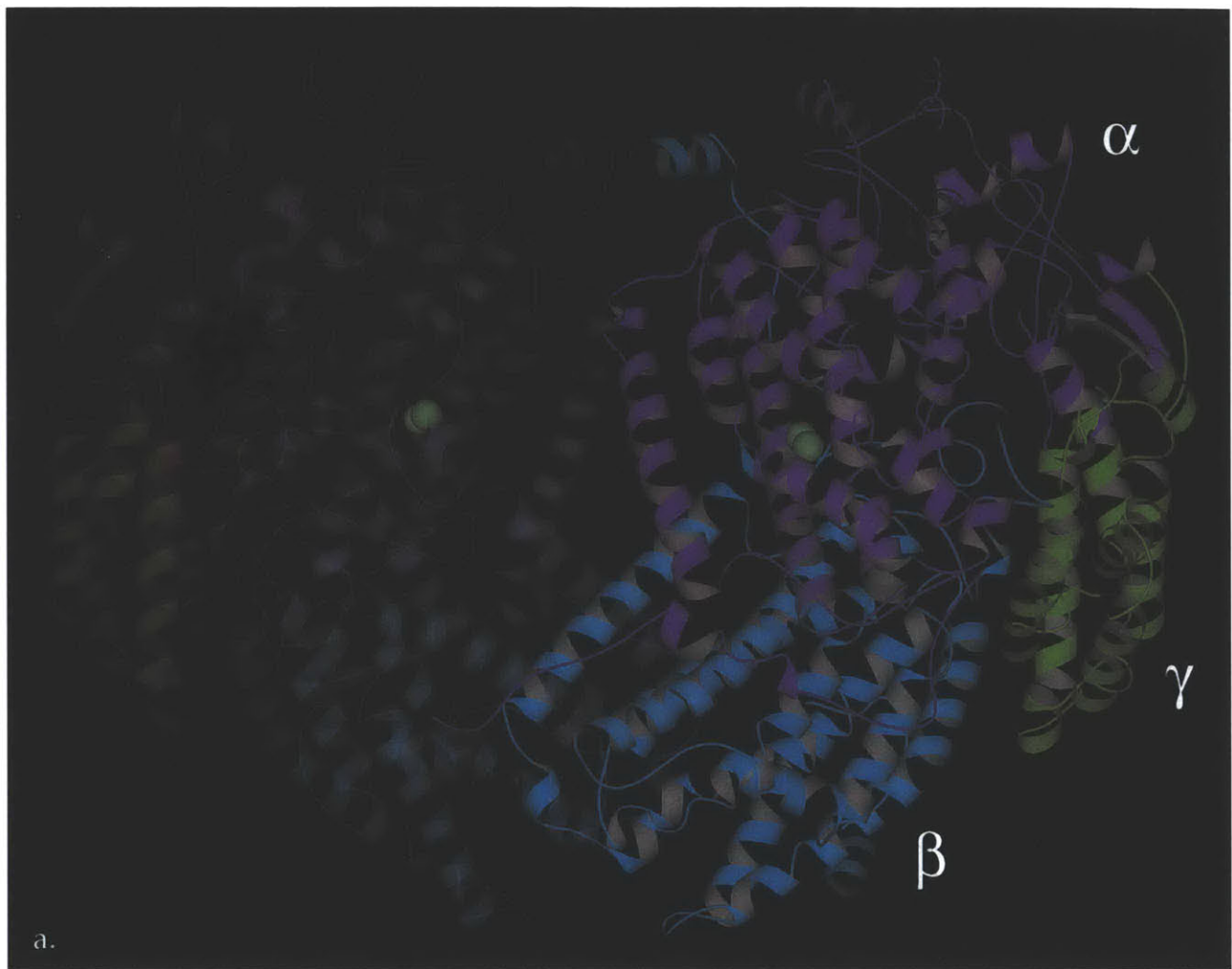
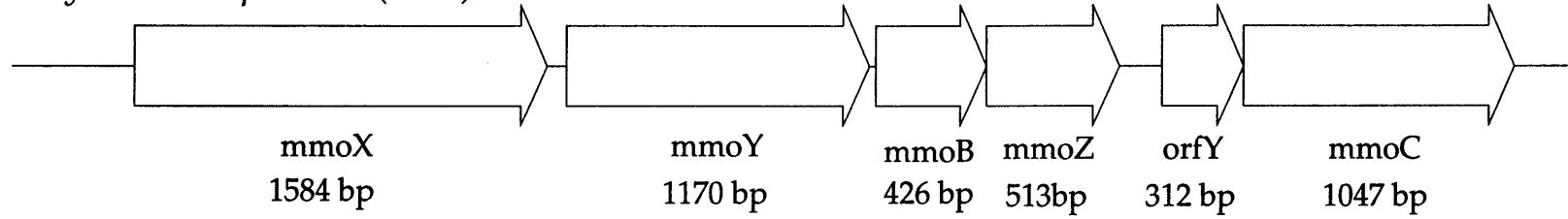


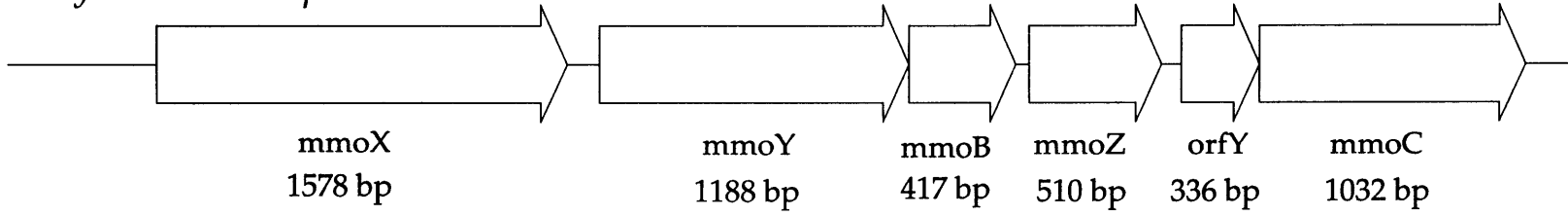
Figure 1-1

Figure 1-2. Organization of the sMMO operons from three different organisms. Gene arrangement is identical between the organisms.

Methylococcus capsulatus (Bath)



Methylosinus trichosporium OB3B



Methylocystis sp. Strain M

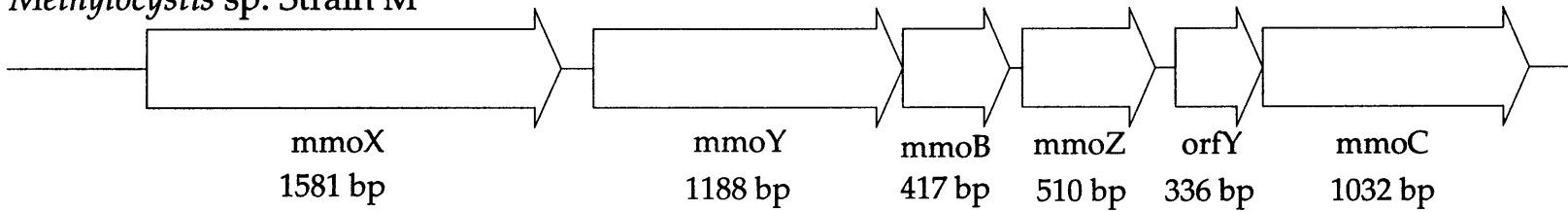
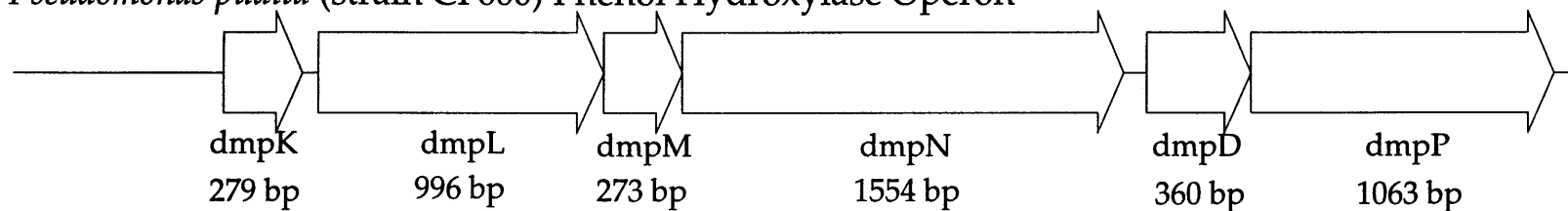


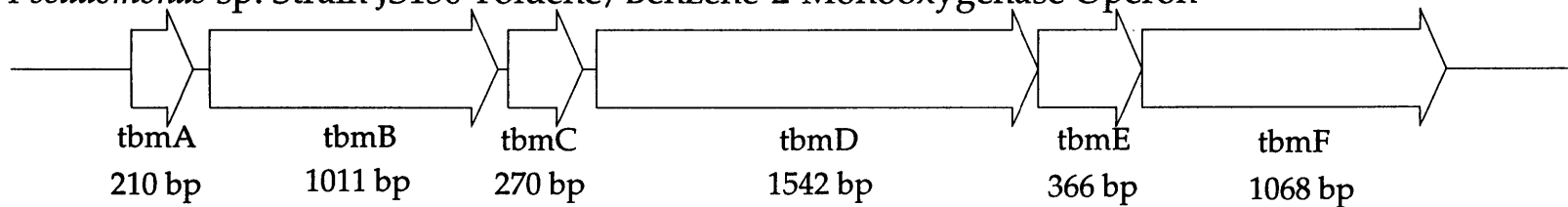
Figure 1-2

Figure 1-3. Organization of other sMMO family multicomponent monooxygenase operons. The gene arrangement is quite different from the sMMO operons and from each other. The alkene monooxygenases are not included, as neither of them are fully sequenced.

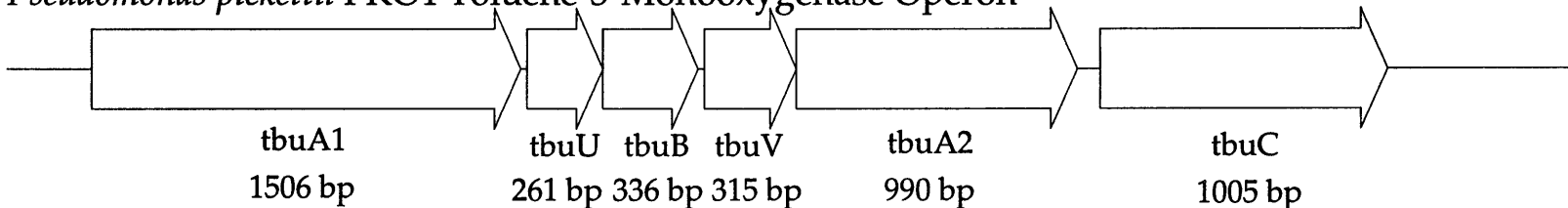
Pseudomonas putida (strain CF600) Phenol Hydroxylase Operon



Pseudomonas sp. Strain JS150 Toluene/Benzene-2-Monooxygenase Operon



Pseudomonas pickettii PKO1 Toluene-3-Monooxygenase Operon



Pseudomonas mendocina KR1 Toluene-4-Monooxygenase Operon

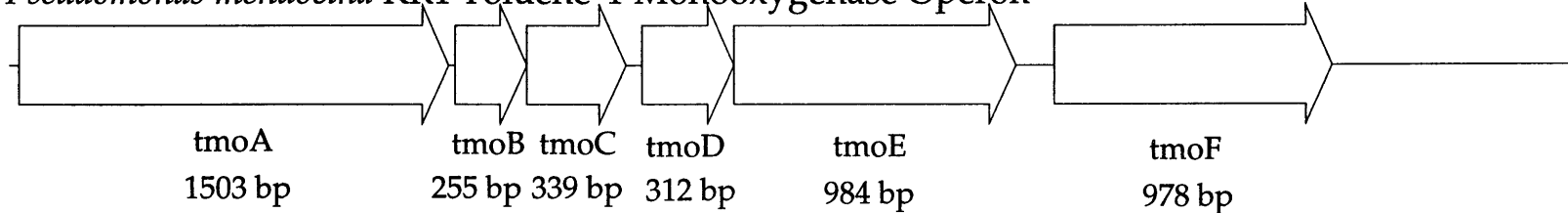


Figure 1-3

Figure 1-4. Binding locations of primers used in sequencing the *M. capsulatus* (Bath) sMMO hydroxylase genes. Primers beginning with a D were the gift of Thanos Salifoglou.

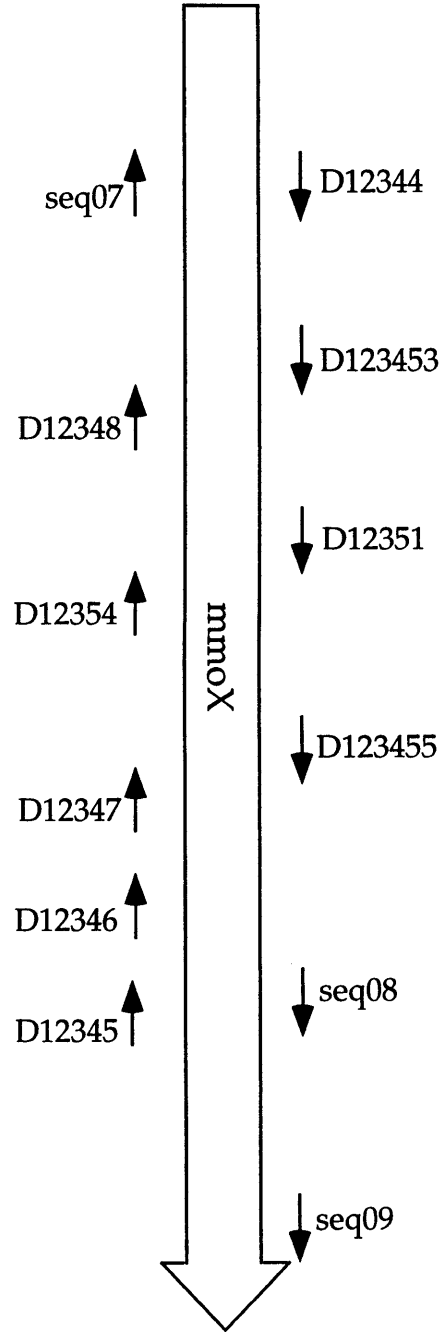
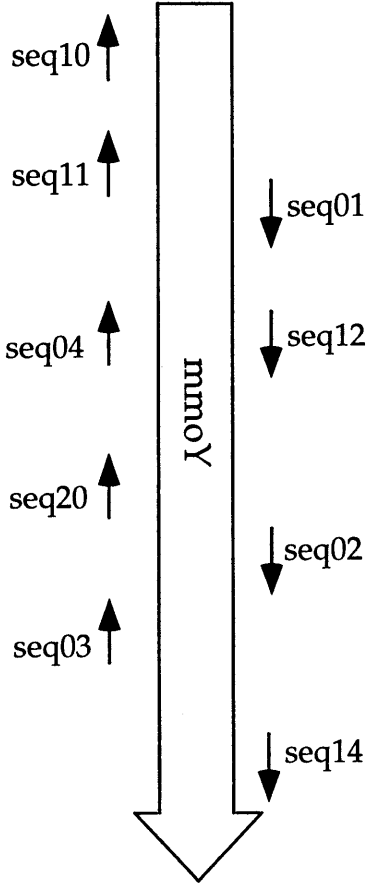
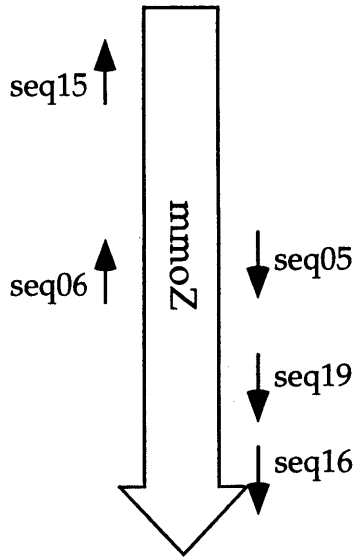


Figure 1-4

Figure 1-5. DNA sequences and deduced peptide sequences of the *M. capsulatus* (Bath) sMMO genes. The hydroxylase, protein B, and reductase genes can be found in the GenEMBL database. All errors in the original sequence as listed in Figures 1-6 and 1-7 are incorporated in this listing.

1450 1470 1490
GTGATCGCCGAACTGCACGGGCTGCGCAGTGATGGCAAGACCCTGATCGCCCAGCCGCAT
ValIleAlaGluLeuHisGlyLeuArgSerAspGlyLysThrLeuIleAlaGlnProHis
481

1510 1530 1550
GTCCGTGGCGACAAGCTGTGGACGTTGGACGATATCAAACGCCTGAACTGCGTCTTCAAG
ValArgGlyAspLysLeuTrpThrLeuAspAspIleLysArgLeuAsnCysValPheLys
501

1570
AACCCGGTGAAGGCATTCAATTGA
AsnProValLysAlaPheAsnEnd
521

M. capsulatus (Bath) *mmoY* sequence

10 30 50
ATGAGCATGTTAGGAGAAAGACGCCGCGTCTGACCGATCCGGAAATGGCGGCCGTCATT
MetSerMetLeuGlyGluArgArgArgGlyLeuThrAspProGluMetAlaAlaValIle
1

70 90 110
TTGAAGGCGCTTCTGAAGCTCCGCTGGACGGCAACAACAAGATGGGTTATTTTCGTCACC
LeuLysAlaLeuProGluAlaProLeuAspGlyAsnAsnLysMetGlyTyrPheValThr
21

130 150 170
CCCCGCTGGAAACGCTTGACGGAATATGAAGCCCTGACCGTTTATGCGCAGCCCAACGCC
ProArgTrpLysArgLeuThrGluTyrGluAlaLeuThrValTyrAlaGlnProAsnAla
41

190 210 230
GACTGGATCGCCGGCGCCTGGACTGGGGCGACTGGACCCAGAAATTCACGGCGGCCGC
AspTrpIleAlaGlyGlyLeuAspTrpGlyAspTrpThrGlnLysPheHisGlyGlyArg
61

250 270 290
CCTTCCTGGGGCAACGAGACCACGGAGCTGCGCACCGTTCGACTGGTTCAAGCACCGTGAC
ProSerTrpGlyAsnGluThrThrGluLeuArgThrValAspTrpPheLysHisArgAsp
81

310 330 350
CCGCTCCGCCGTTGGCATGCGCCGTACGTCAAGGACAAGCCGAGGAATGGCGCTACACC
ProLeuArgArgTrpHisAlaProTyrValLysAspLysAlaGluGluTrpArgTyrThr
101

370 390 410
GACCGCTTCTGCAGGGTTACTCCGCCGACGGTCAGATCCGGGCGATGAACCCGACCTGG
AspArgPheLeuGlnGlyTyrSerAlaAspGlyGlnIleArgAlaMetAsnProThrTrp
121

430 450 470
CGGGACGAGTTCATCAACCGTATTGGGGCGCCTTCTGTTC AACGAATACGGATTGTTC
ArgAspGluPheIleAsnArgTyrTrpGlyAlaPheLeuPheAsnGluTyrGlyLeuPhe
141

970 990 1010
ACCGGCAAGTGGCTGGAGCCCACGATCGCCGCTCTGCGCGACTTCATGGGGCTGTTGCG
ThrGlyLysTrpLeuGluProThrIleAlaAlaLeuArgAspPheMetGlyLeuPheAla
321

1030 1050 1070
AAGCTGCCGGCGGGCACCCTGACAAGGAAGAAATCACC GCGTCCCTGTACCGGGTGCTC
LysLeuProAlaGlyThrThrAspLysGluGluIleThrAlaSerLeuTyrArgValVal
341

1090 1110 1130
GACGACTGGATCGAGGACTACGCCAGCAGGATCGACTTCAAGGCGGACCGCGATCAGATC
AspAspTrpIleGluAspTyrAlaSerArgIleAspPheLysAlaAspArgAspGlnIle
361

1150 1170
GTTAAAGCGGTTCTGGCAGGATTGAAATAA
ValLysAlaValLeuAlaGlyLeuLysEnd
381

490

510

GTGCGGGTGGTGCATCTGCAGTCGCCGCACTGA
ValArgValValHisLeuGlnSerProHisEnd
161

M. capsulatus (Bath) orfY sequence

```

      10              30              50
      .             .             .
ATGGTCGAATCGGCATTTTCAGCCATTTTCGGGCGACGCAGACGAATGGTTCGAGGAACCA
MetValGluSerAlaPheGlnProPheSerGlyAspAlaAspGluTrpPheGluGluPro
  1

      70              90              110
      .             .             .
CGGCCCCAGGCCGGTTTCTTCCCTTCCGCGGACTGGCATCTGCTCAAACGGGACGAGACC
ArgProGlnAlaGlyPhePheProSerAlaAspTrpHisLeuLeuLysArgAspGluThr
  21

     130              150              170
      .             .             .
TACGCAGCCTATGCCAAGGATCTCGATTTTCATGTGGCGGTGGGTCATCGTCCGGGAAGAA
TyrAlaAlaTyrAlaLysAspLeuAspPheMetTrpArgTrpValIleValArgGluGlu
  41

     190              210              230
      .             .             .
AGGATCGTCCAGGAGGGTTGCTCGATCAGCCTGGAGTCGTCGATCCGCGCCGTGACGCAC
ArgIleValGlnGluGlyCysSerIleSerLeuGluSerSerIleArgAlaValThrHis
  61

     250              270              290
      .             .             .
GTACTGAATTATTTTGGTATGACCGAACAACGCGCCCCGGCAGAGGACCGGACCGGCCGA
ValLeuAsnTyrPheGlyMetThrGluGlnArgAlaProAlaGluAspArgThrGlyGly
  81

     310
      .
GTTCAACATTGA
ValGlnHisEnd
 101
```

M. capsulatus (Bath) mmoC sequence

10 30 50
ATGCAGCGAGTTCACACTATCACGGCGGTGACGGAGGATGGCGAATCGCTCCGCTTCGAA
MetGlnArgValHisThrIleThrAlaValThrGluAspGlyGluSerLeuArgPheGlu
1

70 90 110
TGCCGTTTCGGACGAGGACGTCATCACCGCCGCCCTGCGCCAGAACATCTTTCTGATGTCG
CysArgSerAspGluAspValIleThrAlaAlaLeuArgGlnAsnIlePheLeuMetSer
21

130 150 170
TCCTGCCGGGAGGGCGGCTGTGCGACCTGCAAGGCCTTGTGCAGCGAAGGGGACTACGAC
SerCysArgGluGlyGlyCysAlaThrCysLysAlaLeuCysSerGluGlyAspTyrAsp
41

190 210 230
CTCAAGGGCTGCAGCGTTCAGGCGCTGCCGCCGAAGAGGAGGAGGAAGGGTTGGTGTG
LeuLysGlyCysSerValGlnAlaLeuProProGluGluGluGluGluGlyLeuValLeu
61

250 270 290
TTGTGCCGGACCTACCCGAAGACCGACCTGGAAATCGAACTGCCCTATACCCATTGCCGC
LeuCysArgThrTyrProLysThrAspLeuGluIleGluLeuProTyrThrHisCysArg
81

310 330 350
ATCAGTTTTGGTGAGGTCGGCAGTTTCGAGGCGGAGGTCGTCCGCCCTCAACTGGGTTTCG
IleSerPheGlyGluValGlySerPheGluAlaGluValValGlyLeuAsnTrpValSer
101

370 390 410
AGCAACACCGTCCAGTTTCTTTGCAGAAGCGGCCCGACGAGTCCGGCAACCGTGGCGTG
SerAsnThrValGlnPheLeuLeuGlnLysArgProAspGluCysGlyAsnArgGlyVal
121

430 450 470
AAATTCGAACCCGGTCAGTTCATGGACCTGACCATCCCCGGCACCGATGTCTCCCGCTCC
LysPheGluProGlyGlnPheMetAspLeuThrIleProGlyThrAspValSerArgSer
141

970 990 1010
GATGCCGCCTGCGAGCTGGTACGCAGCCGCGGTATCCCCGGCGAACAGGTCTTCTTCGAA
AspAlaAlaCysGluLeuValArgSerArgGlyIleProGlyGluGlnValPhePheGlu
321

1030
AAATTCCTGCCGTCCGGGGCGGCCTGA
LysPheLeuProSerGlyAlaAlaEnd
341

Figure 1-6. Mistakes in the published hydroxylase subunit gene sequences and their corrections. Changes are shown in bold face. All mistakes were confirmed by DNA sequencing.

mmoX Correction A

251

Lituration Gene Sequence CTG CAG ~~GTA~~ GCG CTG
Lituration Protein Sequence Leu Gln Val Ala Leu
Corrected Gene Sequence CTG CAG **GAT** GCG CTG
Corrected Protein Sequence Leu Gln Asp Ala Leu

mmoY Correction B

424

434

Lituration Gene Sequence TGG CGG ~~ACG~~ AGT TCA ~~TGC~~ AAC CCG
Lituration Protein Sequence Trp Arg Thr Ser Ser Cys Asn Arg
Corrected Gene Sequence TGG CGG **GAC** GAG TTC ATC AAC CCG
Corrected Protein Sequence Trp Arg Asp Glu Phe Ile Asn Arg

mmoY Correction C

1086

1164

1170

Lituration Gene Sequence GAC GAT GGA .. 69 bp .. GAT TGA
Lituration Protein Sequence Asp Asp Gly .. 23 res .. Asp End
Corrected Gene Sequence GAC **GAC** TGG .. 69 bp .. GGA TTG AAA TAA
Corrected Protein Sequence Asp Asp Trp .. 23 res .. Gly Leu Lys End

mmoZ Correction D

63 64

Lituration Gene Sequence ATC GCG CAC ~~GTC~~ AAC ACC
Lituration Protein Sequence Ile Ala His Val Asn Thr
Corrected Gene Sequence ATC GCG CAG **CTC** AAC ACC
Corrected Protein Sequence Ile Ala Gln Leu Asn Thr

Figure 1-6

Figure 1-7. Mistakes found in the published DNA sequence for the sMMO genes *mmoB* and *mmoC*. The mistake in the *mmoB* gene was discovered by N-terminal sequencing of the protein B peptide (49) and confirmed via DNA sequencing (52). The mistake in the *mmoC* gene was discovered by DNA sequencing (52). Changes are shown in bold face.

mmoB Correction E

34

Literature Gene Sequence	GCC GGC T TTC ATG GGC
Literature Protein Sequence	Ala Gly Phe Met Gly
Actual Gene Sequence	GCC GGC A TC ATG GGC
Actual Protein Sequence	Ala Gly Ile Met Gly

mmoC Correction F

760

Literature Gene Sequence	GTG AAC C AC GAG CCG
Literature Protein Sequence	Val Trp His Glu Pro
Corrected Gene Sequence	GTG AAC A CC GAG CCG
Corrected Protein Sequence	Val Trp Thr Glu Pro

Figure 1-7

Figure 1-8. Relationships between the genes and proteins of the sMMO multicomponent monooxygenase family. The T3M and T4M systems have ferredoxins encoded in their operons, where the others do not. The gray background behind the *orfY* homologues for T2M and PH indicate that sequence alignments and homology analyses do not indicate that these proteins are related to *orfY*. They are included in the *orfY* category because they are all small open reading frames that have no similarities with any other genes in the GenEMBL database.

	<i>Methylococcus capsulatus</i> (Bath) Soluble Methane Monooxygenase	<i>Methylosinus trichosporium</i> OB3B Soluble Methane Monooxygenase	<i>Methylocystis</i> sp. strain M Soluble Methane Monooxygenase	<i>Pseudomonas putida</i> strain CF600 Phenol Hydroxylase	<i>Pseudomonas</i> sp. strain JS105 Toluene/ Benzene-2- Monooxygenase	<i>Pseudomonas pickettii</i> PKO1 Toluene-3- Monooxygenase	<i>Pseudomonas mendocina</i> KR1 Toluene-4- Monooxygenase	<i>Nocardia corallina</i> Alkene Monooxygenase	<i>Xanthobacter</i> sp. Py2 Alkene Monooxygenase
Hydroxylase α subunit <i>Gene</i> Calc. MW	sMMOH α <i>mmoX</i> 60646	sMMOH α <i>mmoX</i> 60076	sMMOH α <i>mmoX</i> 59973	P3 <i>dmpN</i> 60522	TbmD <i>tbmD</i> 60077	TbuA1 <i>tbuA1</i> 57555	TmoA <i>tmoA</i> 57982	AmoC <i>amoC</i> 57212	XamoA <i>xamoA</i> 58040
Hydroxylase β subunit <i>Gene</i> Calc. MW	sMMOH β <i>mmoY</i> 45132	sMMOH β <i>mmoY</i> 45112	sMMOH β <i>mmoY</i> 45170	P1 <i>dmpL</i> 38208	TbmB <i>tbmB</i> 37042	TbuA2 <i>tbuA2</i> 37525	TmoE <i>tmoE</i> 38386	AmoA <i>amoA</i> 38462	?
Hydroxylase γ subunit <i>Gene</i> Calc. MW	sMMOH γ <i>mmoZ</i> 19847	sMMOH γ <i>mmoZ</i> 19314	sMMOH γ <i>mmoZ</i> 19349	P4 <i>dmpO</i> 13207	TbmE <i>tbmE</i> 13001	TbuU <i>tbuU</i> 9604	TmoB <i>tmoB</i> 9588	?	?
Reductase <i>Gene</i> Calc. MW	sMMOR <i>mmoC</i> 38541	sMMOR <i>mmoC</i> 37991	sMMOR <i>mmoC</i> 37358	P5 <i>dmpP</i> 38477	TbmF <i>tbmF</i> 37990	TbuC <i>tbuC</i> 36101	TmoF <i>tmoF</i> 35983	AmoD <i>amoD</i> 37282	?
Ferredoxin <i>Gene</i> Calc. MW						TbuB <i>tbuB</i> 12254	TmoC <i>tmoC</i> 12326		
Coupling Protein <i>Gene</i> Calc. MW	sMMOB <i>mmoB</i> 15984	sMMOB <i>mmoB</i> 14883	sMMOB <i>mmoB</i> 14901	P2 <i>dmpM</i> 10491	TbmC <i>tbmC</i> 10029	TbuV <i>tbuV</i> 11703	TmoD <i>tmoD</i> 11618	AmoB <i>amoB</i> 12985	?
<i>orfY</i> Product <i>Gene</i> Calc. MW	OrfY <i>orfY</i> 11942	OrfY <i>orfY</i> 11926	OrfY <i>orfY</i> 12499	P0 <i>dmpK</i> 10586	TbmA <i>tbmA</i> 7880				

Figure 1-8

Figure 1-9. Identity statistics between the closely related proteins of the sMMO multicomponent monooxygenase family. These include the α and β subunits of the hydroxylase, protein B and the reductase. Three numbers are given in each comparison; the top is the number of identical residues, the middle is the number of differing residues, and the bottom number is the number of gap placeholders. Numbers right of the diagonal are percentages and left of the diagonal are raw numbers. Percentages do not add up to 100% due to mismatches at the ends of the peptides. Note that two randomly paired proteins would be expected to have identity percentages of 10-15%, depending upon the size of the protein.

Hydroxylase alpha subunit									
	1	2	3	4	5	6	7	8	9
1 Mtri_Halpha	526	96%	81%	34%	17%	17%	17%	18%	17%
	0	3%	18%	61%	74%	73%	74%	73%	74%
	0	0%	0%	4%	7%	9%	7%	8%	8%
2 MstM_Halpha	506	52%	82%	34%	17%	16%	17%	18%	17%
	20	0	17%	61%	75%	74%	74%	73%	74%
	0	0	0%	4%	7%	9%	7%	8%	8%
3 Mcap_Halpha	428	434	527	34%	17%	16%	17%	17%	17%
	98	92	0	61%	74%	73%	74%	74%	73%
	1	1	0	4%	7%	9%	7%	8%	8%
4 AMO_AmoC	177	178	176	501	18%	18%	16%	17%	16%
	316	315	317	0	71%	68%	72%	71%	72%
	21	21	22	0	10%	12%	10%	11%	11%
5 T2M_TbmD	94	91	93	95	513	63%	21%	23%	24%
	399	402	401	369	0	34%	73%	71%	69%
	42	42	42	55	0	2%	5%	5%	6%
6 PH_P3	91	89	91	98	325	517	20%	23%	24%
	394	396	395	358	178	0	73%	70%	69%
	50	50	50	63	12	0	5%	5%	6%
7 T3M_TbuA1	95	94	96	85	109	107	501	66%	43%
	397	398	397	377	379	377	0	32%	55%
	42	42	42	57	29	29	0	0%	0%
8 T4M_TmoA	98	97	96	89	119	120	336	500	44%
	393	394	396	372	368	363	163	0	54%
	43	43	43	58	30	30	3	0	1%
9 AMO_XamoA	95	93	96	84	127	125	219	224	497
	395	397	394	376	357	355	278	271	0
	43	43	44	58	31	31	3	6	0

Coupling Protein

	1	2	3	4	5	6	7	8
1 Mtri_B	138	96%	65%	26%	22%	22%	19%	18%
	0	3%	32%	67%	71%	68%	72%	75%
	0	0%	1%	5%	6%	8%	8%	6%
2 MspM_B	133	138	65%	26%	20%	21%	18%	17%
	5	0	32%	67%	73%	69%	73%	75%
	0	0	1%	5%	6%	8%	8%	6%
3 Mcap_B	92	92	141	22%	19%	18%	20%	20%
	46	46	0	73%	75%	73%	72%	74%
	2	2	0	4%	5%	7%	7%	5%
4 T3M_TbuV	29	29	24	104	55%	33%	25%	30%
	74	74	80	0	43%	63%	70%	66%
	6	6	5	0	0%	3%	3%	2%
5 T4M_TmoD	24	22	21	58	103	35%	27%	18%
	78	80	82	45	0	60%	68%	78%
	7	7	6	1	0	3%	3%	3%
6 T2M_TbmC	22	21	18	31	33	89	48%	23%
	66	67	71	58	56	0	51%	75%
	8	8	7	3	3	0	0%	1%
7 PH_P2	19	18	20	24	26	43	90	21%
	70	71	70	66	64	46	0	76%
	8	8	7	3	3	0	0	1%
8 AMO_AmoB	23	22	25	32	19	21	20	117
	93	94	92	70	82	68	70	0
	8	8	7	3	4	1	1	0

Hydroxylase beta subunit

	1	2	3	4	5	6	7	8
1 Mtri_Hbeta	395	94%	58%	25%	15%	13%	15%	17%
	0	5%	39%	65%	78%	81%	79%	75%
	0	0%	1%	9%	5%	5%	4%	7%
2 MspM_Hbeta	372	395	60%	25%	16%	13%	15%	17%
	23	0	38%	65%	77%	80%	79%	75%
	0	0	1%	9%	5%	5%	4%	7%
3 Mcap_Hbeta	232	237	389	25%	15%	11%	12%	13%
	157	152	0	66%	78%	81%	81%	78%
	6	6	0	8%	6%	6%	5%	7%
4 AMO_AmoA	95	97	94	343	18%	19%	14%	16%
	248	246	249	0	72%	71%	75%	70%
	34	34	32	0	9%	8%	10%	12%
5 T3M_TbuA2	55	57	53	64	329	56%	18%	19%
	270	268	270	245	0	42%	75%	74%
	19	19	21	31	0	0%	5%	5%
6 T4M_TmoE	45	46	41	65	186	327	18%	18%
	278	277	280	243	140	0	75%	76%
	20	20	22	30	2	0	5%	5%
7 T2M_TbmB	54	55	45	49	63	62	336	42%
	278	277	285	262	258	257	0	53%
	17	17	19	37	19	20	0	3%
8 PH_P1	60	63	47	59	67	61	144	331
	267	264	278	246	250	255	182	0
	25	25	27	44	19	18	13	0

Reductase

	1	2	3	4	5	6	7	8
1 Mtri_R	340	71%	41%	20%	18%	22%	22%	21%
	0	23%	51%	67%	68%	66%	65%	67%
	0	5%	6%	11%	13%	10%	11%	10%
2 MspM_R	250	343	50%	24%	21%	26%	25%	26%
	81	0	47%	66%	67%	64%	65%	64%
	21	0	2%	9%	10%	8%	8%	8%
3 Mcap_R	148	174	348	22%	25%	23%	25%	28%
	182	166	0	69%	64%	69%	65%	63%
	24	7	0	8%	9%	7%	8%	7%
4 T3M_TbuC	74	87	80	334	37%	29%	28%	30%
	242	234	243	0	59%	68%	68%	65%
	40	33	29	0	2%	2%	3%	4%
5 T4M_TmoF	64	77	89	125	326	27%	28%	29%
	243	236	226	199	0	67%	66%	63%
	47	38	34	9	0	4%	5%	6%
6 T2M_TbmF	80	96	83	99	94	355	55%	31%
	241	231	248	232	231	0	42%	64%
	39	30	26	10	15	0	1%	3%
7 PH_P2	82	92	92	96	98	198	353	32%
	236	232	235	232	224	153	0	63%
	41	32	30	12	17	6	0	4%
8 AMO_AmoD	77	94	101	103	102	110	114	342
	241	230	226	222	218	228	221	0
	39	30	28	16	21	13	15	0

Figure 1-9

Figure 1-10. Sequence alignments of the peptides corresponding to the α subunit of the hydroxylase. Residues conserved across all peptides are shown in reverse. The top number in each bar is the consensus numbering, the bottom number is the *M. capsulatus* (Bath) residue number. Residues belonging to helices in domain 1 of the hydroxylase are marked.


```

1
Mtri_Halpha .....MAI SLATKAATDA LKVNRAVGV EPQEVHKWLQ SFNWDFK..E
MstM_Halpha .....MAI SLATKAATDA LKVNRAVGV EPQEVHKWLQ SFNWDFK..D
Mcap_Halpha .....MAL STATKAATDA LAANRAPTSV NAQEVHRWLQ SFNWDFK..N
AMO_AmoC .....MAS NPTQLHEKSK SYDWDFTSVE
T2M_TbmD MDTRVAKKKL GLKERYAAMT RGLGWETTYQ PMDKVFP..Y DTYEGIK.IH
PH_P3 MATH.NKKRL NLKDKYRYLT RDLAWETTYQ KKEDVFP..L EHFEGIK.IT
T3M_TbuA1 .....MAL LERAAWYDIA RTTNWTPSYV TESELPDIM TGAQGV.ME
T4M_TmoA .....MAM HPRKDWYELT RATNWTSPSYV TEEQLFPERM SGHMGIP.LE
AMO_XamoA .....MAL LNRDDWYDIA RDVDWTLISV DRAVAFPEEW KGEKDIC.GT
Mcap #

```

```

51
Mtri_Halpha NRTKYPTKYH MANETKEQFK VIAKEARME AANDERQFGT LLDGLTRLGA
MstM_Halpha NRTKYATKYH MANQTKEQFK VIAKEARME AANDERQFGT LLDGLTRLGA
Mcap_Halpha NRTKYATKYK MANETKEQFK LIAKEARME AVANDERQFGS LQDALTRLNA
AMO_AmoC RRPKFETKYK MPKKGKDPFR VLIRDYMKME AEKDDRTHG. FLDGAVRTRE
T2M_TbmD DWDKWQ.... .....DPFR LTMDAYWKYQ GEKPKLYAV IEAFAQNNQ
PH_P3 DWDKWE.... .....DPFR LTMDTYWKYQ AEKPKLYAI FDAFAQNNGH
T3M_TbuA1 TWETYD.... .....EPYK TSYPEYVSIQ REKDAGAYSV KAALERSRMF
T4M_TmoA KWESYD.... .....EPYK TSYPEYVSIQ REKDAGAYSV KAALERAKIY
AMO_XamoA AWDDWD.... .....EPFR VSFREYVMVQ RDEASVGAI REAMVRKAY
Mcap #
Mcap Helix [ -----HELIX A-----]

```

```

101
Mtri_Halpha GNKVHPRWGE TMKVISNFLE VGEYNAIAAS AMLWDSATAA EQKNGYLAQV
MstM_Halpha GNKVHPRWGE TMKVISNFLE VGEYNAIAAS AMLWDSATAA EQKNGYLAQV
Mcap_Halpha GVRVHPKWNE TMKVVSNFLE VGEYNAIAAT GMLWDSAQAA EQKNGYLAQV
AMO_AmoC ATRIEPRFAE AMKIMVPQLT NAEYQAVAGC GMIISAVENQ ELRQGYAAQM
T2M_TbmD LGISDARYVN ALKLFIQGV TPLEYNAHRGF AHVGRQFTGE GARVAAQMOS
PH_P3 QNISDARYVN ALKLFLTAVS PLEYOAFQGF SRVGRQFSGA GARVACQMQA
T3M_TbuA1 ED.ADPGWLS ILKAHYGAIA LGEYAAAMSAE ARMARFGRAP GMRNMATFGM
T4M_TmoA EN.SDPGWIS TLKSHYGAIA VGEYAAAVTGE GRMARFSKAP GNRNMATFGM
AMO_XamoA EK.LDDGHKA TSHLHMGTIT MVEHMAVTMQ SRFVRFAPSA RWRSLGAFGM
Mcap #
Mcap Helix [ -----HELIX B-----] [ -----]

```

```

151
Mtri_Halpha LDEIRHTHQC AFINHYYSKH YHDPAGHND RRTAIGPLW KGMKRVFADG
MstM_Halpha LDEIRHTHQC AFINHYYSKH YHDPAGHND RRTAIGPLW KGMKRVFADG
Mcap_Halpha LDEIRHTHQC AYVNYFAKN QDPAGHND RRTTIGPLW KGMKRVFSDG
AMO_AmoC LDEVVHAQLE MTLRNYAKH WCDPSGFDIG QRG....LY QHPAGLVSIG
T2M_TbmD IDELRHYQTE T...HAISHY NKYFNGMHSP NHWFDRVWYL SVPKSFEDA
PH_P3 IDELRHVQTO V...HAMSHY NKHFDGLHDF AHMYDRVWYL SVPKSYMDDA
T3M_TbuA1 LDENRHGQLQ LYFPDYCAK DRQFDWAHKA YHTNEWG..A IAARSTFDDL
T4M_TmoA MDELRHGQLQ LFFPHEYCKK DRQFDWAWRA YHSNEWA..A IAAKHFFDDI
AMO_XamoA LDETRHTQLD LRFSDLLND SPSFDWSQRA FHTDEWA..V LATRNLFDDI
Mcap #
Mcap Helix 143 147 HELIX C-----] [ ---HELIX D-

```

Figure 1-10

```

201                                     250
Mtri_Halpha    ....FISRDA VECSVNLQLV GACFNPLI VAVTEWASAN GDEITPTVFL
MstM_Halpha    ....FISGDA VECSVNLQLV GACFNPLI VAVTEWASAN GDEITPTVFL
Mcap_Halpha    ....FISGDA VECSLNLQLV GACFNPLI VAVTEWASAN GDEITPTVFL
AMO_AmoC       EFQHFNTGDP LDVIIDLNIV AETAFNILL VATPQVAVAN GDNAMASVFL
T2M_TbmD       ....CTA.GP FEFLTAVSFS FEYVLTNLLF VPFMSGAPHN GDMSTVTFGF
PH_P3          ....RTA.GP FEFLTAVSFS FEYVLTNLLF VPFMSGAYN GDMATVTFGF
T3M_TbuA1     ....FMSRSA IDIAIMLTFA FETGFNMQF LGLAADAAEA GDFTFASLIS
T4M_TmoA      ....ITGRDA ISVAIMLTFS FETGFNMQF LGLAADAAEA GDYTFANLIS
AMO_XamoA     ....MLNADC VEAALATSLT LHGFNIQF VALASDAMEA GDNVNSNLLS
Mcap #        209      214      224      229
Mcap Helix    -----] [ -----HELIX E-----] [ ----

```

```

251                                     300
Mtri_Halpha    SVETDEL RHM ANGYQTV.VS IANDPASAKF LNTDLNNAFW TQQKYFTPVL
MstM_Halpha    SVETDEL RHM ANGYQTV.VS IANDPAAAKY LNTDLNNAFW TQQKYFTPAL
Mcap_Halpha    SIETDEL RHM ANGYQTV.VS IANDPASAKY LNTDLNNAFW TQQKYFTPVL
AMO_AmoC       SIQSDEARHM ANGYGSV.MA LLENEDNLPL LNQSLDRHFW RAHKALDNAV
T2M_TbmD       SAQSDESRHM TLGIECIKFM LEQDPDNVPI VQRWTDKFWF RGYRLLTIV.
PH_P3          SAQSDEARHM TLGLEVIKFM LEQHEDNVPI IQRWIDKFWF RGYRLTLI.
T3M_TbuA1     SIQTDESRHA QIGGPALQIL IASGRKEQA. .QKLVDAIA RAWRLFSLLT
T4M_TmoA      SIQTDESRHA QSGPALQLL IENGKREEA. .QKKVDMAIW RAWRLFVAVLT
AMO_XamoA     SIQTDEARHA QLSFPTLDVM MKHDPK.RA. .QQILDVAFW RSYRIFQAVT
Mcap #        238 242 246 250
Mcap Helix    HELIX F-----] [ -----HELIX G

```

```

301                                     350
Mtri_Halpha    GYLFEYGSKF ..KVEPWVKT WNRWVSEDWG GIWIGRLGKY GVESPRSLRD
MstM_Halpha    GYLFEYGSKF ..KVEPWVKT WNRWVYEDWG GIWIGRLGKY GVESPRVLRD
Mcap_Halpha    GMLFEYGSKF ..KVEPWVKT WNRWVYEDWG GIWIGRLGKY GVESPRSLKD
AMO_AmoC       GWCSEYGARK ..RPWSYKAQ WEEWVDDFV GGYIDRISEF GVQAPACLGA
T2M_TbmD       AMMQDYM..L PKRVMSWKEA WE.MYAEENG GALFKDLARY GIREPAGWKD
PH_P3          GMMMDYM..L PNKVMWSEA WG.VYFEQAG GALFKDLERY GIRPEKYVEQ
T3M_TbuA1     GTSMDYATPL HHRKESFKE. ...FMTEWIV GQFERTLIDL GLDLFPWYWDQ
T4M_TmoA      GPVMDYITPL EDRSQSFKE. ...FMYEWII GQFERSLIDL GLDKFPWYWDL
AMO_XamoA     GVSMDYITPV AKRQMSFKE. ...FMLEWIV KHHERIRDY GLQKFPWYWDT
Mcap #        292                                     321 325 329
Mcap Helix    -----] [ -----HELIX H-----]

```

```

351                                     400
Mtri_Halpha    AKRDAYWAH DLALAAYAMW PLAFARLALP .DEEDQAMFE ANYPG.WADH
MstM_Halpha    AKTDAYWAH DLALAAYALW PLAFARLALP .DEEDQEMFE ANYPG.WADH
Mcap_Halpha    AKQDAYWAH DLYLLAYALW PTGFFRLALP .DQEEMEMFE ANYPG.WYDH
AMO_AmoC       AADEVKWSH TLGQVLSAVW PLNFWRSDAM .GPADFEMFE NHYPG.WSAA
T2M_TbmD       ACEGKDHIS QAWATFYNYG RGRR.STRGS .EREEMQALS EKYPESFDTL
PH_P3          TTIGKEHIT QVWGALYQYS KATSFHTWIP .GDEELNALS EKYPDTFDKY
T3M_TbuA1     MINEFDYQH AYQMGIFWFR PTIWWNPAAG ITPDCRDLE EKYPG.WNDT
T4M_TmoA      FLKDIDELH SYHMGVLDWR TTAWWNPAAG VTPEERDLE EKYPG.WNKR
AMO_XamoA     FEKTLDHGH ALHIGTWFWR PTLFWDPNGG VSREERRLN QKYPN.WEES
Mcap #        344                                     371 377

```

Figure 1-10

	401				450
Mtri_Halpa	YGKIFNEWKK	LGIEDPKSGF	IPYQWLLANG	HDVYIDRVSQ	VVFI.PSLAK
MstM_Halpa	YGKIYNEWKK	LGIEDPKSGF	IPYAWLLENG	HDVYIDRVSQ	VVFI.PSLAK
Mcap_Halpa	YGKIYEEWRA	RGCEDPSSGF	IPLMWFIEEN	HPIYIDRVSQ	VVFC.PSLAK
AMO_AmoC	YQGYWEGYKA	LA..DPAGGR	IMLQELPGLP	P...MCQVCQ	VPCVMPRLDM
T2M_TbmD	YRPAFEFWAR	R..AEEGRRF	YN.....K	TLPMLCTTCQ	VPMFFTEPGD
PH_P3	YRPRFEFWRE	Q..QAKGERF	YN.....D	TLPHLQVCQ	LVVIFTEPDD
T3M_TbuA1	FGKAWDVIID	NLLAGKPELT	VP.....E	TLPIVCNMSQ	LVIC.AVPGN
T4M_TmoA	WGRCWDVITE	NVLNDRMDLV	SP.....E	TLPSVCNMSQ	LVLV.GVPGD
AMO_XamoA	WGLVWDEIIS	NINAGNIEKT	LP.....E	TLPMLCNVTN	LVII..GSHWD
Mcap #					424

	451				500
Mtri_Halpa	GTG.SLRVHE	FNKKHSLTD	DWGERQWLIE	PERYEC.H.NV	FEQYEGRELS
MstM_Halpa	GSG.SLRVHE	FNKKHSLTD	DWGERMWLSE	PERYEC.H.NL	FEQYEGRELS
Mcap_Halpa	GAS.TLRVHE	YNGOMHTFSD	QWGERMWLAE	PERYECQ.NI	FEQYEGRELS
AMO_AmoC	NAA...RIIE	FEGOKIALCS	EPCQRIFTNW	PEAYRHRKQY	WARYHGWDLA
T2M_TbmD	ATKIAIRESD	YFNKYHFCS	DHCKHIFDDE	PEKYVQSWLP	VHQIYQ...G
PH_P3	PTKLSLRSLV	HEGERYQFCS	DGCCDIFKNE	PVKYIQAWLP	VHQIYQ...G
T3M_TbuA1	GWIVKDYPLD	YKERTYHFNS	EIDRWVFQQD	PLRYRDHLTL	VDRFLA...G
T4M_TmoA	DWNIEVFSLE	HNRLYHFSG	EVDRWVFQQD	PVQYQNHMNI	VDRFLA...G
AMO_XamoA	RFHLKPEQLV	YKERLYTFDS	DVSKWIFELD	PERYAGHTNV	VDRFIG...G
Mcap #		443	461	464	

	501				550
Mtri_Halpa	EVIAEGHGVR	SDKTLIAQP	HTRGDNLWTL	EDIKRAGCVF	PDPLAKF*..
MstM_Halpa	EVIAEGHGVR	SDKTLIAQP	HVRGDNLWTL	EDIKRAGCVF	PDPLAKF*..
Mcap_Halpa	EVIAELHGLR	SDKTLIAQP	HVRGDKLWTL	DDIKRLNCVF	KNPVKAFN*..
AMO_AmoC	DVIVDLGYIR	PDEKTLIGQP	LLEMERLWTI	DDIRALQYEV	KDPLQEA*..
T2M_TbmD	HCFPEGTDPT	AEGFDPLMAV	LKYYEMNIGR	DNFDFEGSED	QKNFAAWTGE
PH_P3	NC.....	.EGGDVETVV	QKYYHIKSGV	DNLEYLGSPE	HQRWLALKGQ
T3M_TbuA1	QIQP...PN	LMGALQYMNL	AP.GECGDDA	HHYAWVEAYR	NQRYQKKA*
T4M_TmoA	QIQP...MT	LEGALKYMGF	QSIEEMGKDA	HDFAWADKCK	PAM..KKS*
AMO_XamoA	QIQP...MT	IEVNLNMGL	TP.EVMGKDV	FNYRWAGDYA	ENRIAAE*..
Mcap #		492			

	551	566
Mtri_Halpa
MstM_Halpa
Mcap_Halpa
AMO_AmoC
T2M_TbmD	TA*.....
PH_P3	TPPTAAPADK	SLGAA*
T3M_TbuA1
T4M_TmoA
AMO_XamoA
Mcap #		

Figure 1-10

Figure 1-11. Sequence alignments of the peptides corresponding to the β subunit of the hydroxylase. Residues conserved across all peptides are shown in reverse. The top number in each bar is the consensus numbering, the bottom number is the *M. capsulatus* (Bath) residue number.

	251				300
Mtri_Hbeta	WAGHAVYDAT	FGQFARREFF	QRLATVYGD	LTPFFTAQS	TYFQTTTGAI
MspM_Hbeta	WAGHAVYDAT	FGQFARREFF	QRLATVYGD	LTPFFTAQS	TYFQTTTGAI
Mcap_Hbeta	FSVHAVYDAL	FGQFVRREFF	QRLAPRFGDN	LTPFFINQAQ	TYFQIAKQGV
AMO_AmoA	VAGTLVFEPL	VGHLAKAELE	SRRAPMFGDG	TTPAVLASAL	LDSGRHLESV
T3M_TbuA2	VALSLVVRPA	VEEAVLRSLG	EAAR.HNGDT	LLGLLTDAQ	ADAQRHRRWA
T4M_TmoE	VSLNLVVKPM	IVESIFKPLQ	QQAW.ENNDT	LLPLLIDSQ	KDAERHSRWS
T2M_TbmB	VAQNLALDGL	LYPLIYGHFV	DDHLALQGGT	AVAILTSFMP	EWHDETARWI
PH_P1	LAQNLVLDGL	LQPLMYQRF.	DQWLTEGGG	DVAMLTEFMR	DWYGESTRWW
	301				350
Mtri_Hbeta	DDLFDVYCLAN	DSEFGAHRRT	FLNATEHYL	ASSVAALKDF	VGLYAKVEKV
MspM_Hbeta	DDLFDVYCLAN	DPEFGAHRRT	FLNATEHYL	ARSVTALKDF	VGIYAKVEKV
Mcap_Hbeta	QDLYYNCLGD	DPEFSDYRRT	VMRNMTGKWL	EPTIAALRDF	MGLFAKL..P
AMO_AmoA	QAL.VRLVCQ	DPVHGDQQA	TVRRMIEEWQ	PRCKAAQSF	LPTFS.....
T3M_TbuA2	GALVRMAL..	...EQPGNRE	VITGALAKWE	PLADEAIVAY	CSALPEAPAA
T4M_TmoE	KALVKHAL..	...ENPDNHA	VIEGAIKWR	PLADRAAEAY	LSMLS.SDIL
T2M_TbmB	DAVIKTMANA	AEPEAAGNRA	LLSQMFSQWA	DRAQAALAPV	AEMALGEHGA
PH_P1	DAMFKTVL..	..AENDANRE	QVQAMLEVWE	PRAYEALLPL	AEEA...TGI
Mcap #		313	320	331	
	351				400
Mtri_Hbeta	AG..ATDSAG	VSEALQRVFG	DWKIDYADKI	GFRVDVDQKV	DAVLAGYKN*
MspM_Hbeta	AG..ATDRAG	VSEALQRVFG	DWKVDYADKI	GFKIDVDEKV	AAVLAGYKN*
Mcap_Hbeta	AG..TTDKEE	ITASLYRVVD	DWIEDYASRI	DFKADRDQIV	KAVLAGLK* .
AMO_AmoA	DC..GIDAKE	SANALSRALA	N.....QRAAVE	GAGITA* ...
T3M_TbuA2	QARATAAVRE	FRHSLGL*..
T4M_TmoE	HAQYLERSTS	LRASILTV*
T2M_TbmB	AALGEVRRRA	LDARATKLGL	SL*.....
PH_P1	AALDEV.RSA	FATRLQKIGL	KSREE*....

Figure 1-11

Figure 1-12. Sequence alignments of the peptides corresponding to protein B. Residues conserved across all peptides are shown in reverse. Residues with conservative substitutions are shown with gray background. The top number in each bar is the consensus numbering, the bottom numbers are the *M. capsulatus* (Bath) sMMOB residue number and *P. pudita* P2 residue number.

	1					50
Mtri_B	MSSAHNAYNA	GIMQKTGKAF	ADEFFAEENQ	VVHESNAVVL	VLMKSDEIDA	
MspM_B	MSSAHNAYNA	GIMQKTGKAF	ADEFFAEENQ	VVHESNAVVL	VLMKSDEIDA	
Mcap_B	MSVNSNAYDA	GIMGLKGKDF	ADQFFADENQ	VVHESDTVVL	VLKKSDEINT	
T3M_TbuVMSIDNTA	EAYRNNRVGP	VLRASSITAG	
T4M_TmoDMST.LAD	QALHNNNVGP	IIRAGDLVEP	
T2M_TbmCMSQVFI	AFQANEESRA	
PH_P2MSSLVYI	AFQDNDNARY	
AMO_AmoBMTDVKET	TVTSTPSAAV	PGTKNRRVGI	SLISSSDTEA	
Mcap #				38		
PH P2 #				5		

	51					100
Mtri_B	I E EDIVLKG.	GKAKNPSIVV	EDKAGFWW K	ADGA E EIDAA	EAG L LLSKPF	
MspM_B	I E EMVLKG.	GKAKNPSIVV	EDKAGFWW K	ADGA E EIDAA	EAA L LLSKPF	
Mcap_B	F E EILLTDY	KKNVNPTVNV	EDRAGYWW K	ANGK E EVDCD	EIS L LLGRPF	
T3M_TbuV	V E EAAQEDNP	GKS....IRI	DDKLAYVR D	TDGE E ILRRA	TLE E ALGRPF	
T4M_TmoD	V E ETAEIDNP	GKE....ITV	EDRRAYVR E A	AEGE E ILTRK	TLE E QLGRPF	
T2M_TbmC	V E EAIVTDNP	..E....AVV	TYPTGLVK D	APGR E ITIRRE	TIE E QTGRPF	
PH_P2	V E EAIIQDNP	..H....AVV	QHHPAMIR E	AEKR E EIRRE	TVE E NLGRAW	
AMO_AmoB	A E E H IAETQP	..D....AKI	DFRDCFYK E	RDGQ E SFDMA	ELS E IA E EDI	
Mcap #	53		79	85	94 97	
PH P2 #	20		40	46	55 58	

	101					142
Mtri_B	SVYDLL N NVS	STV G RAYTLG	TKFTITSELM	GLDRALTDI*	..	
MspM_B	SVYDLL N NVS	STV G RAYTLG	TKFTITSELM	GLDRALTDI*	..	
Mcap_B	NVYDFL N DVS	STI G RAYTLG	NKFTITSELM	GLDRKLEDYH	A*	
T3M_TbuV	KMSELE N NLS	SFAGRIETTD	DYVRFYYEKT	L*.....	..	
T4M_TmoD	NMQELE N NLA	SFACQIQADE	DQIRFYFDKT	M*.....	..	
T2M_TbmC	DLQQLH N NLV	TLS G HIDEDD	DQLT S WQH*	
PH_P2	DVQEML N DVI	TIG G NVDEDD	DRFVLEWKN*	
AMO_AmoB	DTDIFL N NMS	TYY G RIVVSD	GRVDIYAEIQ	PARFKD*...	..	
Mcap #	107	114				
PH P2 #	68	75				

Figure 1-12

Figure 1-13. Sequence alignments of the peptides corresponding to the reductase. Residues conserved across all peptides are shown in reverse. The top number in each bar is the consensus numbering, the bottom number is the *M. capsulatus* (Bath) residue number. Domains corresponding to [2Fe-2S], FAD and NADH binding regions are marked (24).

```

1
Mtri_R      ...MYQIVIE TEDGETCR.R MRPSDWISR AEAER.NLLA SQRASG.CATC
MspM_R      ...MYQIVIE TEDGETCSFE CGPSEDVISA GLRQSVILLA SCRAGACATC
Mcap_R      MQRVHTITAV TEDGESLRFE CRSDEDVITA ALRQNIFLMS SREGGCGATC
T3M_TbuC    ...MKHQITI EGGSAFS..V AADEDTLRG ALRGGIALPH EGSVGGCGAC
T4M_TmoF    .....MFNI QSDDLHHEFE ADSNDTLLSA ALRAELVFPY EONS GGCGAC
T2M_TbmF    .....MCNQL TIEPLGRITLD VAEGQTLDA ALRSGVYIPH ACGHGLCGTC
PH_P5       .....MSYNV TIEPTGEVIE VEDGQTILQA ALRQGVWLPF ACGHGTGATC
AMO_AmoD    .....MTTI NVQPFSSHEYS CEDGESLLDG ALRNSLLLKY GAKHGGCGTC
Mcap #      42      47 50
Domain      [ -----

51
Mtri_R      KADCTDGDYE LIDVKVQAVP PDE.EEDGKV LERTFPRSD LHLLV...PY
MspM_R      KADCTDGDYE LIDVKVQALP PDE.EEDGKV LERTFPRSD LHVVV...PY
Mcap_R      KALCSEGDYD LKGC SVQALP PEE.EEEGLV LERTYPKTD LEIEL...PY
T3M_TbuC    RFDLLSGLVE SIWPEAPGLS ERDR.KRGKH LACQSRPLGD CTIRVRCDD.
T4M_TmoF    KIELLEGEVS NLWPDAPGLA AREL.RKNRF LACQCKPLSD LKIKVINRA.
T2M_TbmF    KVQVTSGEVD HGAANPLRRS WISSGEEGKT LACCATALSD VCIEADVDD.
PH_P5       KVQVVEGEVD IGEASPFALM DIER.DERKV LACCAIPLSD LVIEADVDA.
AMO_AmoD    KVRLLDGDVE .EPGSSFALT PEDR.ENDVI LACASVPLEP CTIDVEPSGL
Mcap #      57      80
Domain      -----FE2S2-----]

101
Mtri_R      TYDRISFEAI QTNWLAEILA CDRVSSNVVR LVLQR.SRPM AARISLNIVP
MspM_R      TYDRISFQAI QTNWLAEITE CDRVSSNVVR LVLQPLTADG AAPISLNILP
Mcap_R      THCRISFGEV .GSFEAEVVG LNWVSSNTVQ FLLQKRPEDEC GNR.GVKKEP
T3M_TbuC    ...TYRPVVS PGRWAAVLQA RRELTPDMSE FTFA....V HAP..AEERP
T4M_TmoF    ...EGRASHP PKRFSTRVVS KRFLSDEMFE LRLE....A EQK..VVEESP
T2M_TbmF    .EPDARASFP CGLWWATVTR IDTLTPTIKG LRLK....L DQP..IDFQA
PH_P5       .DPD.FLGHP VEDYRGVVSA LVDLSPTIKG LHIK....L DRP..MPFQA
AMO_AmoD    TEEFFSFGDT SREFQTVVGG VEFLTADIAR VRLR....L EPGEEIATA
Mcap #      142
Domain      [ ---

151
Mtri_R      GQFVDIEIIG THTRRSYSMA SVAE.D..GQ LEFIIRLLPD GAFSKFLQTE
MspM_R      GQFVDIEIIG THTRRSYSMA SVAE.D..GR LEFFIRLLPD GAFSNYLRTQ
Mcap_R      GQFMDLTIPG TDVRSYSIPA NLPNPE..GR LEFLIRVLPE GREFSDYLRND
T3M_TbuC    GQYALLYPH APGARAYSMS NLPNAD..GI WQFVIRRVPG GAGSNALFDQ
T4M_TmoF    GQYFMVDVEE L.GTRAYSAA N.PVDG..NT LTLIVKAVPN GKVSCALAN.
T2M_TbmF    GQYVMVEIIG LGQRFAFSMP MPSDGGPCGE IELQVRRVPG AAGTGVLHEQ
PH_P5       GQYVNLALIG IDGTRAFSLA NPP..SRNDE VELHVRLVEG GAATGFIHKQ
AMO_AmoD    GQFVNVEVIG TGLLTFSLA NAPDDP..SV VELICKLYPD GLFSRFLRDE
Mcap #      145      153      162
Domain      ---FAD-----]

```

Figure 1-13

```

201                                     250
Mtri_R   AKVGM RVDLR  GPAGSFFLHD  HGGRSRVFVA  GGTGLSPVLS  MIRQLGKASD
MspM_R   ARVGQRVALR  GPAGSFSLHK  .SERPRFFVA  GGTGLSPVLS  MIRQLHKESD
Mcap_R   ARVGQVLSVK  GPLGVFGLKE  RGMAPRYFVA  GGTGLAPVVS  MVRQM QEWTA
T3M_TbuC VEIGQTVTLD   GPYGHALRD  DNARDIVCIA  GSGGLAPMLS  VARGALAQEG
T4M_TmoF .ETIETLQLD   GPYGLSVLKT  ADETQSVFIA  GSGGIAPMVS  MVNTLIAQGY
T2M_TbmF LAVGDTLHVT   GPYGRFFVRQ  SAAKPMLFVA  GSGGLSSPRS  MILDLEQGC
PH_P5    LKVGDAVELS   GPYQFFVRD  SQAGDLIFTA  GSGGLSSPQS  MILDLLERGD
AMO_AmoD AAPGTPVRVF   GPYQQLKIRL  SH.RPILMIA  GSGGLAPLLS  MLRDLAAKKC
Mcap #   203                                     222       232
Domain   [ -----NADH--

```

```

251                                     300
Mtri_R   PSPATLLFGV  TNREELFYVD  ELKTLAQSM  TLGVRIAVVN  DDGGNG..VD
MspM_R   PQPATLFFGV  TNYEELFYVD  ELKALQHAMP  SLDVQIAVVN  VSENGN..VA
Mcap_R   PNETRIYFGV  NTEPELFYID  ELKSLERSMR  NLTVKACVWH  PSGDWE..GE
T3M_TbuC AQRVHFFYGG  RSQPDLGAMA  ALDDL.V.GDN  RLALSVVLSA  PGPELQWQGP
T4M_TmoF EKPITVIFYGS  RLEAELEAAE  TL..FG.WKE  NLKLVVSSS  VVGNSEKKYP
T2M_TbmF TLPITLVNGQ  RSREELYGHA  EFVALADRHP  NFSYVPVLSN  EPEGSADWGA
PH_P5    TRRITLFOGA  RNRAELYNCE  LFEELAARHP  NFSYVPALNQ  ANDDPEWQGF
AMO_AmoD DRPVSMFFGA  RSVDDLYLIE  EIREIGESLA  DFEFIPVLS.  ESSPADWHGE
Mcap #   252       259
Domain   -----]

```

```

301                                     350
Mtri_R   KGTVIDLLRA  ELEIDLLLGH  ARRRRRRETA  RSCREDHRDR  CPA.WRSD..
MspM_R   KGTVIDLLQD  EL.....  GRRAEKPDY  LCGPPGMIDA  AFA.AASSAG
Mcap_R   QGSPIDALRE  DLE.....  .SSDANPDY  LCGPPGMIDA  ACE.LVRSRG
T3M_TbuC TGFVHAEVER  VLVAPL....  ...DRFEFY  FAGPPPMIEA  VQALLMHTHR
T4M_TmoF TGYVHEIPE  YMEGLL....  ...GA.EFY  LCGPPQMINS  VQKLLMIENK
T2M_TbmF RGFVHDAAKA  HFNQGF....  ...AGHKAY  LCGPPPMVEA  AIGALM.QGR
PH_P5    KGFVHDAAKA  HFDGRF....  ...GGQKAY  LCGPPPMIDA  AITTLM.QGR
AMO_AmoD TGMVTDAL.L  RWRAEL....  ...A.HDVY  LCGPPPMIDA  AVPLL.V.ERG
Mcap #   292
Domain

```

```

351                                     381
Mtri_R   .....FLEK  FLASG*....  .....
MspM_R   VPKEQVYLEK  FLASG*....  .....
Mcap_R   IPGEQVFFEK  FLPSGAA*..  .....
T3M_TbuC VPFEQMHFDR  EV*.....  .....
T4M_TmoF VPFEAIHFDR  EF*.....  .....
T2M_TbmF LFEDDIYTEK  FLSAADANAR  A..QPLFKRV *
PH_P5    LFERDIFMER  FYTAADGAGE  SSRSALFKRI *
AMO_AmoD VRPRNIYYDA  TPAAQVVVV  *.....
Mcap #   342
Domain

```

Figure 1-13

Figure 1-14. View of the absolutely conserved α subunit residues near the active site of the *M. capsulatus* (Bath) sMMO hydroxylase. Carbons are marked gray, oxygens are red, and nitrogens are blue. The four helices that surround the active site are shown as partially transparent ribbons. The irons are shown in pink, and iron 1 is marked as such. The hydroxide bridge, terminal water and acetate bridge are all omitted for clarity. This Figure was generated by using the program MolScript (47).

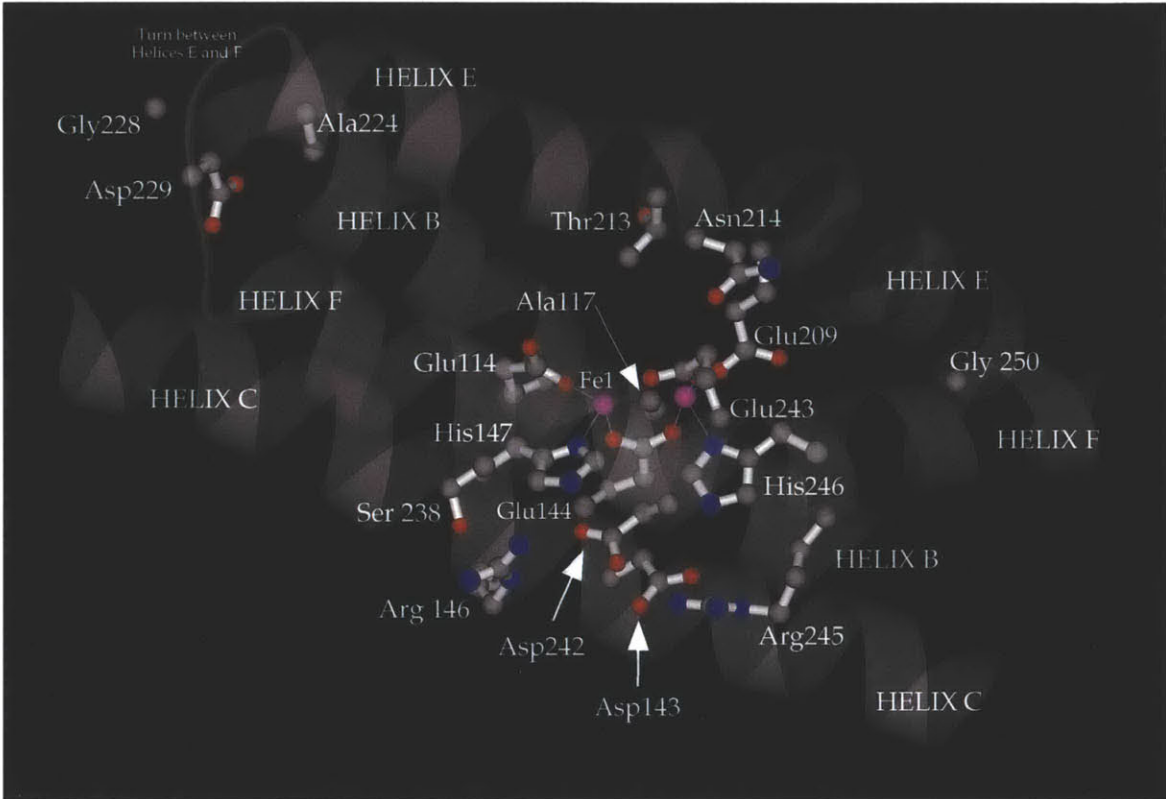


Figure 1-14

Figure 1-15. Schematic of the hydrogen bonding network in the absolutely conserved residues near the active site. Distances as shown in the Figure do not necessarily correspond to actual distances.

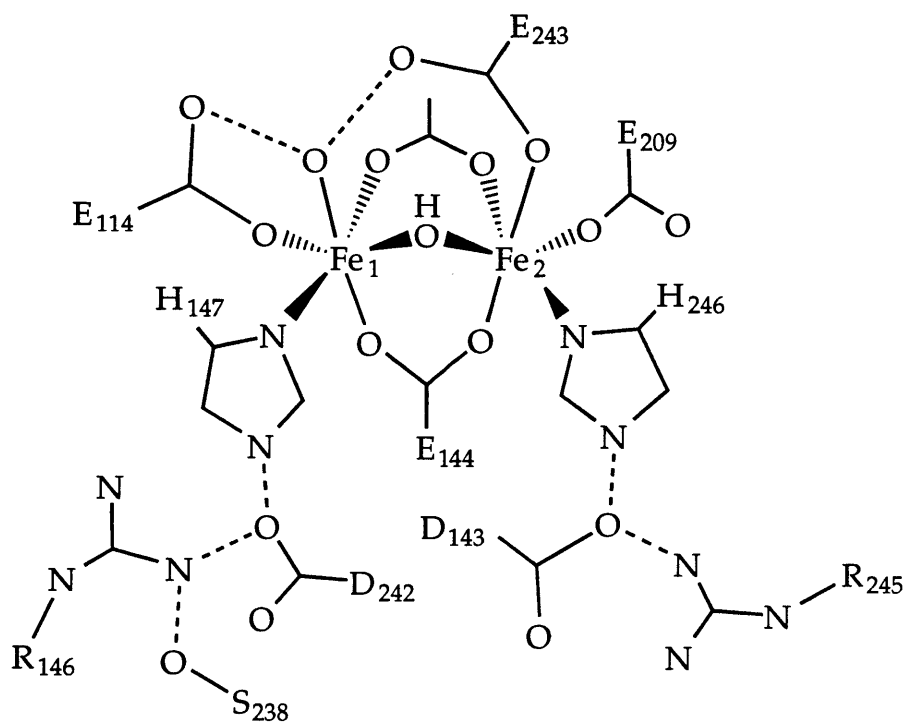


Figure 1-15

Figure 1-16. View of the absolutely conserved α subunit residues not near the active site of the *M. capsulatus* (Bath) sMMO hydroxylase. All peptides but the rightmost α subunit are partially transparent for clarity. Residues lining the canyon are shown in yellow, the aromatic cluster residues on top of the hydroxylase are in red, and the cluster of residues under the γ subunit are shown in white. This Figure was generated by using the program MolScript (47).

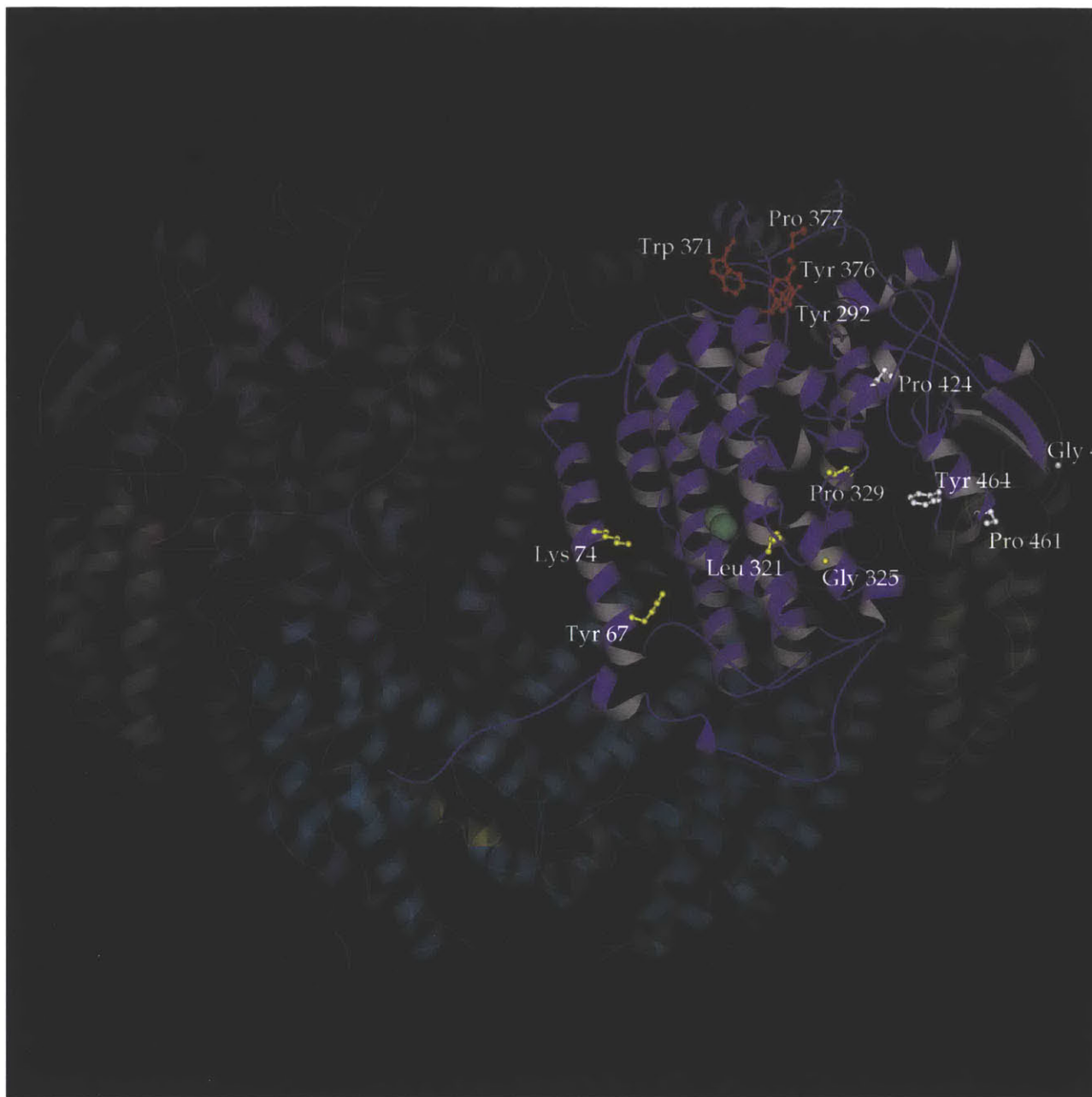


Figure 1-16

Figure 1-17. View of the absolutely conserved β subunit residues in the *M. capsulatus* (Bath) sMMO hydroxylase. All peptides but the rightmost β subunit are partially transparent for clarity. Conserved residues are shown in white. This Figure was generated by using the program MolScript (47).

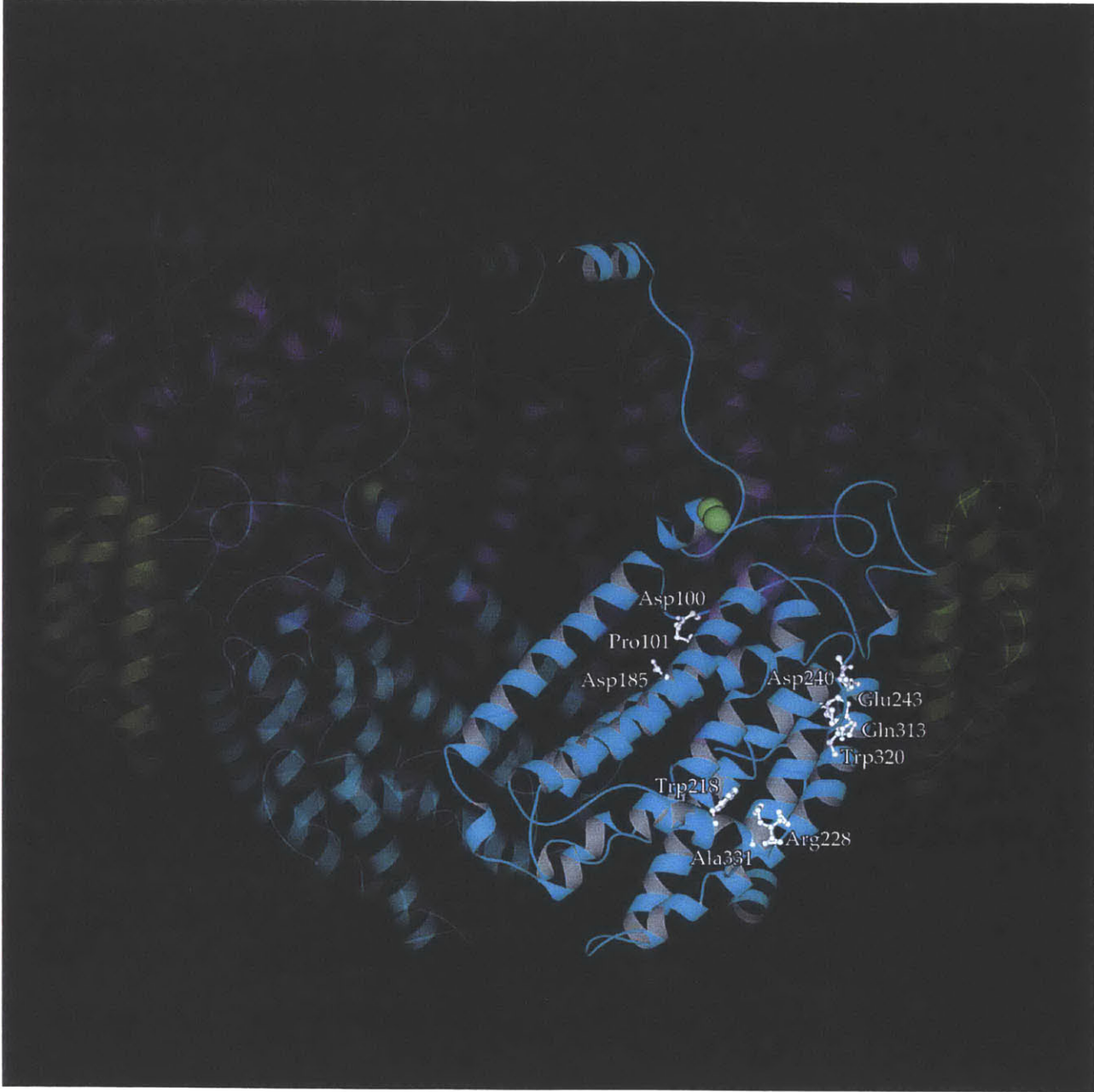


Figure 1-17

Figure 1-18. View of the absolutely conserved residues in the *P. pudita* CF600 phenol hydroxylase P2 protein (model 1). Conserved residues are shown in white. Conservative substitutions are shown in yellow. This Figure was generated by using the program MolScript (47).

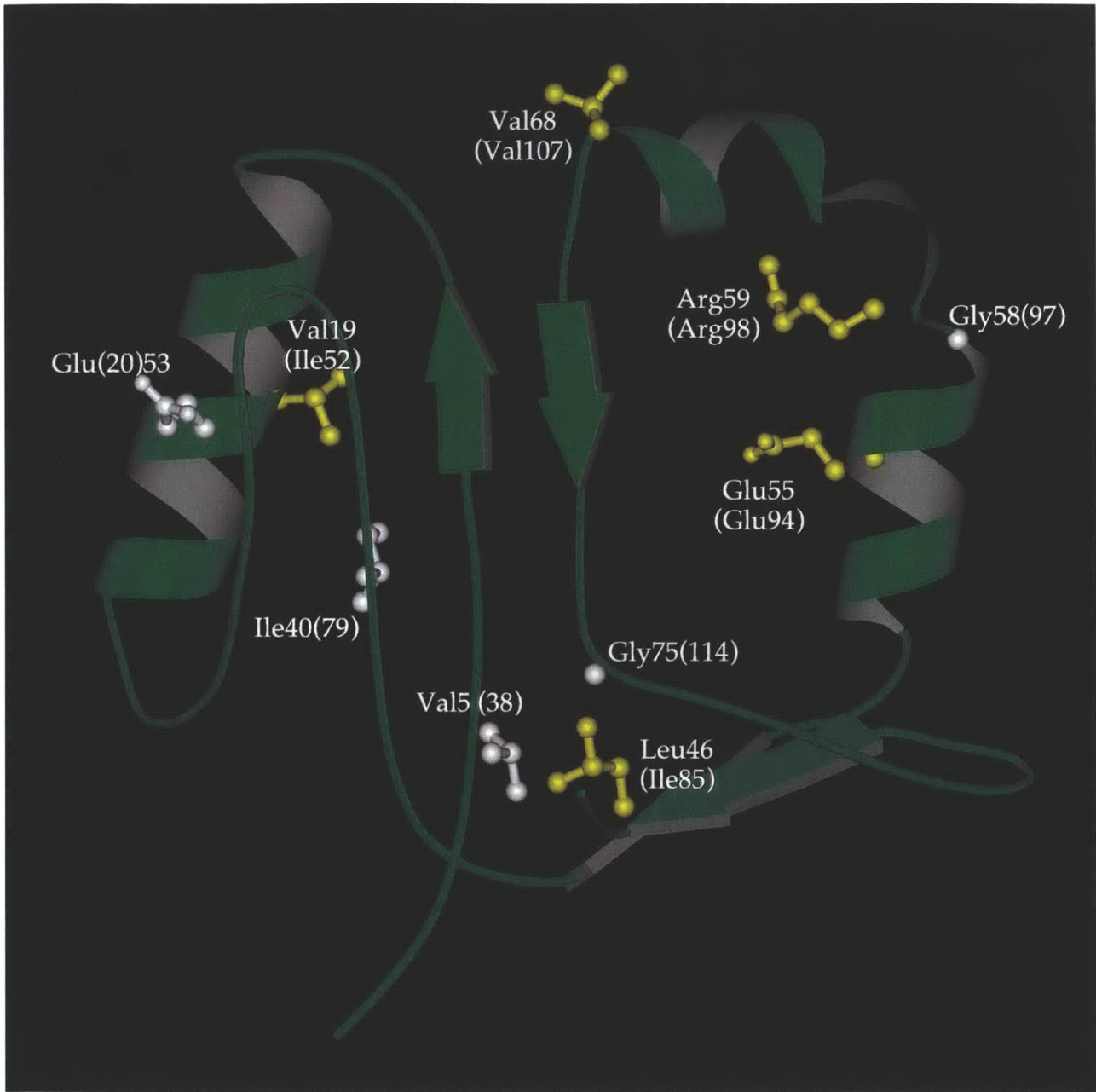


Figure 1-18

Figure 1-19. Cartoon of two possible sMMO family interprotein interactions.

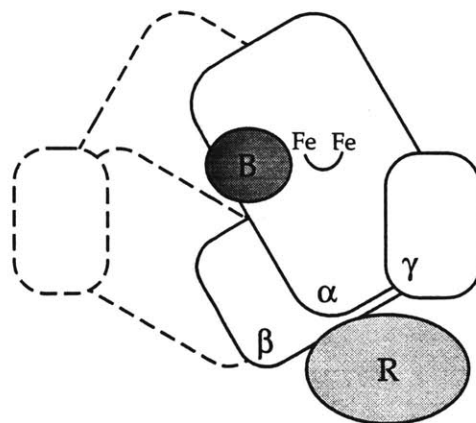
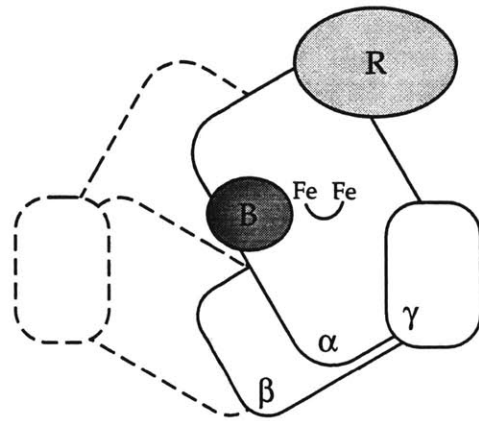


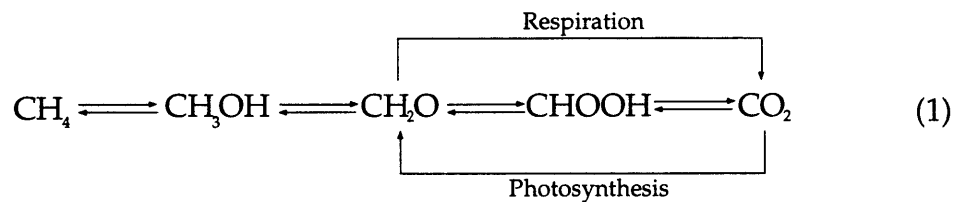
Figure 1-19

Chapter Two

Heterologous Expression of the *Methylococcus capsulatus* (Bath) Soluble Methane Monooxygenase Hydroxylase

Introduction

Carbon atoms, along with other elements necessary for the chemistry of life, circulate in the biosphere in a characteristic pattern. This pattern, termed the carbon cycle, can be represented in a redox fashion as shown in eq. 1 below:



This equation shows the circulation of carbon between high oxidation states (carbon dioxide in the atmosphere and carbonates in the hydro/geosphere) and low oxidation states (methane in the atmosphere and petrochemicals in the geosphere). The two most well known processes in the carbon cycle are labeled in eq. 1. Photosynthesis is the process of storing solar energy in carbon by reducing carbon dioxide to the formaldehyde oxidation state, generally in the form of saccharides. Respiration is the release of that energy through the oxidation of saccharides to carbon dioxide.

There are biological participants in the carbon cycle at all oxidation levels. The metabolic oxidation of methane to carbon dioxide occurs in methylotrophic bacteria (1-5). About half of the total organic matter degraded by anaerobic microbes is converted to methane, but only 0.5% of this methane reaches the

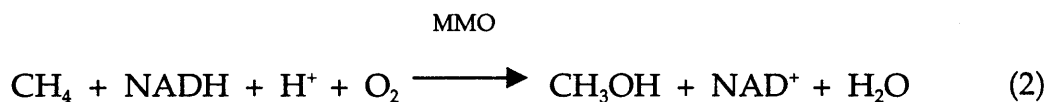
atmosphere (2). Most is consumed by methanotrophs. These organisms, some of which are capable of subsisting on methane as a sole source of carbon and energy, form a small but crucial ecological niche for recycling carbon from decaying biomass. Figure 2-1 portrays a greatly simplified schematic of the role methanotrophs play in the carbon cycle. Complex carbon molecules that are not easily broken down settle in soil layers that are very low in oxygen. Heterotrophs and methanogens anaerobically break down these complex molecules into smaller and more reduced pieces. Methane gas is the ultimate product of this process, for it can be neither disassociated into smaller pieces nor further reduced. It diffuses upward into soil containing relatively high oxygen levels where it is oxidized by methanotrophs to form either biomass or carbon dioxide. Since this methane would otherwise reach the atmosphere where methane can act as a greenhouse gas, methanotrophs occupy an important and interesting niche in the carbon cycle.

Methanotrophs are capable of subsisting on nothing but methane and oxygen for all of their carbon and energy. Methane metabolism in these organisms is summarized in Figure 2-2. The first two steps, catalyzed by methane monooxygenase (MMO) and methanol dehydrogenase, are energy neutral, since the MMO reaction consumes NADH and the second step produces a NADH equivalent. The organism then makes a choice between carbon fixation or energy production in the form of NADH. This metabolism mimics the larger scale carbon cycle, in that energy is stored as CH_2O units and released by burning those units to form CO_2 .

The methanotroph metabolic reactions are interesting from both a chemical and economic standpoint. The first step in the process, the controlled oxidation of methane to methanol by dioxygen, is particularly interesting due to its kinetic difficulty. Current industrial processes to produce methanol from

methane require two steps (6). The first is the conversion of methane to "synthesis gas" (CO + H₂), which takes place over Ni, Al or Si catalysts, and the second is conversion of the "synthesis gas" to methanol, which is done by using Zn/Cu or Zn/Cr catalysts. Both reactions require pressures of 50-200 bar and reaction temperatures of 250-900 °C. The MMO system performs this reaction at 25 °C and 1 atmosphere utilizing water as a solvent. It would clearly be cheaper and safer to use catalysts that mimic the chemistry of MMO in industrial methanol production processes. To further that goal, examination of the reaction of methane and dioxygen in the MMO system is a first step in the design of new catalysts.

The enzymes that catalyze the MMO reaction come in two forms, a particulate MMO (pMMO) that contains copper and is membrane bound, and a soluble MMO (sMMO) that contains iron and is found in the cytoplasm (7-10). The sMMO enzymes are relatively simple to purify and are quite robust when compared to the pMMO, and they have therefore been studied in more detail. The stoichiometry of the MMO reaction is shown below in eq. 2.



The sMMO hydroxylase protein (sMMOH) is the site of methane activation. It is a heterodimer consisting of two copies each of three subunits, MMOH α (60646 Dal), MMOH β (45132 Dal) and MMOH γ (19847 Dal), resulting in a holoenzyme with a molecular weight of 251 kDal. It contains a non-heme, carboxylate-bridged diiron center that is the site of methane oxidation. This diiron unit is similar to centers found in a wide variety of enzymes, including ribonucleotide reductase (RR) (11, 12), stearoyl acyl carrier protein Δ -9 desaturase (13), phenol hydroxylase (14) and toluene-4-monooxygenase (15). The sMMO

system also contains a reductase and a coupling protein. The structure of the hydroxylase has recently been determined under a variety of conditions (16, 17), and those data supplied important information about the mechanism of the enzyme.

Three proposals relate the structure of the hydroxylase to its function. Specifically, the MMOH α residues cysteine 151, threonine 213 and leucine 110 are hypothesized to have functions suggested by their positions in the crystal structure. It was first postulated by Dalton and Nordlund that C151 in the *M. capsulatus* (Bath) MMOH would occupy the same position in the active site as tyrosine 122 from ribonucleotide reductase subunit R2, based on sequence comparisons (18). The R2 iron center is responsible for converting Tyr122 to a radical. Subsequently, it was proposed that a thiyl radical at C151 might be a part of the mechanism of methane hydroxylation (19). The crystal structure confirmed that C151 occupies a position similar to the RR R2 tyrosine residue, although the sulfur atom of the cysteine is farther away from the iron center than the tyrosine oxygen atom due to the difference in size between tyrosine and cysteine side chains. A thiyl radical intermediate was recently observed by EPR spectroscopy in a coenzyme B12-dependent RR that is responsible for abstraction of a hydrogen atom from a ribose ring (20). A thiyl radical is possibly involved in the mechanism of hydrocarbon hydroxylation.

Threonine 213 also has a corresponding residue in RR R2 subunit. It occupies a position similar to that of serine 211 in the R2 protein, which is responsible for shuttling protons from solvent into the active site (21). In the structures of the reduced and oxidized frozen crystals, T213 is hydrogen bonded to a solvent molecule and an acetate ion, respectively (17, 22). Both the water molecule and acetate are further linked by hydrogen bonds to the diiron center

via solvent ligands. The threonine residue is, therefore, part of an extensive hydrogen bonding network that may function to feed protons into the active site.

Another possible interpretation of the roles of the Cys151 and Thr213 residues is based on the observation that they are among the few protonated residues in the largely hydrophobic active site cavity. As such, they may serve to communicate structural changes via hydrogen bonding in the hydroxylase caused by binding of protein B or the reductase to the diiron center, tuning its activity to reflect the state of the protein.

The third residue mentioned above is leucine 110, which crystallographic methods reveal to adopt two different orientations in different crystal forms (23). This residue may act as a gate between two hydrophobic pockets, termed cavities 1 and 2, which are proposed to be involved in substrate access to the active site iron center.

The ideal method to approach the testing of these proposals is site-directed mutagenesis, combined with analysis methods previously established in our laboratory, including X-ray crystallography and stopped-flow kinetics. Interesting mutants at position 151 would include C151A and C151S. MMOH C151S preserves the proton, but changes the electronic character of the residue. The net effect would be that the hydrogen bonding role of C151 will very likely be preserved, but that any radical that may be formed at that position in the native enzyme may not be formed in the mutant C151S. The C151A mutant will be useful as a control since neither hydrogen bonding nor radical formation is possible. The mutants at T213 that would be most informative include T213A, T213S, and T213C. Both T213S and T213C preserve the hydrogen bonding capability, but remove a methyl group. The hydrogen bonding strengths of serine and cysteine differ, and that difference may be observable kinetically if T213 were responsible for delivering protons to the active site during turnover.

The T213A mutant is, again, a control that removes the hydroxyl proton completely. L110 mutants would include a number of smaller residues to observe the effects of removing the proposed gate.

Generating these site-directed mutants depends on having the hydroxylase expressed in a system that allows for easy changes in the hydroxylase subunit gene sequence, and that allows the production of significant amounts of protein for study. This topic is the subject of the present thesis chapter.

A number of proteins homologous to the sMMOH have been expressed in *E. coli*, including ruberythrin (24). It was produced in an insoluble, iron-deficient form, which could be reconstituted by denaturing the protein with guanidinium chloride, followed by dilution in the presence of Fe(II). The Δ -9 desaturase has also been expressed in *E. coli* (25). High yields of soluble desaturase were prepared through the use of an optimized lactose fed-batch fermentation methodology, where lactose was used instead of IPTG as an inducer (26). The toluene-4-monooxygenase (T4M) system is quite similar to the sMMO system (15, 27). It has a hydroxylase with three subunits, a reductase and a protein B homologue. It has been expressed in *E. coli* by inducing the expression systems at very high cell densities, at low temperatures, at low IPTG concentrations and with Fe(II) media supplements. All three of these proteins were produced in an insoluble form under standard expression conditions, requiring specialized conditions for production of soluble material.

All of the proteins mentioned above, with the exception of T4M, are single polypeptides. Expression of proteins with more than one subunit is often a particular challenge, due to the need for subunit assembly in a foreign environment. Few multisubunit proteins have been expressed in *E. coli* (28). The most common strategy for expressing those kinds of systems is to prepare the

individual subunits separately, and recombine them at a later stage to form the holoprotein. Examples of this type of expression include recombinant actin and myosin subunits (29, 30), the two subunits of the human class I histocompatibility antigen (HLA)-A2 (31), RNA polymerase I initiation factor SL1 (32), and two subunits from the corrinoid/iron-sulfur protein from *C. thermoaceticum* (33). A second strategy for expression is to produce an "operon" on a plasmid, either by replication of the wild-type operon or by construction of an artificial operon. The T4M system described above was expressed by using the latter methodology.

Several groups have reported progress in expressing the sMMO genes. The *M. capsulatus* (Bath) sMMOB and sMMOR proteins have been expressed in *E. coli* (34-36). sMMOH⁻ mutants have also been generated in *M. trichosporium*, an important step for producing homologous mutants (37). Heterologous expression of the *M. trichosporium* sMMO system in *P. putida* F1 has been accomplished by using the pMMB broad host range (38), but no subsequent purification of the protein products was reported.

Expression of heterologous proteins in *E. coli* often results in the formation of protein aggregates, termed inclusion bodies (28, 39-42). These inclusion bodies contain the protein of interest in a non-native and non-active form.

Inclusion bodies are the result of the absence of some condition required for protein folding in a heterologous system. This problem has been most evident for eukaryotic proteins that have post-translational modification requirements, in proteins that have more than one subunit, in proteins that may require specific chaperonins for correct folding, and in proteins requiring the assistance of other proteins for insertion of a cofactor (43).

There are two broad methods for solving the problem of inclusion bodies, *in vivo* and *in vitro*. *In vivo* methods prevent the formation of inclusions by

changing the conditions inside the cell during protein induction (28). Examples include growing cultures at a lower temperature, using lower IPTG concentrations, using higher media salt concentrations (to increase the hydrostatic pressure inside the cell), and changing expression systems or organisms. *In vivo* methods often fail, since there is very little that one can do to change the physical environment inside the cell. *In vitro* solutions involve collecting the inclusions and subjecting them to a procedure to refold the protein (42, 44). There are two common examples of such procedures. One can solubilize the inclusion bodies by using a denaturant such as urea or guanidinium hydrochloride and then refold them by dialysis to remove the denaturant. Alternatively one can solubilize the inclusions by using a detergent such as sarcosyl, and then renature the protein by detergent removal. *In vitro* methods are the most common solutions reported in the literature, and if they work well, the formation of inclusion bodies can be an advantage since they are easily isolated in high purity from soluble protein impurities.

This chapter reports on progress toward the expression of the soluble MMOH in *E. coli*. Construction of a series of vectors for both "operon" and individual subunit expression is described, together with the use of those systems to produce substantial amounts of the three sMMOH subunits as inclusion bodies. Both refolding and expression conditions were systematically changed in attempts to produce active sMMOH. Finally, based on observations and deductions from on the data reported, a future course of action to express the hydroxylase is outlined.

Materials and Methods

All chemicals were from Sigma-Aldrich, except IPTG (Boeringer-Mannheim) and when noted otherwise. All enzymes were from New England Biolabs unless stated explicitly. Manufacturer's instructions were followed exactly in their use unless stated. All restriction digests were carried out at 37 °C over 6 h. Double digests were performed first with low-salt optimal enzyme (3 h) followed by addition of high-salt buffer and the second enzyme (3 h). Ligations were carried out overnight at 14 °C. *E. coli* strains INV α F' or XL1-Blue were used for all DNA manipulations. *E. coli* strain JM105 was used as expression host at 37 °C unless mentioned otherwise.

Low Pressure Chromatography sMMOH Purification Procedure. The sMMOH and a crude mixture of sMMOB and sMMOR (termed B/C mix) were prepared as described previously (45, 46). Average iron content of the hydroxylase was 3.4-3.6 Fe/protein and the average activity (in units as described in the literature) was 220-250 mU/mg. An SDS-PAGE gel showing the quality of the protein obtained in this manner is presented in Figure 2-3.

Production of MMOH Polyclonal Antibodies. Two female New Zealand white rabbits were obtained. Blood samples (15 mL) were taken from each animal before any injections were made. The blood was incubated at room temperature for 4 h to clot, then left at 4 °C for 12 h to retract the clot. The serum was decanted and spun in a table-top centrifuge for 10 min at 200 rpm to remove additional blood particulates. The serum was frozen in liquid nitrogen and stored at -20 °C.

Protein antigen injections were prepared by first exchanging and concentrating a native sMMOH sample into PBS at a concentration of 3 mg/mL. A 2 mL sample of the exchanged protein solution was mixed with 2 mL of

Freund's Complete Adjuvant for the first injection or 2 mL of Freund's Incomplete Adjuvant for all subsequent injections. This solution was either vortexed vigorously at 4 °C for 30-60 min or exchanged rapidly between two syringes connected by a narrow stopcock until a thick emulsion formed. This emulsion was divided into two 2 mL syringes and given to MIT Animal Care personnel to inject each rabbit at multiple subcutaneous sites. Two to three weeks after each injection, the animals were bled (15 mL), and serum containing antibodies to the hydroxylase was isolated as described above.

This cycle was repeated 6 times. The final bleed was done by fatal cardiac puncture in which most of the blood from the rabbit was collected, resulting in approximately 50 mL of material. Total serum collected was approximately 120 mL. The serum was used in subsequent experiments without further purification. Protein concentration was approximately 25 mg/mL in the sera samples.

ELISA Assays. A standard sMMOH solution of known purity and quality was used as the standard for all ELISA assays. ELISA 96-well polystyrene plates were purchased from Corning.

In each ELISA assay, one column was reserved as a blank, no-protein control, and another was reserved for a sMMOH standard. Each row was a 1:3 dilution of the row above it, resulting in a typical range of concentrations in the sMMOH column from 160 µg/mL to 73 ng/mL. All dilutions were done in PBSN buffer (140 mM NaCl, 10 mM KCl, 25 mM NaPO₄ at pH 7.4). The protein solution to be tested was diluted and treated in an identical manner to the sMMOH standard.

Protein aliquots of 50 µL were placed in each well. The plate was wrapped in plastic and either baked at 37 °C for 2 h or left to incubate at 25 °C overnight. The protein solution was washed out of the wells with 3 rinses of deionized

water. The remaining sites for protein binding in the wells were blocked by filling each well to the brim with approximately 500 μL ELISA blocking buffer (170 mM H_3BO_4 at pH 8.5, 120 mM NaCl, 0.5% Tween 20, 1 mM EDTA, 0.25% BSA, 0.05% NaN_3) and soaking for 30 min. The blocking buffer was removed by using 3 rinses of deionized water. A solution of 625 ng/mL antiserum was made by dilution of the anti-sMMOH stocks described above in blocking buffer. Aliquots of 50 μL anti-sMMOH antibody were added to each well and allowed to soak at room temperature for 2 h. The antibody was washed out by rinsing 3 times with deionized water, soaking in blocking buffer for 10 min, and rinsing again 3 times in deionized water. A solution of 500 ng/mL Protein A-alkaline phosphatase conjugate was made by dilution of a stock solution in blocking buffer. Aliquots of 50 μL volume of the conjugate were added to each well and allowed to soak in for 2 h. The conjugate was washed out by rinsing 3 times with deionized water, soaking in blocking buffer for 10 min, and rinsing again 3 times in deionized water. A solution of 1.0 mg/mL *p*-nitrophenol phosphate (pNPP) was prepared by dissolving a pre-weighed tablet in an appropriate volume of 200 mM Tris buffer at pH 8.0. Aliquots of 200 μL volume of the pNPP solution were added to each well. The color of the pNP product of the alkaline phosphatase reaction was allowed to develop over 2 to 16 h, depending on the strength of the color.

The plates were read on an EFLab Titertek Multiskan model 110V multiwell plate reader utilizing a lamp filter set to 405 nm. The absorbance values for the sMMOH standard were used to construct a standard curve, and the protein concentration of sMMOH in the unknown samples was determined from that curve.

Western Blots. An SDS-PAGE gel containing one lane of sMMOH pure standard and other lanes with unknown samples were prepared and blotted onto

nitrocellulose. After blotting, the nitrocellulose membrane was sealed in a chamber containing 100 mL TTBS (0.1% Tween 20, 100 mM Tris pH 7.5, 0.9% NaCl) and allowed to soak for 1 h. The TTBS was removed and replaced with 40 mL of a 12.5 µg/mL solution of anti-sMMOH serum, which was prepared by dilution of the stock antisera described above in TTBS. After a 1 h soak, the membrane was removed and washed four times with 50 mL TTBS. A stock solution of goat anti-rabbit IgG(H+L)-horseradish peroxidase (HRPO) conjugate (obtained from Biorad) was diluted 1:3000 in 20 mL of TTBS. The membrane was soaked in that solution for 1 h, and washed four times with 50 mL TTBS. A 20 mL solution of 0.015% H₂O₂, 3 mM 4-chloro-1-naphthol, 0.9% NaCl and 100 mM Tris pH 7.5 was prepared and the membrane was soaked in that solution until adequate color development was observed. The HRPO reaction was stopped by a water wash, and the membrane was allowed to dry in air. A sample western blot prepared by using that protocol is shown in Figure 2-4.

Genomic DNA Sample Preparation. All procedures were carried out at 25 °C unless noted. *M. capsulatus* (Bath) cell paste (1 gram) was thawed and resuspended in 9.8 mL of TE (pH 8). SDS (200 µL of a 25% solution) and 1.5 mg proteinase K were added and mixed gently, followed by incubation at 37 °C for 2 h and 60 °C for 20 min. SDS (600 µL of a 25% solution) was added and incubated at 60 °C for 10 min. Sodium perchlorate (2.5 mL of a 5 M solution) was added, mixed gently, then the solution was again incubated at 60 °C for 15 min. The resulting solution was extracted with an equal volume of 25:24:1 phenol:chloroform:isoamyl alcohol by shaking gently for 30 min and centrifuged at 20,000 g for 20 min. The viscous aqueous layer containing the genomic DNA was removed by using a wide end pipet tip. This extraction procedure was repeated until no white precipitate formed at the phase boundary (typically 2-3 times). The DNA/RNA solution was precipitated by slow addition of 95%

ethanol at $-80\text{ }^{\circ}\text{C}$ to form two layers. The layers were mixed slowly by gentle agitation with a thin glass rod, curved at the tip. The DNA/RNA pellet accumulated on the glass, and was subsequently dried and resuspended in 7 mL of 150 mM NaCl/150 mM sodium citrate (pH 7). DNase-free RNase was added to the solution to 50 mg/mL, and the mixture was incubated at $37\text{ }^{\circ}\text{C}$ for 30 min. The solution was phenol extracted and precipitated as above, except that the DNA pellet was washed in 70% ethanol before speed-vac drying. The pellet was resuspended in 5 mL TE (pH 7.4).

Purification of PCR Primers for pDEC002. The following primers (5' to 3') were ordered from MIT Biopolymers and stored as deprotected, lyophilized powders at $-20\text{ }^{\circ}\text{C}$: XN1.1: GGCCATGGAGGAGGTAAGTAATGGCACTTAG-CACCGCA, XC1.1: CTCGAATTCTCAATTGAATGCCTTCACCG-GGTT, YN1.1: GGGAAATTCAGGAGGTTTCGATATGAGCATGTTAGGACAA, YC1.1: CTCAC-GCGTTCAATCCTGCCAGAACCGCTTTAA, ZN1.1: GGACGCGTAGGAGGTA-TGACATGGCGAAACTGGGTATA, ZC1.1: CTCGAGCTCTCAGTGCGGGCA-CTGCAGATGCAC. Each primer sample was resuspended in 100 μL of water, a 40 μL aliquot of which was mixed with 10 μL of USB Sequenase stop solution. These six samples were loaded onto 7 M urea 12% polyacrylamide gels, which were run for 1.75 h at 250 mV at $50\text{ }^{\circ}\text{C}$. The bands corresponding to the desired primers were visualized by using UV shadowing and were excised from the gel by using fresh, clean razor blades. The gel slices were crushed and the DNA was eluted by soaking overnight at $37\text{ }^{\circ}\text{C}$ in 1 mL of 3 M sodium acetate. The samples were extracted by addition of an equal amount of 25:24:1 phenol:chloroform:isoamyl alcohol, vortexing for 15 s, spinning down in a microcentrifuge for 30 s, and pipetting off the top aqueous layer. The water layer was added to 2.5X volumes of 95% ethanol, vortexed and kept at $-80\text{ }^{\circ}\text{C}$ for 30 min. The tubes were spun at 4,000 rpm for 30 min to pellet the primers. The supernatant was decanted

and the pellets were washed in 1 mL of 70% ethanol. The samples were spun down at 4,000 K for 30 min and the supernatant was decanted. The pellet was dried under vacuum and resuspended in 40 μ L TE (pH 7.4).

PCR Conditions for pDEC002. The following were added to a total volume of 100 μ L for each of the three subunits: 1000 ng of genomic DNA, 100 pmol of the N-terminal primer (_N1.1), 100 pmol of the C-terminal primer (_C1.1), 1 μ L of 20 mM dNTPs, 10 μ L of 10X *Taq* polymerase reaction buffer and 1 μ L *Taq* polymerase (5 units). These samples were placed in a thermocycler that was programmed to with the following cycle: 1 x (7 min at 94 °C, 2 min at 60 °C, 2 min at 72 °C), 38 x (2 min at 94 °C, 2 min at 60 °C, 2 min at 72 °C), 1 x (2 min at 94 °C, 2 min at 60 °C, 10 min at 72 °C). Each of the three samples was purified from reaction buffer salts, primers and dNTPs by using the Qiagen PCR spin quantitation kit. An agarose gel showing the results of the PCR reactions is given in Figure 2-5.

Construction of pDEC002. Direct 4-piece ligations of *mmoX*, *mmoY*, *mmoZ* and the chosen expression vector pTrc99A did not perform adequately, so a more complex serial cloning procedure was adopted, as diagrammed in Figure 2-6. A double digest of 1 μ g of pSL301 (Novagen) and 1 μ g of X1.1 PCR product was performed by using EcoR I and Nco I. The cut pSL301 was treated with CIP (Boeringer-Mannheim) and both restriction digests were purified by agarose gel electrophoresis followed by treatment with the USBioClean kit. A ligation was performed with 2 μ L Boeringer-Mannheim T4 ligase, 2 μ L 10X T4 ligation buffer, 2 μ L 10 mM ATP, 0.1 μ g digested, phosphatased pSL301, and 0.1 μ g digested X1.1 in a total volume of 20 μ L. The reaction was carried out at 4 °C overnight. The entire ligation reaction was transformed into *E. coli* strain JM105 made competent by using the RbCl Hanahan protocol (47). The transformed cells were plated onto LB plates (75 μ g/mL ampicillin). Colonies were screened by

restriction mapping with EcoR I and Nco I. The positives were labeled pSL301-*mmoX*. Approximately 1 µg of pSL301-*mmoX* and 1 µg of Y1.1 PCR product were double digested with EcoR I and Mlu I. The cut pSL301-*mmoX* was treated with CIP and both digests were purified by agarose gel electrophoresis followed by treatment with the USBioClean kit. A ligation was done with 2 µL Boeringer-Mannheim ligase, 2 µL 10X ligation buffer, 2 µL 10 mM ATP, 0.1 µg digested, phosphatased pSL301-*mmoX*, and 0.1 µg digested Y1.1 in a total volume of 20 µL. The reaction was carried out at 4 °C overnight. The entire ligation reaction was transformed into competent *E. coli* strain JM105. The transformed cells were plated onto LB plates (75 µg/mL ampicillin). Colonies were screened by restriction mapping with EcoR I and Mlu I. The positives were labeled pSL301-*mmoXY**. Approximately 1 µg of pSL301-*mmoXY** and 1 µg of Z1.1 PCR product were double digested with Mlu I and Sac I. The cut pSL301-*mmoXY** was treated with CIP, and both restriction digests were purified by agarose gel electrophoresis followed by treatment with the USBioClean kit. A ligation was carried out with 2 µL ligase, 2 µL 10X ligation buffer, 2 µL 10 mM ATP, 0.1 µg digested, phosphatased pSL301-*mmoXY**, 0.1 µg digested Z1.1 in a total volume of 20 µL. The reaction was performed at 4 °C overnight. The entire ligation reaction was transformed into competent *E. coli* strain JM105. The transformed cells were plated onto LB plates (75 µg/mL ampicillin). Colonies were screened by restriction mapping with Mlu I and Sac I. The positives were labeled pSL301-*mmoXY*Z*.

A mistake in the published sequence of the *mmoY* gene was discovered midway through the cloning procedure described above (see chapter one for a description of the error). The C-terminal cloning primer for the *mmoY* gene was, therefore, designed erroneously, and the sequence of the pDEC002 gene was not as expected. A new PCR primer, YC20 (5'-TAGTTACGCGTTTATTTTCAGTC-

CTGCCAGAAC-3') was designed to correct the error. YC20 was synthesized on a Cruachem DNA synthesizer and PAGE-purified according to manufacturer's instructions. A PCR reaction was carried out by adding 20 pmol of primer YC20, 20 pmol primer YC11, 0.1 μ g of pCH4, 2 μ L of 10 μ M dNTPs, 10 μ L 10X *Taq* polymerase reaction buffer and 1 μ L of Gibco BRL *Taq* polymerase (licensed for PCR by Hoffman-La Roche) in a total volume of 100 μ L. The samples were overlaid with 75 μ L mineral oil and placed in a thermocycler set to run the following cycle: 1X (5 min at 94 $^{\circ}$ C), 30 X (1 min at 94 $^{\circ}$ C, 1 min at 60 $^{\circ}$ C, 1 min at 72 $^{\circ}$ C), 1 X (8 min at 72 $^{\circ}$ C). The PCR reactions were cloned into the pCRII vector (purchased from Invitrogen) directly by adding 1 μ L of the PCR reaction without purification to a 10 μ L ligation reaction containing 1 μ L pCRII vector, 1 μ L ligase (from Boeringer-Mannheim) and 1 μ L ligase buffer. The ligation reactions were transformed into INV α F' cells and selection of positive *mmoY* insert clones was done by using a combination of α -complementation and restriction mapping. The *mmoY* insert of interest was isolated by cutting selected pCRII-*mmoY* clones with Mlu I and EcoR I. A sample of plasmid pSL301-*mmoXY**Z was also cut by Mlu I and EcoR I to excise the incorrect *mmoY* insert. The appropriate DNA fragment from each restriction digest was purified by use of Millipore MP filter units for purification of DNA from agarose gel slices. The *mmoY* correction insert and the pSL301-*mmoXY**Z plasmid shell were ligated together to form pSL301-*mmoXYZ*. The corrected sMMOH artificial operon was cut with Nco I and Hind III to excise the operon fragment, which was subsequently ligated into the multiple cloning site of pTrc99A to form pDEC002. The structure of this plasmid was verified by restriction mapping and is shown in Figure 2-7.

Sequencing of pDEC002. The entirety of the pDEC002 plasmid was sequenced by using the protocols and primers described in chapter one. The *mmoX*, *mmoY* and *mmoZ* genes were all sequenced completely on both sense and

antisense strands, along with approximately 100 bp on either side of the cloned genes.

Expression of MMOH by using the pDEC002 system. The pDEC002 plasmid was transfected into JM105. The standard MMOH expression experiment was as follows. A 5 mL culture grown in LB media supplemented with 100 µg/mL of ampicillin was grown to saturation overnight. A 100 µL sample of this culture was diluted into 100 mL of LB media containing 100 µg/mL ampicillin. The culture was allowed to grow until the cells reached an O.D. of 0.6 to 0.8. IPTG was added to a final concentration of 0.4 mM and the cells were allowed to grow for another 2 h. The culture was centrifuged at 4,000 rpm in a Sorvall centrifuge for 10 min, and the media was discarded. The cells were resuspended in 20 mL of cracking buffer (25 mM MOPS at pH 7, 5 mM MgCl₂, 5 mM sodium thioglycolate, 1 mM 6-aminocaproic acid, 1 mM 3,5-diaminobenzoic acid, and approximately 1 mg/mL DNase), and passed through a French Pressure Cell (SLM-Aminco) at 15,000 psi twice. The crude cell lysate was ultracentrifuged at 40,000 rpm in a Beckman ultracentrifuge for 90 min. The supernatant was saved as the soluble fraction, and the pellet was solubilized in cracking buffer with the addition of 6 M urea. An SDS-PAGE gel showing the results of a sample pDEC002 expression experiment is shown in Figure 2-8.

MMOH Inclusion Purification. A 10 mL sample of pDEC002 system inclusions (approximately 1 mg/ml) solubilized in standard cracking buffer plus 6 M urea was loaded on a 30 mL DEAE Biogel (Pharmacia) column equilibrated in 25 mM MOPS (pH 7)/6 M urea. The column was washed with 32 mL of buffer at 1 mL/min, and was washed in a NaCl gradient from 0 to 300 mM over 192 min at 1 mL/min. The column was washed with 300 mM NaCl buffer for 76 min (at 1 mL/min).

Post-Expression Refolding Experiments

Dialysis Reconstitution of Native MMO Hydroxylase Isolated from M. capsulatus (Bath). A 10 mL sample of active hydroxylase (1 mg/mL) was prepared. Powdered urea was added slowly with slow stirring to bring the sample to 6M. Stirring continued for 1 h to insure complete denaturation of protein. This sample was placed in a dialysis bag and dialyzed against 1 L of cracking buffer plus 0.5 mM ferrous ammonium sulfate for 8 h. The buffer was exchanged and dialysis was continued for another 8 h. During this time, a flocculent precipitate formed in the bag. After dialysis was complete, the contents of the bag were ultracentrifuged at 40,000 rpm for 90 min. The supernatant was drop frozen at -80 °C and the pellet was solublized in 5 mL of cracking buffer plus 6M urea. Similar experiments were performed by using 4 M guanidinium hydrochloride in place of the 6 M urea, with identical results.

Dialysis Reconstitution of Insoluble Expressed Hydroxylase Isolated from E. coli. A 3 mL sample of the insoluble sMMOH pellet described above was diluted in 27 mL of cracking buffer plus 4 M guanidine hydrochloride (approximately 1 mg/mL). A 10 mL sample of the diluted protein was placed in each of three dialysis bags (10 kDa MW cutoff). These three bags were each placed in 1 liter of cracking buffer, 1 liter of cracking buffer plus 0.5 mM ferric EDTA, and 1 liter of cracking buffer plus 0.5 mM ferrous ammonium sulfate respectively. Stirring continued for 8 h, after which time the outer buffer was exchanged, and stirring was continued for another 8 h. During this dialysis, a white flocculent precipitate formed in the bags, usually after 1 or 2 h. After dialysis was complete, the contents of the bags were ultracentrifuged at 40,000 rpm for 90 min. The supernatant was drop frozen at -80 °C and the pellet was solublized in cracking

buffer plus 4M guanidine hydrochloride. The supernatant from each of the three dialyses was analyzed on SDS-PAGE gels, shown in Figure 2-9.

Anaerobic Fe(II) Dialysis Reconstitution of Insoluble Expressed Hydroxylase Isolated from E. coli. In analogy with the *Desulfovibrio vulgaris* rubrerythrin refolding procedure (24), an anaerobic denaturant dialysis was attempted to refold the MMOH inclusions. A 5 mL volume of a 50 μ M MMOH solution in 6 M urea/cracking buffer solution was thawed in a 500 mL RB flask with a 70 μ L aliquot of β -mercaptoethanol. The flask was sealed with a septum and degassed by 20 cycles of evacuation followed by back filling with argon gas. This protein sample along with 250 mL of degassed 25 mM MOPS (pH 7) buffer and a vial of 0.1 g $\text{Fe(II)(NH}_4)_2(\text{SO}_4)_2$ and 0.01 g ascorbic acid were cycled into an anaerobic box, where the iron/ascorbate powders were added to the 250 mL of buffer. The buffer was added slowly to the protein solution over two h, diluting the urea to 120 mM. The protein solution was ultracentrifuged to remove the precipitated protein and concentrated to a volume of 10 mL in an Amicon concentrator.

This anaerobic Fe(II) refolding experiment was also carried out by using denatured MMO hydroxylase as isolated from *M. capsulatus* (Bath). All conditions were identical, except that the starting concentration of MMOH in the 5 mL sample was 5 μ M.

Sarcosyl Lysis Growth. The standard growth protocol was followed up to the resuspension step. The cells were resuspended in 10 mL of cracking buffer. A 200 μ L aliquot of 10% w/v N-lauroyl sarcosine (sarcosyl detergent) was added, and the sample was passed through the French press (2 passes, 1000-1200 psi). A 1 mL sample of 20% 1-O-octyl- β -D-glucopyranoside (octylglucoside detergent) was added and the mixture was stirred for 20 min to allow the sarcosyl to diffuse into the octylglucoside micelles. The sample was ultracentrifuged at 40,000 rpm for 90 min. The supernatant was drop frozen at -80 $^{\circ}$ C and the pellet was

solublized in cracking buffer plus 6 M urea. Both the supernatant and pellet were examined by SDS-PAGE gels, shown in Figure 2-10. All of the hydroxylase remained in the insoluble form.

Detergent Lysis Screening. Four buffer solutions containing various detergents were made according to the following procedure. All buffers contained 25 mM MOPS (pH 7), 1 mM aprotinin, 1 mM pepstatin, 1 mM PMSF and 5 mM sodium thioglycolate. Buffer NI contained 0.5 mM Nonidet P40. Buffer TW contained 0.1 mM Tween 20. Buffer DM contained 1.6 mM dodecylmaltoside. Buffer OG contained 25 mM octylglucoside.

For each of these buffers, the standard MMOH inclusion preparation was followed, excepting that the cracking buffer was replaced by detergent buffer. An SDS-PAGE gel of those samples is shown in Figure 2-11.

Sarcosyl Pellet Solubilization. The standard growth protocol for the pDEC002/JM195 system was followed to the ultracentrifugation step. After ultracentrifugation, the supernatant was drop frozen, and the pellet was resuspended in 3 mL of SPS buffer (25 mM MOPS at pH 6.95, 5 mM sodium thioglycolate {added immediately before use}, 1 mM PMSF, 20 µg/mL aprotinin, 5 µg/mL leupeptin, 2.5 µg/mL pepstatin, 1.5% sarcosyl detergent). This suspension was homogenized in a glass homogenizer. The sample was ultracentrifuged at 40,000 rpm for 20 min and the supernatant was mixed gently into 24 mL OG buffer (25 mM MOPS at pH 6.95, 5 mM sodium thioglycolate {added immediately before use}, 1 mM PMSF, 20 µg/mL aprotinin, 5 µg/mL leupeptin, 2.5 µg/mL pepstatin, 2.5% octylglucoside detergent, 1 M NaCl). This sample was ultracentrifuged for 30 min at 40,000 rpm. The supernatant was drop frozen at -80 °C and the pellet was solublized in 5 mL cracking buffer plus 6 M urea. The first and second supernatants and the pellet were analyzed by SDS-PAGE as shown in Figure 2-12. A 10 mL sample of the second supernatant was

placed in a 10 mL dialysis bag and dialyzed against 1 liter cracking buffer for 8 h to remove the octylglucoside/sarcosyl micelles. During this initial period, no protein precipitated. The outer buffer was exchanged and dialysis continued for 8 h. During this period, a white precipitate formed in the bag. After dialysis, the sample was ultracentrifuged for 30 min at 40,000 rpm. The supernatant was concentrated to 2 mL by using Centricon-10 concentrators, and the pellet was solubilized in 2 mL cracking buffer plus 6 M urea.

Alteration of Expression Conditions

Low Temperature Induction Growths. The standard growth protocol was followed, except that the 2 h induction period after addition of IPTG was carried out at 30 °C and 25 °C for two separate 500 mL growths. An additional trial was done under standard conditions, excepting that the IPTG was added at O.D. 0.2. Results as monitored by SDS-PAGE gels were identical to the 37 °C induction growths.

E. coli Strain Screening. The pDEC002 vector was transfected into the following *E. coli* strains: BL21(DE3), HMS174, HMS174(DE3), C600, HB101, K12, XL1-Blue, and JM105 (as a control). These strains were grown by following the pDEC002 protocol. All strains performed identically to JM105.

Variation of Media Content. Variants on the protein expression procedure were attempted to induce production of soluble protein. The medium was changed to M-9 minimal media, and to TYPGN (super-rich). Results were identical to those obtained under standard conditions.

Expression System Screening (pDEC010). The fragment of pDEC002 containing the artificial operon (*mmoXYZ*) was excised from the plasmid by using Nco I and Hind III and ligated into the pET11d vector to form pDEC010.

This plasmid was transfected into the BL21(DE3) strain and grown by using the pDEC002 protocol. An SDS-PAGE gel showing the results of that system is shown in Figure 2-13.

Individual Subunit Expression

Construction of pDEC05x. Linker oligonucleotides linkX1 (5'-AATTTGC-GGATCCGCTCGA-3'), linkX2 (5'-AGCTTCGAGCGGATCCGCA-3'), linkY1 (5'-CATGGAATGAGGATCCGCGT-3') and linkY2 (5'-AATTACGCGGGATCC-TCATTC-3') were synthesized on a Cruachem DNA synthesizer and were purified by PAGE according to Cruachem directions.

Plasmid pDEC002 was cut with BamH I and EcoR I and was purified from an agarose gel slice by using a Millipore MP filter unit. Approximately 0.1 µg of the pDEC002 fragment was ligated with 100 pmol of each linker oligonucleotide linkX1 and linkX2. The resulting plasmid, with the EcoR I site removed and a BamH I site added via linker design, was restriction mapped and labeled pDEC050.

Plasmid pDEC002 was cut with Nco I and EcoR I and was purified from an agarose gel slice by using a Millipore MP filter unit. Approximately 0.1 µg of the pDEC002 fragment was ligated with 100 pmol of each linker oligonucleotide linkY1 and linkY2. The resulting plasmid, with the EcoR I site removed and a BamH I site added via linker design, was restriction mapped and labeled pDEC055. The construction and structure of plasmids pDEC050 and pDEC055 are shown in Figures 2-14 and 2-15, respectively.

Construction of pDEC060. This construction is diagrammed in Figure 2-16. Plasmids pDEC050 and pET20b were digested with Nco I and Hind III. The agarose gel bands corresponding to the *mmoX* cassette and the pET20b fragment

were purified by using Millipore MP filter units. Approximately 0.1 µg of each DNA fragment were ligated together. The resulting pDEC060 plasmid was restriction mapped to confirm its structure as shown in Figure 2-17.

Construction of pDEC070. Primer oligonucleotides XN30 (5'-GCGCCATGGCACTTAGCACCGCAACC-3') and XC30 (5'-CTCAAGCTTTCA-ATTGAATGCCTTCACCGG-3') were synthesized on a Cruachem DNA synthesizer and purified by PAGE according to manufacturer's specifications. The PCR reactions were carried out by adding 2.60 µg pCH4 template DNA, 20 pmol of each primer, 2 µL of 10 µM dNTPs, 10 µL 10X *Taq* polymerase reaction buffer and 1 µL of Gibco BRL *Taq* polymerase in a total volume of 100 µL. They were placed in a thermocycler set to cycle for 1X (2 min at 94 °C), 10 X (2 min at 94 °C, 2 min at 60 °C, 6 min at 72 °C), 1 X (10 min at 72 °C). The reaction products were cloned into the pCRII vector (purchased from Invitrogen) directly by adding 1 µL of the PCR reaction directly to a 20 µL ligation reaction containing 1 µL pCRII vector, 1 µL ligase (from Boeringer-Mannheim) and 2 µL ligase buffer. The ligation reactions were transformed into INVαF' cells. Selection of insert clones was done by using α-complementation followed by EcoR I digests to identify inserts of the correct size.

The *mmoX* insert was excised by using Nco I and Hind III and ligated into the multiple cloning site of pET32a. The plasmid was labeled pDEC070 and restriction mapped. Its construction is shown in Figure 2-16, and its structure is shown in Figure 2-17.

Simple MMOH subunit expression - pDEC05x. Both pDEC050 and pDEC055 were transformed into JM105. A 5 mL culture of each strain was grown in LB amp media (100 µg/mL ampicillin) to saturation overnight. A 1 mL sample of this culture was diluted into 1000 mL of LB amp media. The culture was allowed to grow until the cells reached an O.D. of 0.6. IPTG was added to a final

concentration of 0.4 mM and the cells were allowed to grow for another 2 h. The culture was centrifuged at 4,000 rpm in a Sorvall centrifuge for 10 min, and the LB supernatant was discarded. The cells were resuspended in 40 mL of cracking buffer (25 mM MOPS at pH 7, 5 mM MgCl₂, 5 mM sodium thioglycolate, 1 mM 6-aminocaproic acid, 1 mM 3,5-diaminobenzoic acid, and approximately 1 mg/mL DNase), and passed through a French Pressure Cell (SLM-Aminco) at 15,000 psi twice. The crude cell lysate was ultracentrifuged at 40,000 rpm in a Beckman ultracentrifuge for 90 min. The supernatant was saved as the soluble fraction, and the pellet was solublized in cracking buffer with the addition of 6 M urea. The results of this expression are shown in Figure 2-18.

Periplasmic Expression of sMMOH α - pDEC060. The pDEC060 plasmid was transformed into BL21(DE3) cells. A cell culture procedure identical to the one described above was carried out by using that strain. Results are shown in Figure 2-19.

Thioredoxin-sMMOH α subunit expression. A 10 mL culture of an AD494(DE3)/pDEC070 strain containing the sMMOH α -thioredoxin fusion gene was grown in LB amp media (100 μ g/mL ampicillin) to saturation overnight. A 6 mL culture sample was diluted into 6 L of LB amp media. The culture was cooled to 20 °C after the cells reached an O.D. of 0.6. IPTG (Boehringer-Mannheim) was added to a final concentration of 0.4 mM and the cells were allowed to grow for another 2 h at 20 °C. The culture was centrifuged at 4,000 rpm in a Sorvall centrifuge for 10 min, and the LB supernatant was discarded. The cells were resuspended in 40 mL of cracking buffer (25 mM MOPS at pH 7, 5 mM MgCl₂, 5 mM sodium thioglycolate, 1 mM Pefabloc SC, and approximately 1 mg/mL DNase), and passed through a French Pressure Cell (SLM-Aminco) at 15,000 psi twice. The crude cell lysate was ultracentrifuged at 40,000 rpm in a Beckman

Ultracentrifuge for 90 min. The supernatant contained the soluble portion of the sMMOH alpha-thioredoxin fusion, and was saved for purification.

Purification of sMMOH α . The soluble cell lysate was applied to a 25 mL Ni²⁺-NTA resin column at 1 mL/min. Following loading, the column was washed with buffer containing 20 mM Tris at pH 7.9, 500 mM NaCl and 5 mM imidazole at 1 mL/min. The bound proteins were eluted by using a gradient of 5 mM imidazole to 150 mM imidazole over 1 h at 1 mL/min, followed by washing of the column with 150 mM imidazole over 1 h at 1 mL/min. The alpha-thioredoxin fusion elutes at approximately 100 mM in a very broad peak.

The crude alpha-thioredoxin fraction was exchanged into buffer containing 20 mM Tris pH 7.9, 150 mM NaCl and 2.5 mM CaCl₂ and concentrated to a volume of approximately 10 mL. 3 units of thrombin (Novagen) were added to the crude mixture, and the cleavage reaction was allowed to proceed for 16 h at 4 °C.

The crude protein solution was applied to a 25 mL Ni²⁺-NTA resin column at 1 mL/min. The flow-through fractions containing pure alpha subunit were collected.

Protein samples were analyzed by using SDS-PAGE gels and Western blotting. Protein concentrations were determined by using ELISAs. Iron concentration was determined by using the ferrozine assay. Results are shown in Figure 2-21.

EPR Mixed-Valent Sample Preparation. Protein samples, either native hydroxylase or expressed sMMOH α , of approximate concentration 50 μ M and approximate volume of 250 μ L were prepared by concentration in Centriprep 10 concentrator units. Stoichiometric amounts of the mediators potassium indigo tetrasulfonate, methylene blue and phenazine methosulfate were added to the sample. The sample was degassed by 15 cycles of vacuum evacuation followed

by argon backfilling. A degassed solution of 5 mM sodium dithionite in 50 mM MOPS (pH 8.6) buffer was made and used to titrate the protein solution until the methylene blue changed from blue to yellow. The sample was anaerobically transferred to a quartz EPR tube and frozen in liquid nitrogen. Results are shown in Figure 2-22.

EPR Reduced Sample Preparation. Expressed sMMOH α samples of approximate concentration 100 μ M and approximate volume of 250 μ L were prepared by concentration in Centriprep 10 concentrator units. A stoichiometric amount of the mediator methyl viologen was added to the sample. The sample was degassed by 15 cycles of vacuum evacuation followed by argon backfilling. A degassed solution of 5 mM sodium dithionite in 50 mM MOPS (pH 8.6) buffer was made and used to titrate the protein solution until the methyl viologen changed from yellow to blue. The sample was anaerobically transferred to a quartz EPR tube and frozen in liquid nitrogen.

Results

The template for most of the PCR cloning discussed above was the pCH4 plasmid, a gift from Prof. J. Colin Murrell. This plasmid is a cDNA copy of the entire sMMO operon cloned into pBR325 (48). The sequence and structure of this operon can be found in chapter one. The initial pDEC002 plasmid cassettes (*mmoX*, *mmoY** and *mmoZ*) were amplified from a genomic DNA sample directly prepared from *M. capsulatus* (Bath) cell paste.

The plasmids in this chapter were designed by using the commonly used expression-cassette strategy (49). This methodology allows for very precise control over the design of the expression plasmid. By designing PCR primers with mismatches at the 5' end, one can insert any desired sequence at the ends of

the PCR cassettes, including spacers, restriction sites and ribosome binding sites. The disadvantage is that PCR based cloning often results in sequences with mistakes since *Taq* polymerase does not have the full array of error checking machinery that many other DNA polymerases do.

The design for the first useful plasmid constructed, pDEC002, shown in Figure 2-7, was intended to create a simplified sMMO operon that would only express the three subunits of the hydroxylase. Upon induction of expression, the *E. coli* cell culture color changed from an ordinary yellowish color to white. Observation of the cells under the microscope revealed that the cells had large white organelles taking up approximately 10-25% of the cell volume. These white 'bodies' were collected by cell lysis followed by centrifugation. The peptide component of the aggregate was solubilized with denaturants such as urea and guanidinium hydrochloride, which showed the white material to be entirely protein. SDS-PAGE analysis revealed that the protein was approximately 50% hydroxylase peptides that had been misfolded and packaged as inclusion bodies.

Several lines of research were followed in an attempt to obtain active hydroxylase from the pDEC002 plasmid. A system that produces inclusion bodies can actually be an advantage if one is able to induce the collected protein to refold into an active form. The packaging of the misfolded, expressed protein allows it to be easily collected and purified away from other *E. coli* proteins. Therefore, among the first experiments tried was to refold the hydroxylase via a denaturation/renaturation cycle.

Use of hydrogen-bond disrupting salts such as urea and guanidinium hydrochloride as a denaturant and then removing those salts by dialysis or dilution did not afford any detectable soluble hydroxylase. This basic theme was varied by changing the rate of dialysis/dilution, the presence of 'helper' molecules such as thiols, Fe(III) or Fe(II), and the nature of the denaturant. A few

detergents were screened, including N-lauroyl sarcosine, which is reported in the literature as an excellent additive for refolding. The only method that exhibited encouraging results was a technique labeled in the text above as sarcosyl pellet solubilization. The detergent N-lauroyl partially solubilized the sMMOH aggregate, but removal of the detergent induced the protein to precipitate out of solution.

Since the sMMOH expresses and folds correctly in its native host, *M. capsulatus* (Bath), it seems reasonable to conclude that there is either some factor missing in the *E. coli* cytoplasm that is necessary for correct folding, or some factor present in *E. coli* that is causing misfolding. It follows that an effort to make the *E. coli* cytoplasm more like the *M. capsulatus* (Bath) cytoplasm might cause the sMMOH to fold properly upon expression

One of the most basic differences between the sMMOH native expression system and the designed system is the speed of expression. The native system produces peptides slowly and steadily. The artificial system produces peptides very quickly upon induction. One consequence of this difference is that there is a large number of folding intermediates present in the cell after induction. One might imagine that these folding intermediates might interact with one another, forming long, polymeric, insoluble chains that would aggregate. This model for inclusion body formation is the most prevalent one in the literature (43).

To reduce this folding intermediate problem, there are a number of methods one can employ. Reducing the temperature, the IPTG concentration, or both, can greatly reduce the amount of folding intermediates. This method often works in the literature, but was unsuccessful in the sMMOH case. Changing media content has also been successful in some cases, but was not useful for the pDEC002 system.

Changing the expression system has been helpful in producing soluble protein from some inclusion body systems. In particular, with multisubunit proteins, expression of the subunits individually can be of use. Accordingly, a series of plasmids with the three subunits separated was constructed. Emphasis was placed on expression of the MMOH α subunit, as there was the possibility of it being useful on its own, even if expression of MMOH β and MMOH γ were unsuccessful, or if reconstitution of the three subunits was not possible.

The first vector constructed, pDEC050, was designed to express the native MMOH α . Not unexpectedly, the subunit was expressed as inclusion bodies. The pDEC055 plasmid, constructed as a counterpart to pDEC050, was intended to serve as a source of β and γ subunit. The system failed to produce any proteins, either soluble or insoluble. It seems most likely that the long space between the pTrc promoter and the ribosome binding site, which was enforced by the linker design, caused expression to fail. The plasmid pDEC060 was designed to attach the *pelB* leader sequence onto the α subunit. The *pelB* sequence directs the nascent polypeptide to be secreted into the periplasmic space. The periplasm is a very different environment from the cytoplasm. The protein concentration is lower, and the reduction potential is much more oxidizing. Unfortunately, no soluble protein was afforded by this system.

The next vector made, pDEC070, was much more promising. The construction of the vector expressed a fusion protein of the MMOH α with the protein thioredoxin. Thioredoxin fusions are often quite soluble, and are popular for use in solving inclusion body problems. In addition, the vector contained a His6 site for simple purification and an S-Tag site for simple detection via Western blot. Although approximately 90% of the expressed MMOH α -thioredoxin was insoluble, the rest was soluble. It was quite unstable to protease digestion, however, requiring the presence of the protease inhibitor Pefabloc SC

(Boeringer-Mannheim). Purification on two successive nickel resin columns, with a thrombin cleavage step between the two to separate the thioredoxin from the MMOH α , afforded milligram amounts of pure α with approximately 2 irons per subunit, as expected.

The expressed soluble MMOH α has no measurable hydroxylase activity, however. The recombinant material also exhibited no mixed-valent or reduced signal in the EPR, which are hallmarks of the native hydroxylase. It seems, therefore, that the expressed material is folded only into a soluble form, not a native one. It is not unusual to see small amounts of soluble, non-native, misfolded material produced along with insoluble inclusion bodies. Samples of MMOH α with no measurable properties are of limited utility.

Discussion and Conclusions

The work described above has taught us about the folding pathway of the hydroxylase. The MMOH γ subunit can refold into a soluble unit spontaneously, as shown by refolding experiments. This result is not surprising, given knowledge of the crystal structure. The MMOH γ subunit caps the ends of the flat hydroxylase molecule. A large proportion of its surface area is exposed to solvent. This property contrasts with that of the MMOH α and MMOH β subunits, which have extensive contacts with one another. It seems likely that the α and β subunits might have to fold together to reach a native conformation.

However, the folding of the MMOH α subunit must proceed normally to a point. The material obtained from the inclusion bodies contained iron at an approximate level of two irons per MMOH α . There are two domains in the α subunit, domain 1 and domain 2 (16). It is possible that domain 1, which houses

the iron site and that has the same fold as the soluble R2 subunit, folds well, and that domain 2 does not.

Nevertheless, the hydroxylase does not fold into its native form in the *E. coli* cytoplasm or under *in vitro* conditions. It seems that there is some specific, unknown condition for correct folding that has not been met in the experiments described above. There are several possibilities for the identity of this condition. It may be some cytoplasmic physical condition, such as pH, salt concentration or reduction potential, that was not reproduced in the conditions described above. It may be that some specific *M. capsulatus* (Bath) "foldase" protein is necessary for refolding, such as a chaperonin, or a disulfide bridge reducing protein. It might also be that it is important for the sMMO polypeptides to be produced with specific timing enforced by the *M. capsulatus* (Bath) ribosomal machinery. This might be controlled by the spacing between the ribosomal binding sites and the beginnings and ends of the sMMO genes, or by pauses induced by *M. capsulatus* (Bath) codon preferences.

These possibilities suggest several possible methods for expression of the hydroxylase. The possibilities for use of the *E. coli* organism as a host have not been exhausted. Most of the simple "*in vivo*" experiments have been done. It does not seem that the *E. coli* cytoplasm is a hospitable place for sMMOH refolding. Refolding the collected hydroxylase inclusion bodies outside the cell is still a viable possibility. The refolding work described above does not exhaust all possibilities. A methodical search through possible refolding conditions, varying pH, temperature, salt concentration, thiol concentration and reduction potential, might result in native enzyme.

A second possibility is to use the existing system for producing soluble α subunit and combine it with a system for producing β and γ subunit. Since the existing samples of the α subunit have 2 irons per peptide, as expected, this

subunit is most likely partially assembled. It is possible that combining the expressed α subunit with expressed or native β and γ subunit would produce active hydroxylase indistinguishable from the native material. It is not clear how to recombine the subunits to form active material, because the native hydroxylase cannot be disassembled except under highly denaturing conditions. Nevertheless, this method is a possible avenue for hydroxylase expression.

A third possibility for expression of the sMMO hydroxylase is to extend efforts into other organisms that may have cytoplasmic conditions more like *M. capsulatus* (Bath). The pseudomonad *Pseudomonas putida* would be a prime choice, since the *M. trichosporium* sMMOH has been expressed successfully in it already (38). The methylotrophic yeast *Pichia pastoris* is a possibility. It is a valuable alternative in expression of proteins that have been problematic in *E. coli*, and it may share C1 metabolic enzymes with *M. capsulatus* (Bath). A final option is to express in *M. capsulatus* (Bath) itself. This is, by far, the most challenging option, but it is the only organism that the sMMOH is known to fold correctly in. It is challenging because little is known of its molecular biology, other than it is very difficult to culture on solid media. In addition, there is the problem of *M. capsulatus* (Bath) expressing large amounts of the native sMMOH in addition to the mutant sMMOH. This problem could be solved by expressing the pMMO, instead of the sMMO, by use of culture media containing copper. Alternatively, one could produce *M. capsulatus* (Bath) hydroxylase knock-out strains by using procedures described in the literature (37). If one assumes that the technical problems associated with *M. capsulatus* (Bath) could be solved, then use of a wide host range plasmid that contains both the genes necessary for its own replication and the sMMO genes under an inducible promoter would be the favored route for expression.

References

1. Higgins, I. J., Best, D. J., Hammond, R. C., and Scott, D. (1981) *Microbiol. Rev.* 45, 556-590.
2. Higgins, I. J., Best, D. J., and Hammond, R. C. (1980) *Nature* 286, 561-564.
3. Dalton, H. (1992) in *Methane and Methanol Utilizers* (Murrell, J. C., and Dalton, H., Eds.) pp 85-114, Plenum Press, New York.
4. Lidstrom, M. E., and Stirling, D. I. (1990) *Annu. Rev. Microbiol.* 44, 27-58.
5. Best, D. J., and Higgins, I. J. (1983) in *Topics in Enzyme and Fermentation Biotechnology I* pp 38-75.
6. Sheldon, R. A. (1983) *Chemicals from Synthesis Gas*, D. Reidel Publishing Co., Dordrecht, Holland.
7. Valentine, A. M., and Lippard, S. J. (1997) *J. Chem. Soc., Dalton Trans.* 21, 3925-3931.
8. Wallar, B. J., and Lipscomb, J. D. (1996) *Chem. Rev.* 96, 2625-2657.
9. Liu, K. E., and Lippard, S. J. (1995) *Adv. Inorg. Chem.* 42, 263-289.
10. Lipscomb, J. D. (1994) *Annu. Rev. Microbiol.* 48, 371-399.
11. Nordlund, P., and Eklund, H. (1993) *J. Mol. Biol.* 232, 123-164.
12. Stubbe, J. (1990) *J. Biol. Chem* 265, 5329-5332.
13. Fox, B. G., Shanklin, J., Ai, J., Loehr, T. M., and Sanders-Loehr, J. (1994) *Biochemistry* 33, 12776-12786.
14. Powlowski, J., and Shingler, V. (1990) *J. Bact.*, 6834-6840.
15. Yen, K.-M., Karl, M. R., Blatt, L. M., Simon, M. J., Winter, R. B., Fausset, P. R., Lu, H. S., Harcourt, A. A., and Chen, K. K. (1991) *J. Bact.* 173, 5315-5327.
16. Rosenzweig, A. C., Frederick, C. A., Lippard, S. J., and Nordlund, P. (1993) *Nature* 366, 537-543.

17. Rosenzweig, A. C., Nordlund, P., Takahara, P. M., Frederick, C. A., and Lippard, S. J. (1995) *Chemistry & Biology* 2, 409-418.
18. Nordlund, P., Dalton, H., and Eklund, H. (1992) *FEBS Lett.* 307, 257-262.
19. Feig, A. L., and Lippard, S. J. (1994) *Chem. Rev.* 94, 759-805.
20. Licht, S., Gerfen, G. J., and Stubbe, J. (1996) *Science* 271, 477-481.
21. Regnström, K., Åberg, A., Ormö, M., Sahlin, M., and Sjöberg, B.-M. (1994) *J. Biol. Chem.* 269, 6355-6361.
22. Rosenzweig, A. C., Frederick, C. A., and Lippard, S. J. (1996) in *Microbial Growth on C1 Compounds* (Lidstrom, M. E., and Tabita, F. R., Eds.) pp 141-149, Kluwer Academic Publishers, Dordrecht.
23. Rosenzweig, A. C., Brandstetter, H., Whittington, D. A., Nordlund, P., Lippard, S. J., and Frederick, C. A. (1997) *Proteins* 29, 141-152.
24. Gupta, N., Bonomi, F., Kurtz, D. M., Ravi, N., Wang, D. L., and Huynh, B. H. (1995) *Biochemistry* 34, 3310-3318.
25. Fox, B. G., Shanklin, J., Somerville, C., and Münck, E. (1993) *Proc. Natl. Acad. Sci. USA* 90, 2486-2490.
26. Broadwater, J. A., and Fox, B. G. (1996) *iNovations* 4a, 8-9.
27. Yen, K.-M., and Karl, M. R. (1992) *J. Bact.* 174, 7253-7261.
28. Teschke, C. M., and King, J. (1992) *Curr. Op. Biotech.* 3, 468-473.
29. McNally, E., Sohn, R., Frankel, S., and Leinwand, L. (1991) *Meth. Enz.* 196, 368-389.
30. Frankel, S., Sohn, R., and Leinwand, L. (1991) *Proc. Natl. Acad. Sci. USA* 88, 1192-1196.
31. Garboczi, D. N., Hung, D. T., and Wiley, D. C. (1992) *Proc. Natl. Acad. Sci. USA* 89, 3429-3433.
32. Zomerdijk, J. C. B. M., Beckmann, H., Comai, L., and Tijan, R. (1994) *Science* 266, 2015-2018.

33. Lu, W.-P., Schiau, I., Cunningham, J. R., and Ragsdale, S. W. (1993) *J. Biol. Chem.* 268, 5605-5614.
34. Wu, W., Rosenzweig, A., and Lippard, S. J. (1989) *Unpublished Results*.
35. Blazyk, J., and Lippard, S. J. (1998) *Unpublished Results*.
36. West, C. A., Salmond, G. P. C., Dalton, H., and Murrell, J. C. (1992) *J. Gen. Microbiol.* 138, 1301-1307.
37. Martin, H., and Murrell, J. C. (1995) *FEMS Microbiol. Lttrs.* 127, 243-248.
38. Jahng, D., and Wood, T. K. (1994) *App. Env. Microbiol.* 60, 2473-2482.
39. Mitraki, A., and King, J. (1989) *Biotechnology* 7, 690-697.
40. Jaenicke, R., and Ruldolph, R. (1990) in *Protein structure: A practical approach* (Creighton, T., Ed.) pp 191-223, IRL Press, Oxford.
41. Marston, F. A. O. (1986) *Biochem. J.* 240, 1-12.
42. Fischer, B., Sumner, I., and Goodenough, P. (1993) *Biotech. Bioeng.* 41, 3-13.
43. Mitraki, A., Haase-Pettingell, C., and King, J. (1991) in *Protein Refolding* (Georgiou, G., and Bernardez-Clark, E. D., Eds.), ACS Symposium Series.
44. Lin, K.-H., and Cheng, S.-Y. (1991) *BioTechniques* 11, 748-751.
45. DeWitt, J. G., Bentsen, J. G., Rosenzweig, A. C., Hedman, B., Green, J., Pilkington, S., Papaefthymiou, G. C., Dalton, H., Hodgson, K. O., and Lippard, S. J. (1991) *J. Am. Chem. Soc.* 113, 9219-9235.
46. Liu, K. E., Johnson, C. C., Newcomb, M., and Lippard, S. J. (1992) *J. Am. Chem. Soc.* 115, 939-947.
47. Hanahan, D. (1985) in *DNA Cloning: A Practical Approach* (Glover, D. M., Ed.) pp 109-35, IRL press, Oxford.
48. Stainthorpe, A. C., Murrell, J. C., Salmond, G. P. C., Dalton, H., and Lees, V. (1989) *Arch. Microbiol.* 152, 154-159.
49. MacFerrin, K. D., Chen, L., Terranova, M. P., Schreiber, S. L., and Verdine, G. L. (1993) in *Meth. Enz.* pp 79-102.

Figure 2-1. Methylotrophs in the carbon cycle.

This schematic depicts the reclamation of small organic compounds into the carbon cycle. The process begins with heterotrophic catabolism of complex hydrocarbons, typically biological in origin, to small molecules. The products of this process descend to lower layers of the soil where the dioxygen concentration is low. Organisms called methanogens reductively metabolize the small organic waste products to methane, generating energy for themselves. The methane gas produced diffuses towards the surface. Where the dioxygen concentration is high, the methylotrophs can subsist on this methane as a source of carbon and energy, releasing carbon dioxide as a waste product. Thus, carbon is returned to the large pool of CO₂ in the atmosphere.

This cartoon shows one location where methylotrophs can prosper. Any space where methane and oxygen coexist, such as marshlands or geothermal gas vents, could be imagined as a home for these unique organisms.

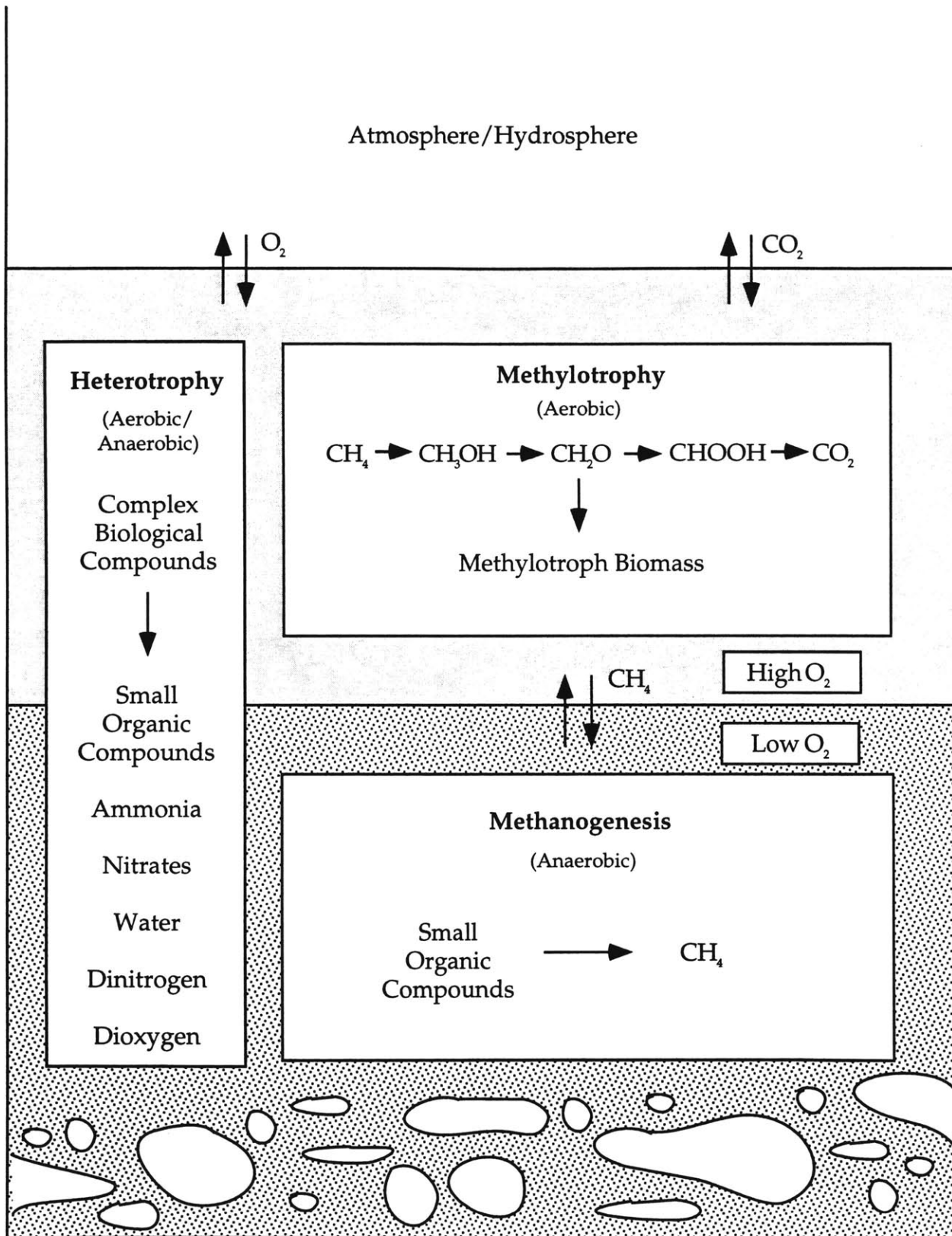


Figure 2-1

Figure 2-2. Metabolism of methane in *M. capsulatus* (Bath).

The first step, oxidation of methane to methanol, is catalyzed by MMO. One NADH molecule must be consumed for every turnover. The second step, oxidation of methanol to formaldehyde, is catalyzed by methanol dehydrogenase. A NADH equivalent, PQQH₂, is generated by this reaction, making the first two reactions energy neutral up to this point. At the formaldehyde step, the organism can choose between assimilation of the carbon or generation of energy by oxidizing the CH₂O to CO₂ via formaldehyde dehydrogenase and formate dehydrogenase.

A more detailed account of this metabolic pathway along with related reactions can be found at <http://www.expasy.ch/cgi-bin/show_image?D5>.

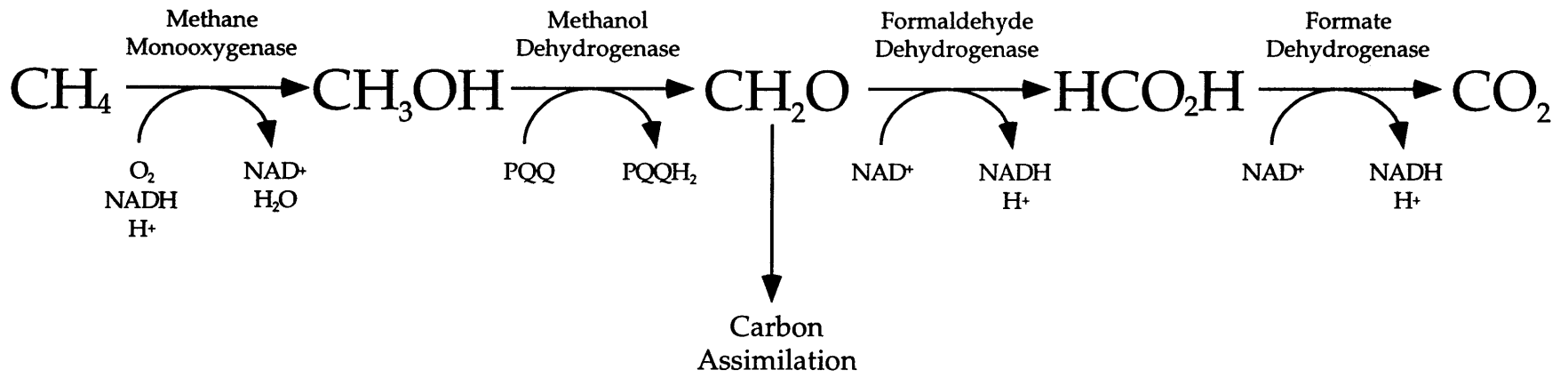


Figure 2-2

Figure 2-3. Native sMMOH PAGE.

An SDS-PAGE gel showing the purified native sMMOH from *M. capsulatus* (Bath). The samples vary in quality, and represent a range of the purest protein available at the time.

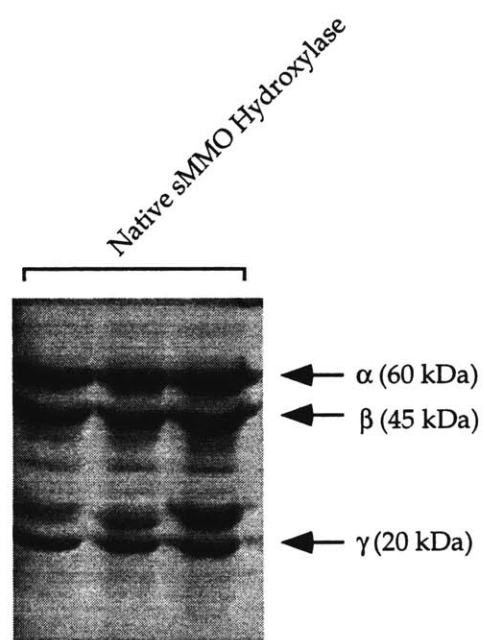
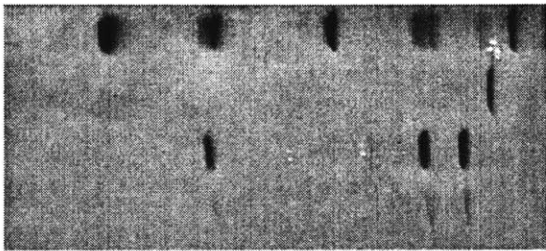


Figure 2-3

Figure 2-4. Sample Western Blot.

An SDS-PAGE gel with a matched Western blot showing typical results obtained. The sMMOH α variation shown in the Figure is a sMMOH α -thioredoxin fusion protein discussed later in the chapter. The additional proteins visible in the hydroxylase lane of the Western blot are due to strong interactions between the hydroxylase impurities and antibodies against those impurities in the sMMOH polyclonal antiserum.

SDS-PAGE



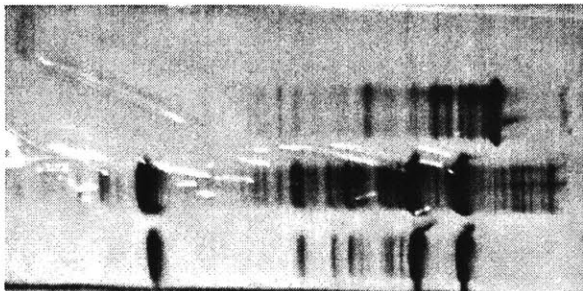
MW Standards

Variation on sMMOH α

sMMOH

sMMOH (1/10 loading)

Western



MW Standards

Variation on sMMOH α

sMMOH

sMMOH (1/10 loading)

Figure 2-4

Figure 2-5. PCR of the sMMOH genes.

Agarose gel showing the results of PCR amplifications of the *mmoX*, *mmoY* and *mmoZ* genes from *M. capsulatus* (Bath) genomic DNA.

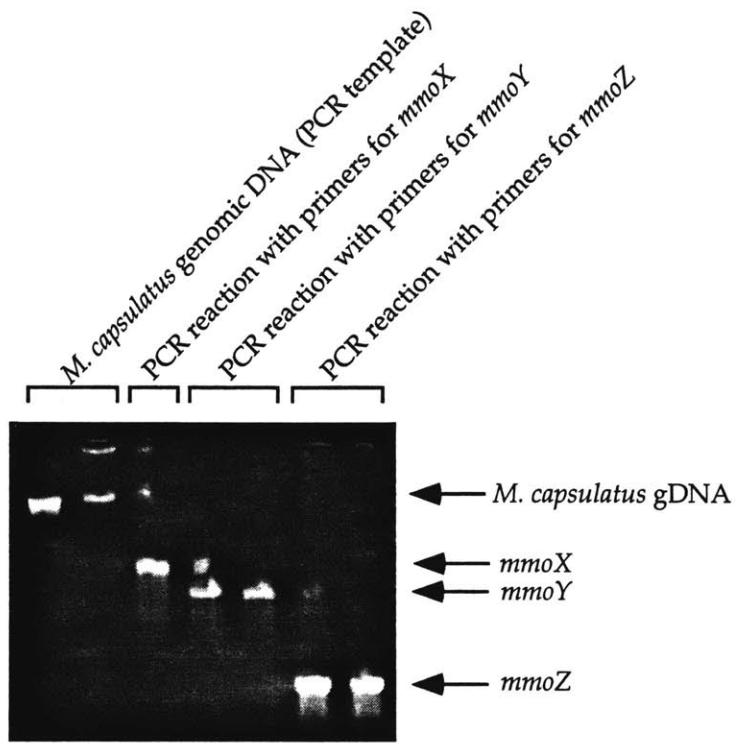


Figure 2-5

Figure 2-6. Construction of pDEC002.

PCR cassettes for the *mmoX*, *mmoY* and *mmoZ* genes were inserted one at a time into the superlinker plasmid pSL301. The *mmoY** gene was generated from an incorrect PCR primer pair that was designed before it was discovered that the published gene sequence of the *mmoY* gene contained a frame shift mistake (see chapter one). A new primer pair based on the correct sequence was designed and the new *mmoY* gene was inserted into the pSL301-*mmoXY*Z* plasmid. The assembled artificial sMMOH operon was excised and ligated into the pTrc99A gene to make pDEC002.

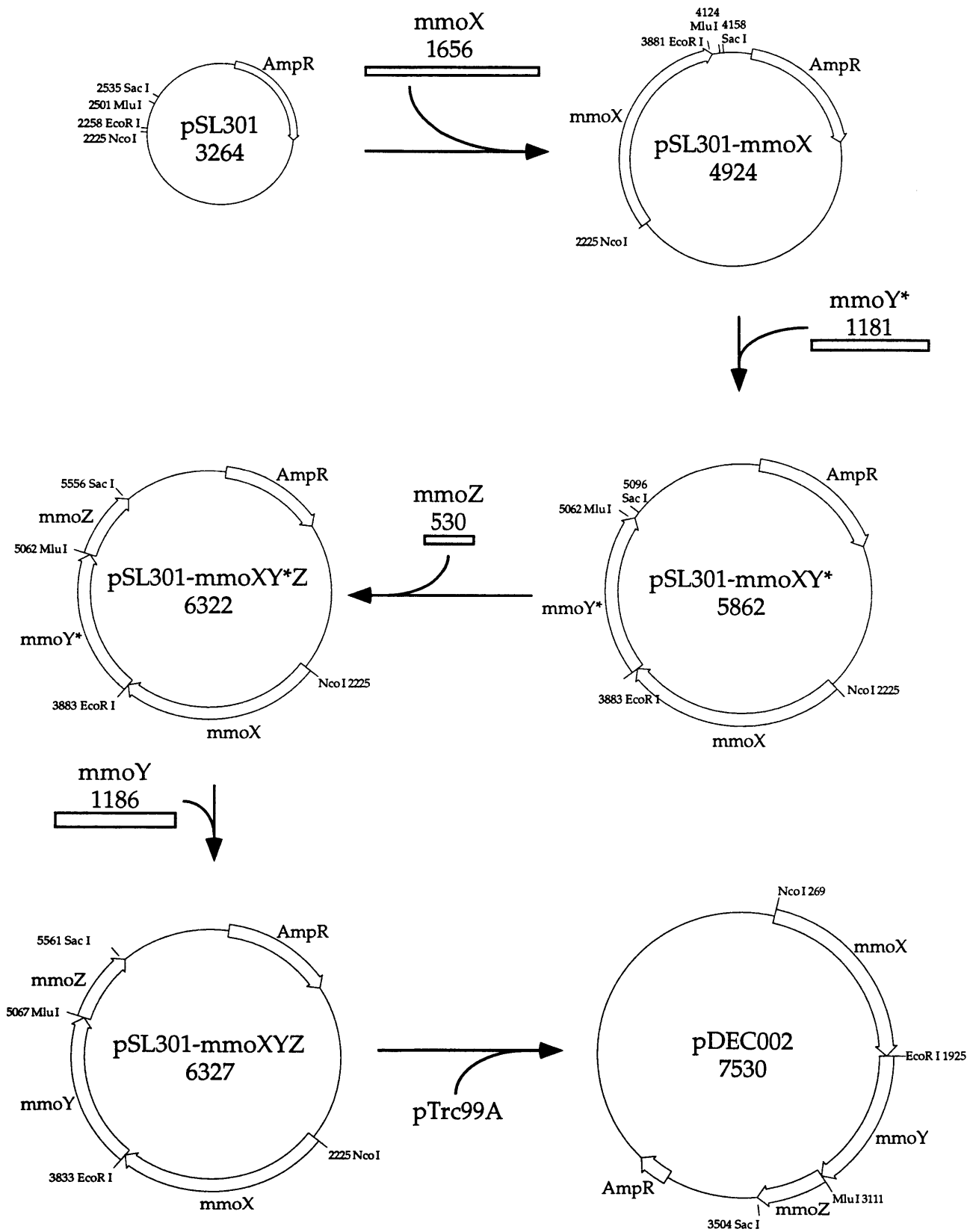


Figure 2-6

Figure 2-7. Structure of pDEC002.

Expression of the *mmoX*, *mmoY* and *mmoZ* genes are controlled by the pTrc promoter, based on a combination of the *E. coli* lac and trp promoters. Immediately following the *mmoZ* gene is a small multiple cloning site and the *rrnB* transcription termination region, designed to prevent run-through transcription. Additional features of the plasmid include the β -lactamase gene for ampicillin resistance, the pBR322 origin of replication, and a copy of the *lacIq* gene for production of the lac repressor and successful expression in *lac*⁻ hosts.

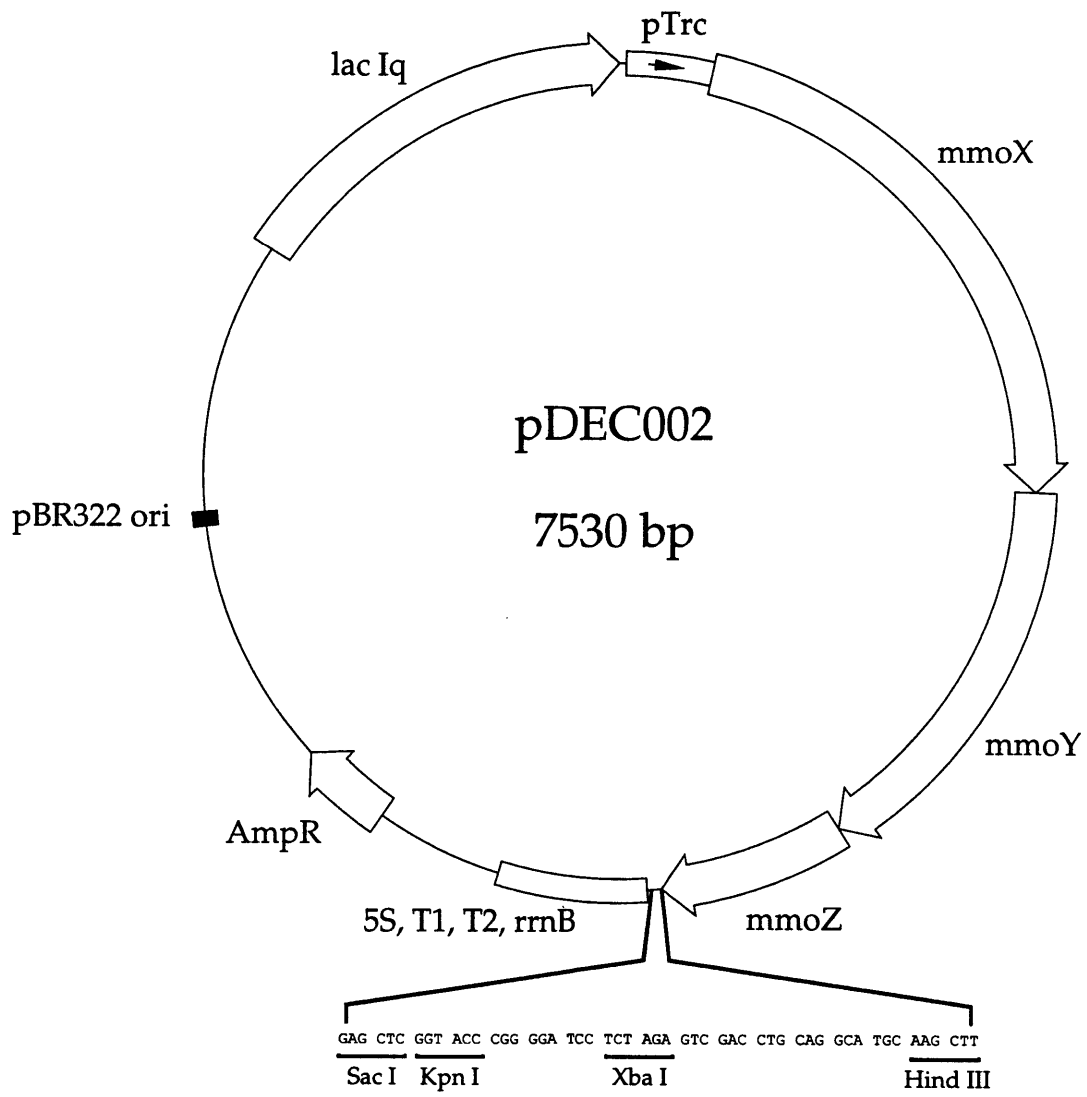


Figure 2-7

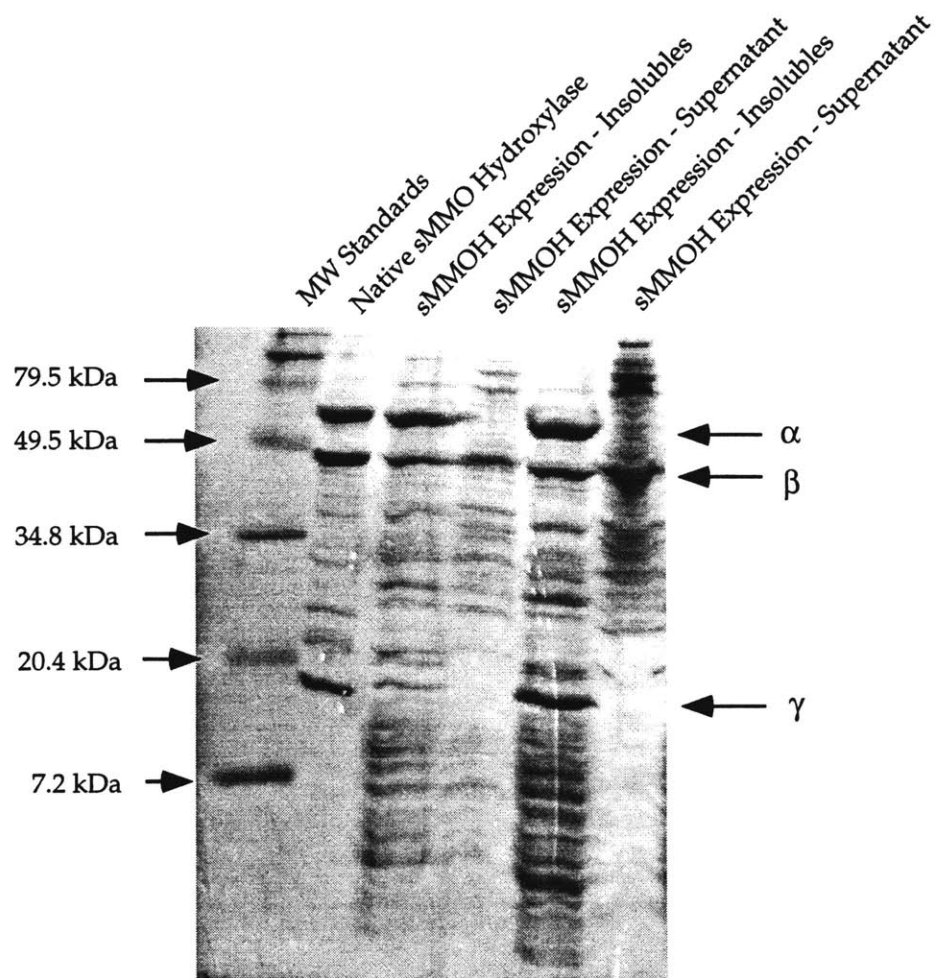


Figure 2-8

Figure 2-8. Expression of sMMOH genes in *E. coli* results in inclusion bodies.

An SDS-PAGE gel showing the results of expression of the sMMOH genes in pDEC002 in *E. coli* JM105. The sMMOH subunits are clearly visible in only the insoluble lanes. The dark band near the MMOH β subunit in the soluble fractions is a native *E. coli* protein present in controls.

Figure 2-9. Attempted refolding of expressed, insoluble sMMOH under a variety of conditions.

An SDS-PAGE gel shows the results of several refolding experiments with two different iron sources. Note that the γ subunit refolds.

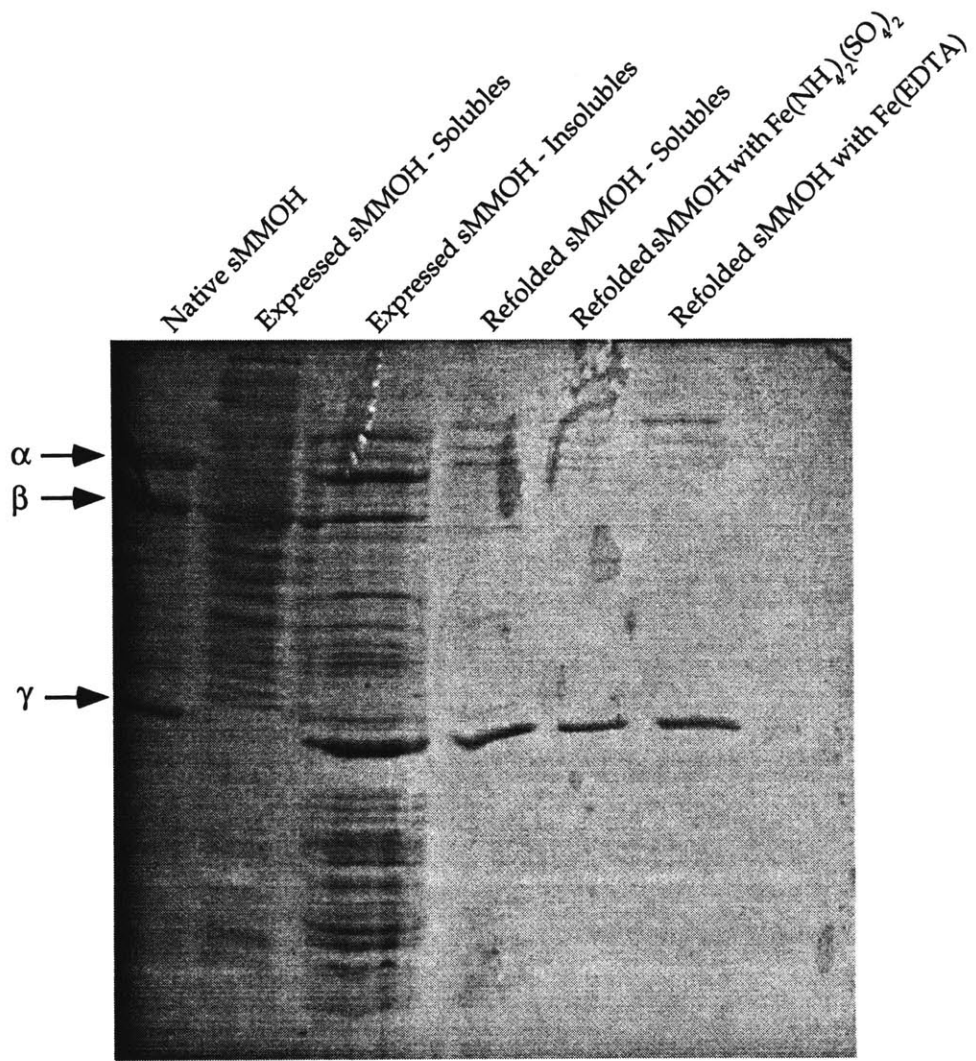


Figure 2-9

Figure 2-10. Expression of sMMOH from pDEC002 by using a sarcosyl lysis procedure.

An SDS-PAGE gel shows the results of lysing the *E. coli* containing expressed sMMOH inclusions in the presence of sarcosyl detergent. The photo is a compilation of several lanes from a single gel.

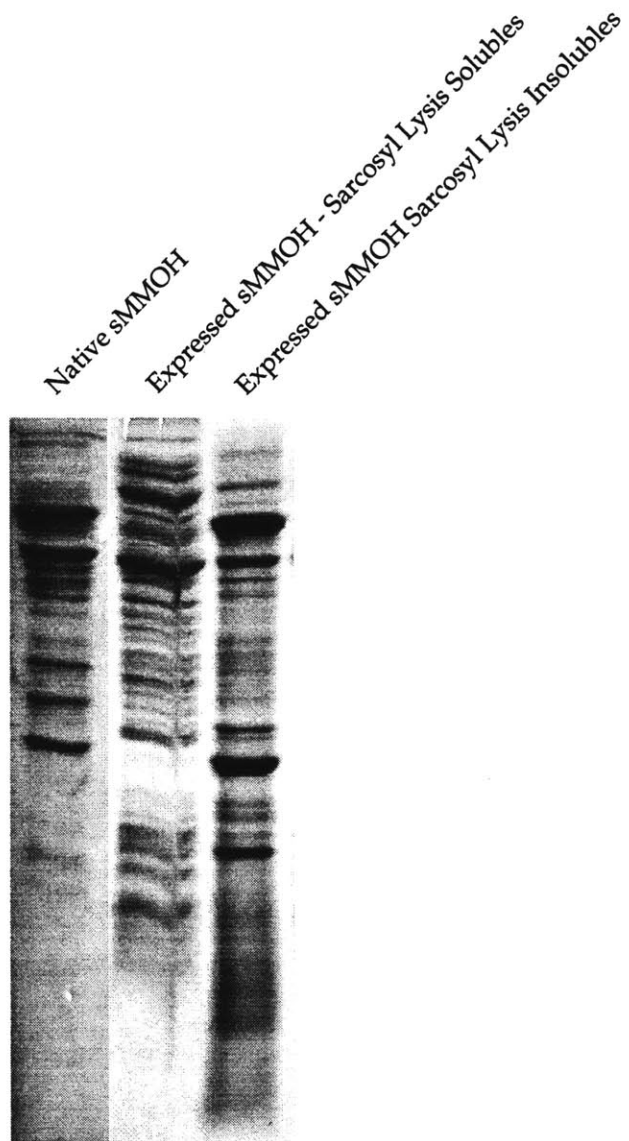


Figure 2-10

Figure 2-11. Attempted reconstitution of the expressed, insoluble sMMOH by using detergents.

An SDS-PAGE gel shows the results of reconstituting the expressed sMMOH in a variety of detergents.

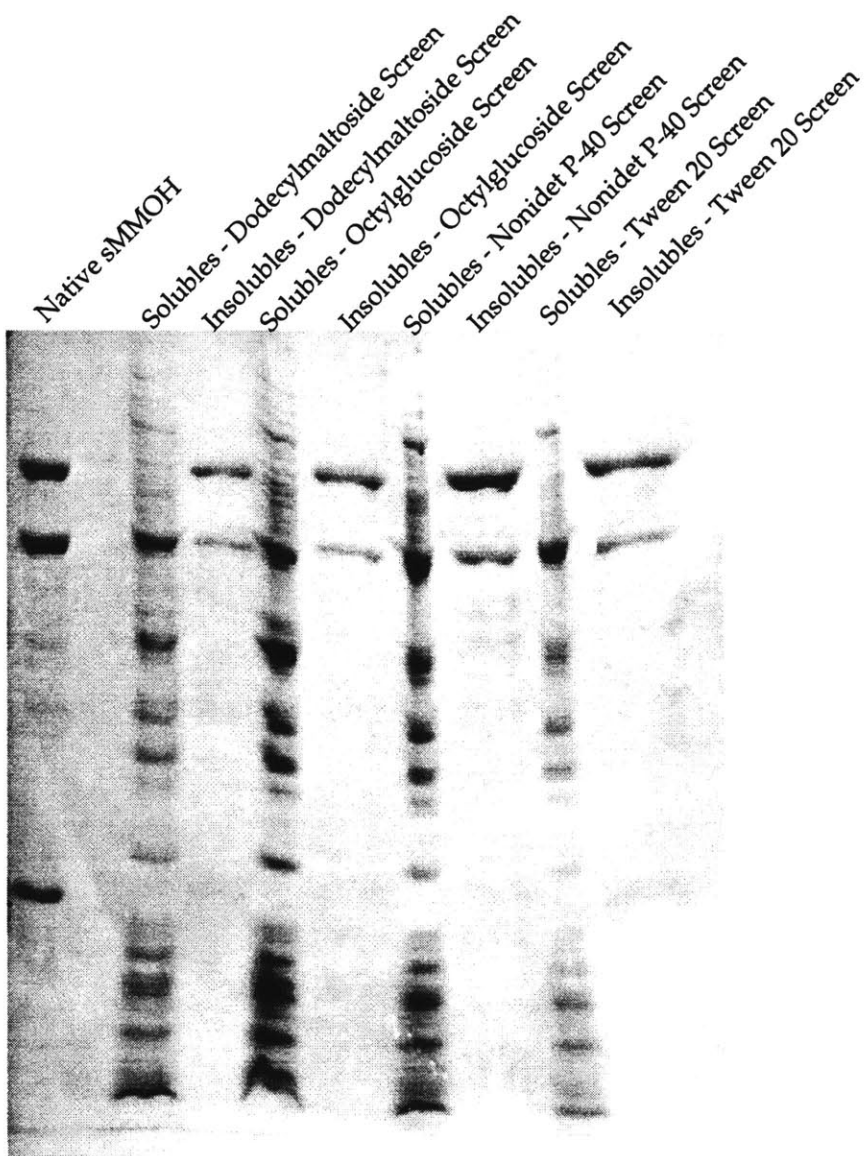


Figure 2-11

Figure 2-12. Attempted reconstitution of the expressed, insoluble sMMOH by using sarcosyl detergent.

An SDS-PAGE gel shows the results of reconstituting the expressed sMMOH with sarcosyl detergent. Note that the sarcosyl resolubilized a portion of the sMMOH, but removal of the sarcosyl resulted in the reprecipitation of the protein.

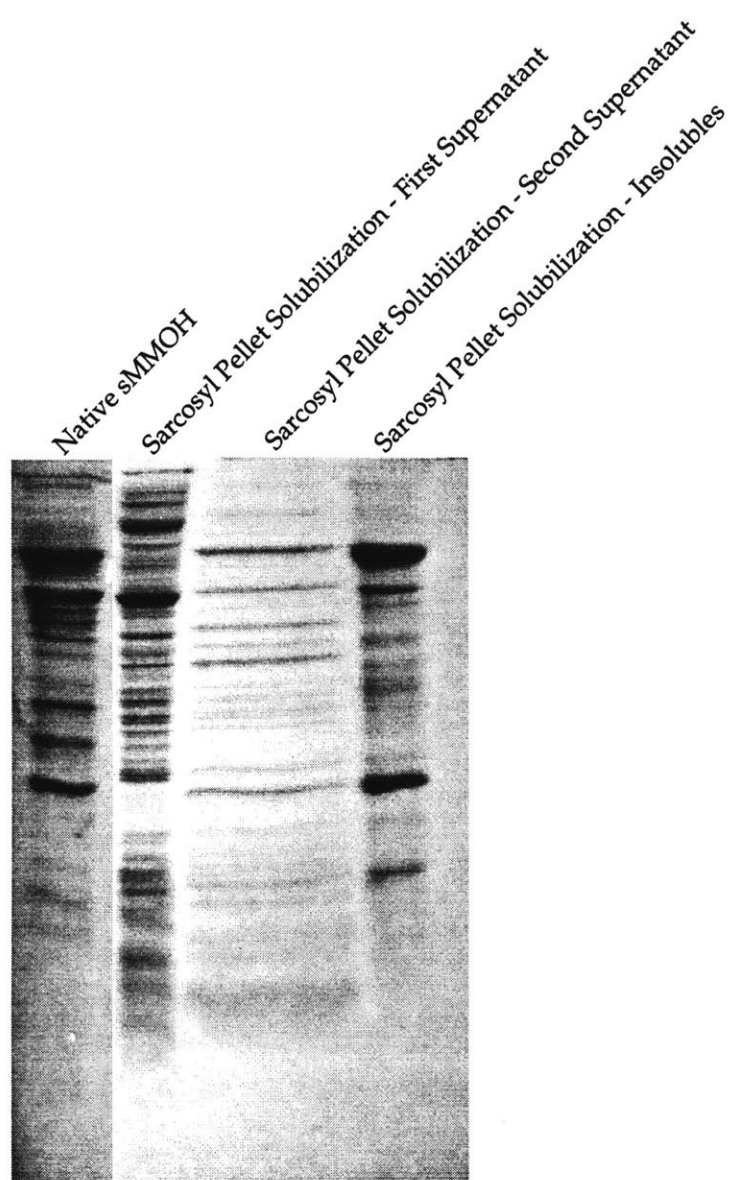


Figure 2-12

Figure 2-13. Expression by using the pDEC010 plasmid in *E. coli*.

An SDS-PAGE gel shows the result of expression of the sMMOH and B genes in *E. coli*. Note that *mmoZ* does not seem to be expressed in this system. The soluble protein near the α subunit is not MMOH α , but an *E. coli* protein.

sMMOH
pDEC010 Expression Solubles
pDEC010 Expression Insolubles

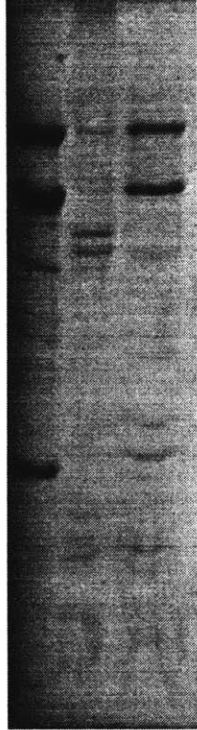


Figure 2-13

Figure 2-14. Construction of pDEC050 and pDEC055.

pDEC050 and pDEC055 were constructed by using similar methods. A fragment (either *mmoYZ* or *mmoX*) was cut out of pDEC002. The remaining plasmid was spliced together by using a short linker. These linkers were designed to remove the single EcoR I site in pDEC002, and insert a BamH I site in its place. This allowed for easy screening of the resulting plasmids.

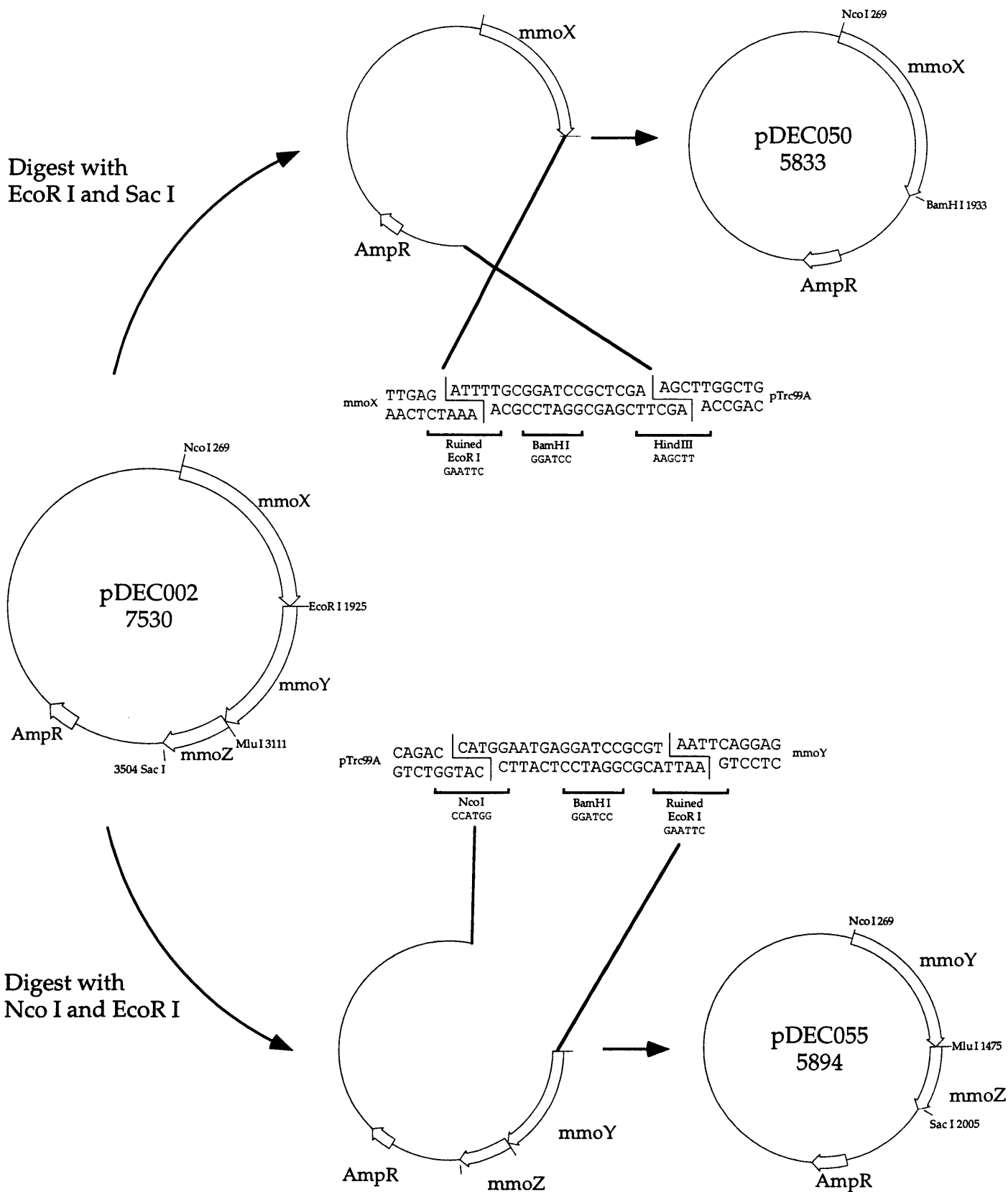


Figure 2-14

Figure 2-15. Structure of pDEC050 and pDEC055.

These plasmids are very similar to their parent pDEC002, including the pTrc promoter, the *rrnB* terminator, ampicillin resistance, and a copy of the *lac* repressor. pDEC050 was intended for expression of the *mmoX* gene, and pDEC055 was intended for expression of the *mmoY* and *mmoZ* genes.

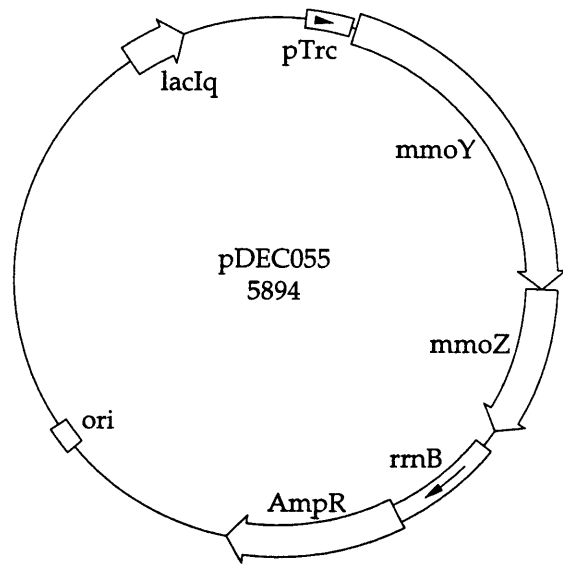
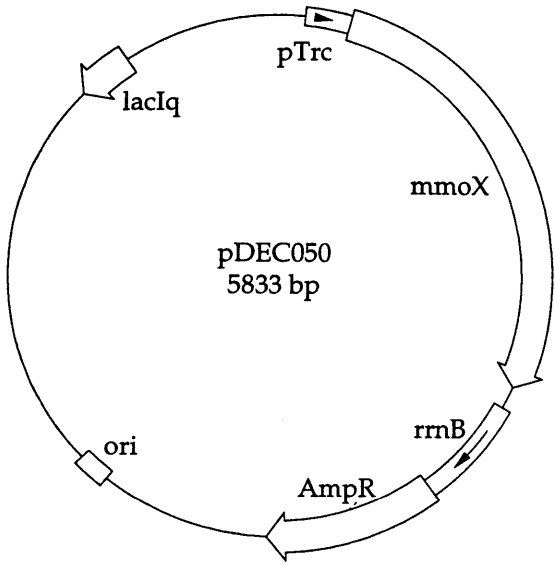


Figure 2-15

Figure 2-16. Construction of pDEC060 and pDEC070.

The plasmid pDEC060 was constructed by excision of the *mmoX* gene from pDEC050 and insertion into the pET20b plasmid. Use of the Nco I site allowed fusion with the pelB tag. Due to the design of the pDEC050 plasmid, there are nine amino acids in between the pelB and *mmoX* genes that are part of neither sequence.

The plasmid pDEC070 was constructed by designing a new set of PCR primers tailored for the pET32a plasmid. These primers were used to amplify the *mmoX* gene from the pCH4 cDNA copy of the sMMO operon. The *mmoX* PCR product was directly cloned into pCRII. This procedure was done to solve to problem often seen in earlier cloning work of cutting restriction sites close to the end of PCR products. The *mmoX* gene was excised from pCRII-*mmoX* and ligated into the pET32a plasmid.

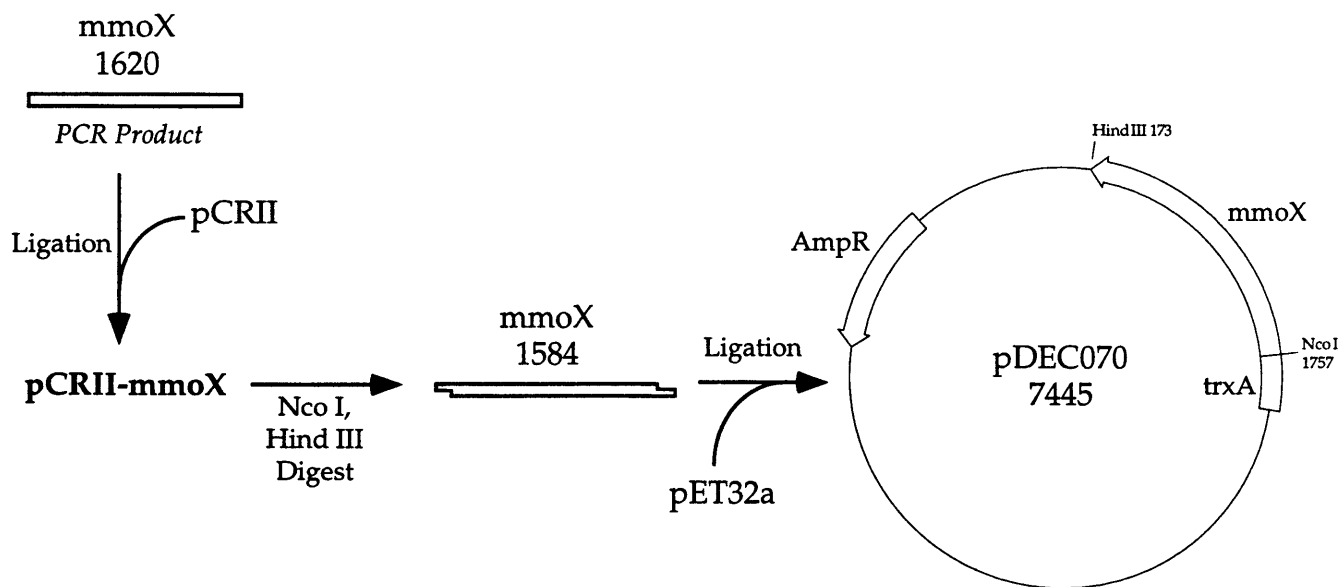
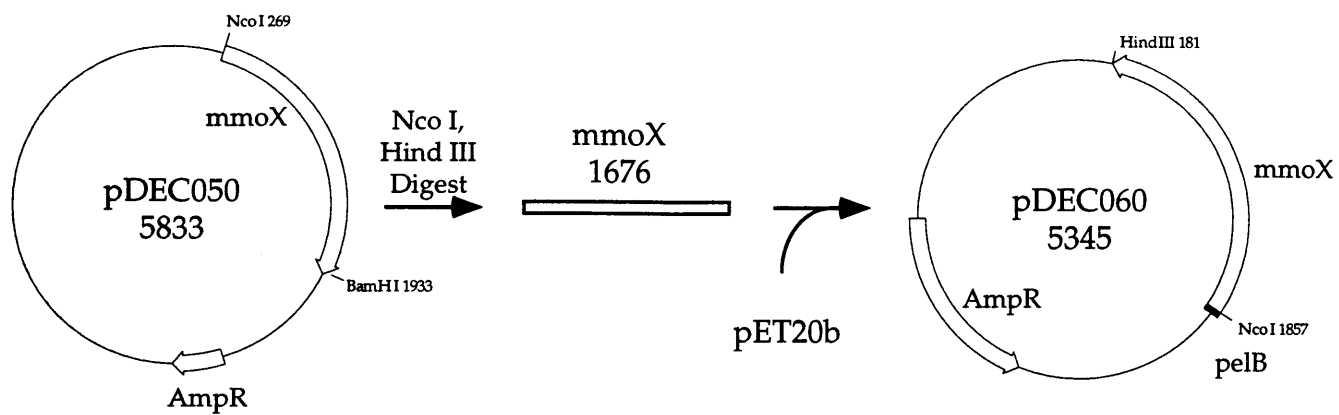


Figure 2-16

Figure 2-17. Structure of pDEC060 and pDEC070.

The pDEC060 plasmid's major feature is a fusion with the *pelB* leader sequence. This allows proteins that are attached to it to be exported to the periplasm. This can be advantageous in a variety of ways. The periplasm is different from the cytoplasm, in that the protein concentration is lower and the reduction potential is oxidizing. Periplasmic expression also allows for easy harvest of the expressed protein, as the cell wall can be broken via a simple freeze/thaw cycle.

The pDEC070 plasmid has several useful features. It fuses the *mmoX* gene with the thioredoxin gene. This feature is specifically designed to help solubilize difficult to fold proteins. In between the *mmoX* and *trxA* genes are a number of small useful sequences, including a His6 tag for easy purification, an S-Tag for easy Western blots, and thrombin and enterokinase cleavage sites to remove the thioredoxin fusion at will.

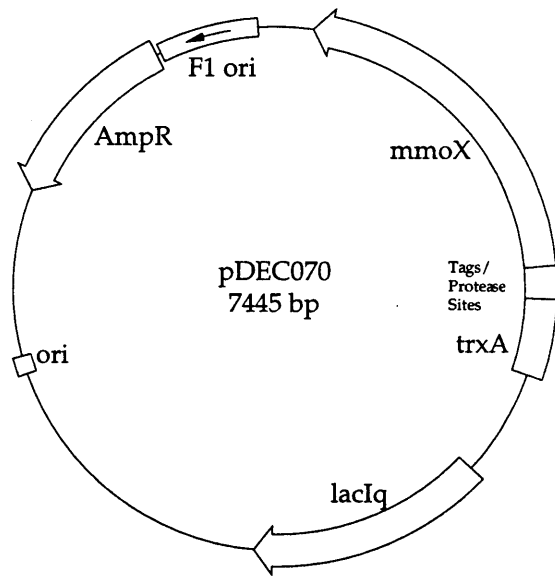
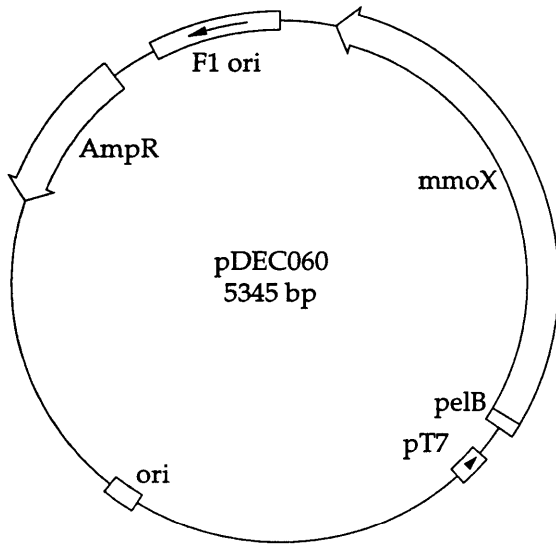


Figure 2-17

Figure 2-18. Expression of sMMOH genes from pDEC050 and pDEC055.

An SDS-PAGE gel shows the results of expression of the pDEC050 and pDEC055 plasmids in *E. coli*. The pDEC050 plasmid exhibits strong expression of the α subunit in an insoluble form. The pDEC055 plasmid does not show any expression of the β and γ subunits at all. This indicates that the space between the promoter and the RBS of the *mmoY* gene, which is enforced by the linker design, may be too long.

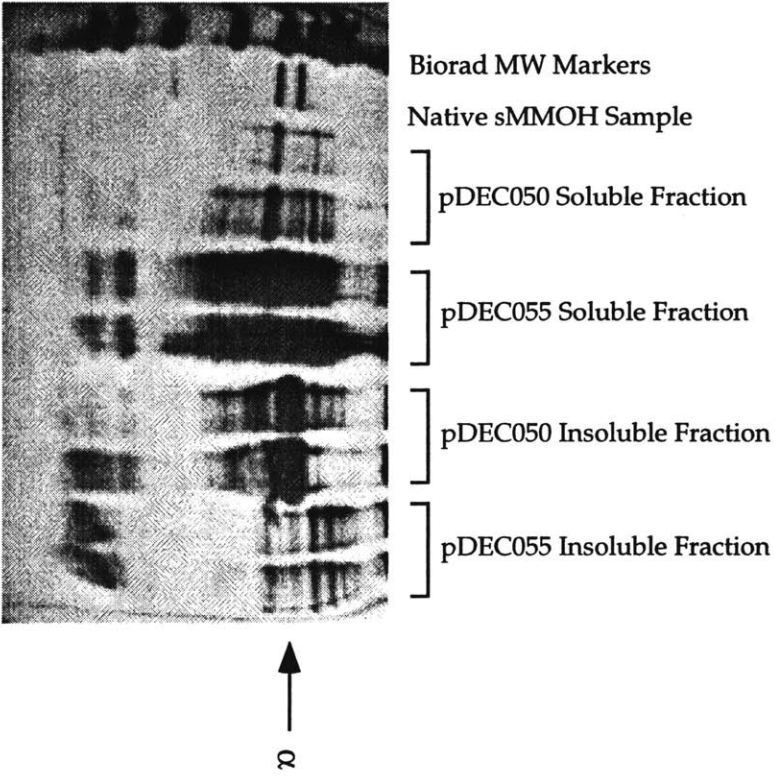


Figure 2-18

Figure 2-19. Periplasmic expression of the sMMOH α from pDEC060.

An SDS-PAGE gel shows the results of expression of the pDEC060 plasmid in *E. coli*. The pelB-tagged α subunit did not fold correctly, and was found in the insoluble fraction, despite its direction to the periplasm. No soluble protein was visible in the soluble fractions.

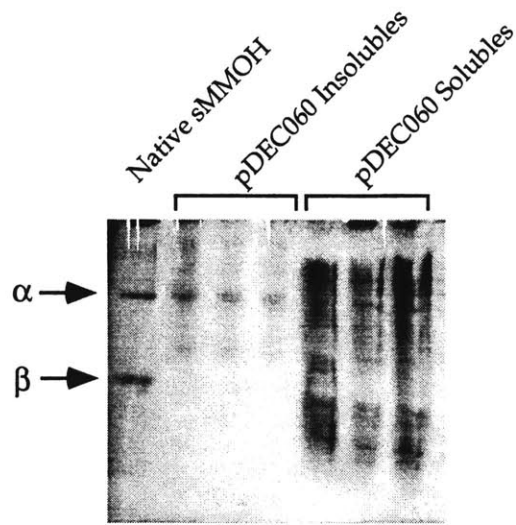


Figure 2-19

Figure 2-20. Expression of the thioredoxin- α subunit fusion protein from pDEC070.

An SDS-PAGE gel shows the results of the expression of the pDEC070 plasmid in *E. coli*. At 37 °C the thioredoxin fusion protein is expressed as insoluble inclusion bodies.

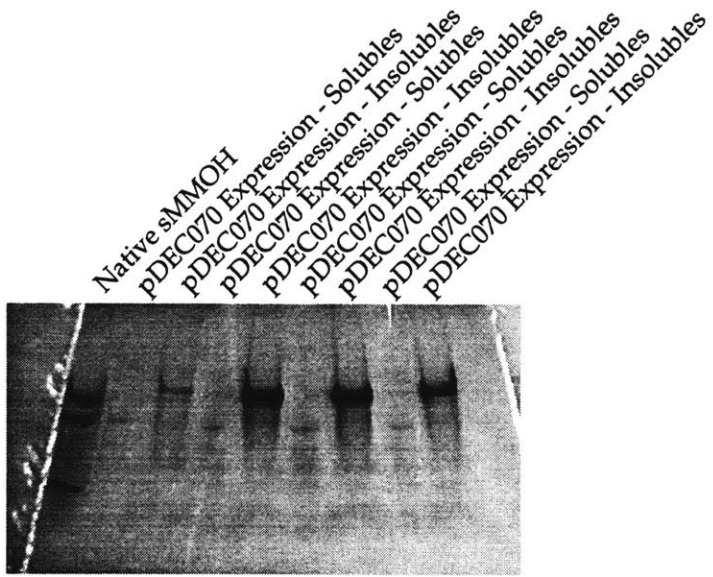


Figure 2-20

Figure 2-21. Purification of the thioredoxin- α subunit fusion protein.

An SDS-PAGE gel and Western blot show the purification of the thioredoxin fusion protein from the bulk of the soluble *E. coli* proteins by using a Ni²⁺-NTA column.

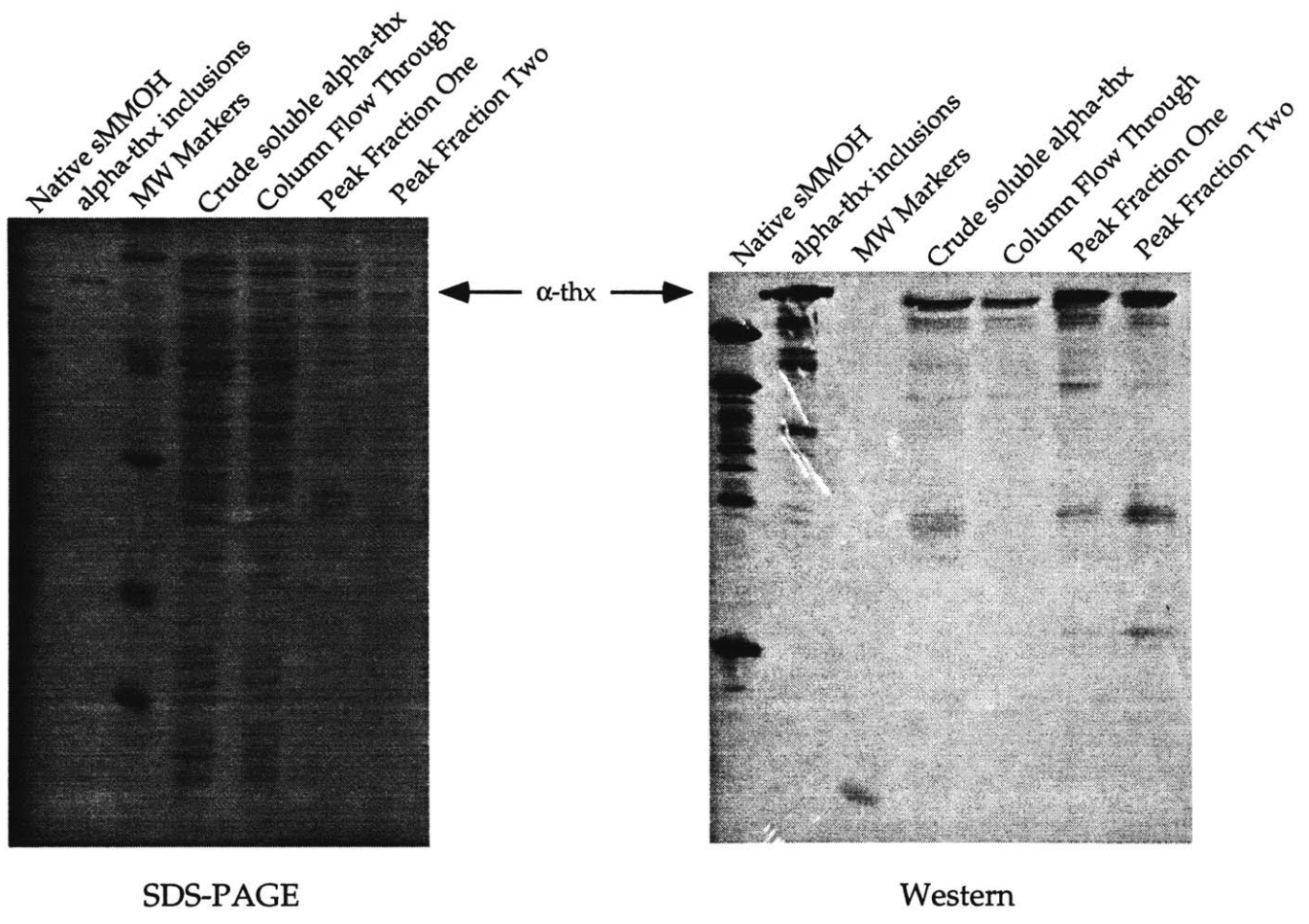


Figure 2-21

Figure 2-22. EPR spectrum of putatively Fe(II) Fe(III) thioredoxin- α subunit fusion protein.

a. EPR spectrum of 150 μ M thioredoxin fusion protein prepared under conditions expected to produce mixed-valent diiron center at 7.2 K. b. EPR spectrum of native sMMOH prepared under conditions expected to produce mixed-valent diiron center at 8.0 K. Both spectra: 100 kHz modulation frequency, 6.67 G modulation amplitude, 9.41 GHz microwave frequency, 1 mW microwave power. The signals at $g \sim 4.3$ and $g = 2.00$ are due to ferric iron impurities and protein-based radical induced by the chemical reduction, respectively. The $g = 1.93, 1.90, 1.85$ signal is due to the antiferromagnetically coupled $S = 1/2$ Fe(II) Fe(III) center in the hydroxylase (45).

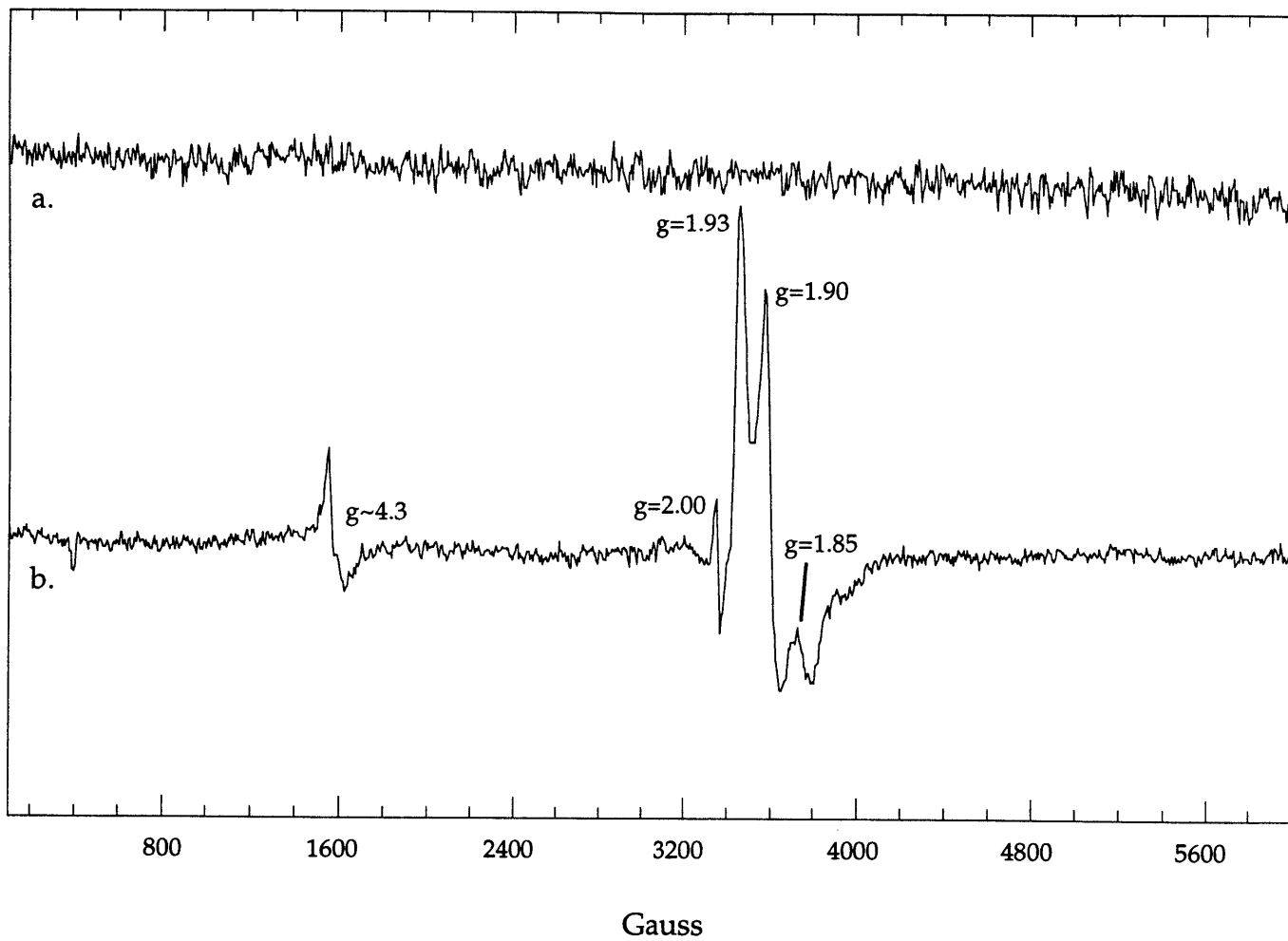


Figure 2-22

Chapter Three

Reactions of Nitric Oxide with the Reduced Non-Heme Iron Center of the Soluble Methane Monooxygenase Hydroxylase

Introduction

The soluble methane monooxygenase (sMMO) enzyme system in methanotrophic bacteria catalyzes the oxidation of methane to methanol and water by using dioxygen as an oxidant at a non-heme carboxylate-bridged diiron center (1-5). One atom of the dioxygen molecule is incorporated into the product alcohol and the other is released as water. Two electrons from NADH and two protons are also required. The controlled oxidation of hydrocarbons by this and similar systems is a topic of considerable current interest.

The sMMO system has three known protein components. The hydroxylase (H) is a homodimer ($\alpha_2\beta_2\gamma_2$) that contains a non-heme diiron center in each of its α subunits. The iron center is the locus of dioxygen activation and methane hydroxylation. The reductase (R) is responsible for transferring electrons from NADH through protein-bound FAD and [2Fe-2S] centers to the diiron center in the hydroxylase. A third component, protein B or the coupling protein, serves to couple this electron transfer to alkane hydroxylation.

The catalytic cycle of the hydroxylase enzyme has been examined in detail by using a variety of rapid kinetics methodologies, including optical stopped-flow and freeze-quench Mössbauer spectroscopy. Typically, the iron center is chemically reduced to the diiron(II) state, designated H_{red} , and mixed rapidly with solutions containing dioxygen. The first well characterized intermediate after H_{red} is H_{peroxo} (6, 7), assigned as a (μ -1,2-peroxo)diiron(III) species through

spectroscopic comparison with crystallographically characterized model compounds (8-10). The H_{peroxo} intermediate spontaneously transforms into intermediate Q (7, 11), which has been assigned a di(μ -oxo)diiron(IV) structure based on EXAFS evidence (12), although other interpretations of the data are possible (1). Intermediate Q reacts with alkane substrates to form hydroxylated products, returning the catalytic center to its resting, diiron(III) state, designated H_{ox} .

The role of protein B is not well understood. The catalytic cycle described above does not take place if protein B is absent. The diiron(II) center is instead oxidized to the diiron(III) state without observable accumulation of the H_{peroxo} and Q intermediates. Under steady state conditions, protein B from the *M. capsulatus* (Bath) sMMO system has a dramatic effect on turnover (13, 14). When it is not present, hydroxylation of products is completely uncoupled from dioxygen and NADH consumption. Instead, dioxygen is reduced to water. As protein B is added to the system, the coupling of hydroxylated product formation to dioxygen consumption increases. At a 1:1 ratio of protein B to hydroxylase the system is fully coupled. As the ratio of protein B to hydroxylase increases beyond 1, the hydroxylation reaction is inhibited. These observations are consistent with protein B having a role as a regulatory protein. The coupling protein also has a direct effect on the iron center. The presence of protein B causes the $g = 16$ integer spin EPR signal of H_{red} from *M. trichosporium* OB3b to become sharper and more intense (15). Magnetic circular dichroism experiments indicate that protein B effects a major coordination change at one of the iron atoms in the active site (16, 17), the details of which are obscure. Knowledge of these changes is crucial both structurally modeling and comprehending the mechanism of the sMMO system.

Nitric oxide is a useful surrogate for dioxygen (18) and reacts similarly with iron to afford complexes having useful spectroscopic properties. Species produced by the reaction of iron(II) with nitric oxide typically are brightly colored, $S = 3/2$ systems (19-21) with characteristic EPR signals (22-24), and are designated as $\{\text{Fe}(\text{NO})\}^7$ (21), where the superscript refers to the sum of d electrons from iron and π^* electrons from the NO molecule.

Nitric oxide has been useful as a probe of non-heme, carboxylate-bridged diiron centers. In hemerythrin (Hr), one NO molecule binds to a single iron atom (25, 26). The resulting $\{\text{Fe}(\text{NO})\}^7$ center couples antiferromagnetically with the other high-spin iron(II) center to form an EPR-active, $S = 1/2$ spin system. The mode of NO binding was proposed to be very similar to that of O_2 , with the uncoordinated oxygen atom of the NO ligand forming a hydrogen bond with the hydroxide bridge present in deoxyhemerythrin. This proposal was supported by a shift in the Raman spectrum due to changes in the Fe–N–O bending mode upon deuteration of the bridge. In the R2 subunit of ribonucleotide reductase, a more complex, heterogeneous reaction was observed (27). Addition of NO to the diiron(II) center of this protein afforded a complex having optical features at 450 and 620 nm. Mössbauer spectra of the product revealed a mixture comprising 77% of a diiron dinitrosyl species, $[\{\text{Fe}(\text{NO})\}^7]_2$, 13% of mononuclear $\{\text{Fe}(\text{NO})\}^7$, and 10% of an unidentified species. The two $S = 3/2$ $\{\text{Fe}(\text{NO})\}^7$ centers in the diiron dinitrosyl adduct were antiferromagnetically coupled to form an EPR-silent species, which decomposed with first order kinetics, reductively coupling the two NO molecules to form N_2O and oxidized RNR-R2. This diiron dinitrosyl species was proposed to be a model of the peroxo intermediate in the RNR-R2 reaction cycle. The spectroscopic properties of these and selected model compounds with carboxylate-bridged, non-heme diiron centers complexed with NO are listed in Table 1.

The present article describes a study of the reactions of NO with the reduced diiron center of the sMMO hydroxylase from *M. capsulatus* (Bath). These experiments afford the opportunity not only to model the O₂ binding step, but also to probe the role of protein B. The results provide important information about how the coupling protein can alter the dinuclear iron center for reaction with dioxygen.

Experimental Procedures

Preparation and Purification of sMMO Hydroxylase (H) and Protein B.

Samples of sMMO hydroxylase and of ⁵⁷Fe-enriched sMMO hydroxylase were prepared from *Methylococcus capsulatus* (Bath) as previously described (28). Protein B was prepared from a cloned source in *E. coli* as reported (29). Purity of the components was assured by SDS-PAGE electrophoresis. Specific activity and iron content were measured as described and were in the range of 250-350 nmol propylene formed mg⁻¹ min⁻¹ and 3.4-3.7 Fe/protein, respectively.

Preparation of Diiron(II) sMMO Hydroxylase (H_{red}). Purified sMMOH samples were prepared in 25 mM MOPS pH 7.0 with stoichiometric amounts of the mediator methyl viologen. The sample was degassed by 15-20 cycles of vacuum evacuation followed by argon backfilling. A degassed solution of ~10 mM sodium dithionite in 50 mM MOPS (pH 8.6) buffer was prepared and used to titrate the protein solution until the methyl viologen changed from yellow to blue. A 30 min time period was sufficient for complete reduction. The sample was then anaerobically dialyzed against two successive 500 mL volumes of 25 mM MOPS pH 7.0 to remove the mediator and reductant.

Addition of NO Gas. H_{red} samples were prepared and placed in vials sealed with rubber septa both with and without the presence of 2 equiv of protein B.

Nitric oxide (99+%, Matheson) was purified by passage through a concentrated NaOH solution to remove NO₂. The NO gas was passed over the protein solution for 5 min with manual agitation to ensure complete reaction. A change from colorless to green-brown was immediately observed. The NO stream was replaced by an argon stream for 10 min to remove excess NO. Samples for EPR and Mössbauer were anaerobically transferred to appropriate cells and frozen in liquid nitrogen approximately 45 min after NO addition.

Addition of NO via NONOates. NONOates are compounds that are stable at high pH, but decompose to NO gas at pH 7 (30, 31). They are useful as a means for delivering precisely known amounts of NO in aqueous solutions. NONOates are stored as concentrated stocks in 10 mM NaOH. The rate of decomposition was determined by introducing a small volume of concentrated NONOate into a 25 mM MOPS pH 7.0 solution and observing the disappearance of the NONOate UV absorption in mock reactions. This known rate of decomposition was used to determine how much NO is present in a protein solution at any given time after introduction of the NONOate.

H_{red} samples were prepared and placed in septum-sealed vials both with and without the presence of 2 equiv of protein B. A small amount (< 1% of sample volume) of concentrated diethylamine-NONOate (Cayman Chemicals) was added, and the reaction was allowed to proceed until the desired amount of NO was generated. Samples were frozen in EPR tubes or Mössbauer cells.

Stopped-flow Spectrophotometry. Stopped-flow experiments were performed to observe the reaction of H_{red} with nitric oxide both with and without the presence of 2 equiv of protein B. This ratio of B to H was chosen for direct comparison with previously reported stopped-flow studies with dioxygen (11). Protein samples, typically 50-150 μM in H_{red}, were loaded anaerobically into Hamilton gastight syringes with Luer-lock fittings. Saturated NO solutions were

prepared by first saturating 25 mM MOPS pH 7.0 solutions with argon gas to remove O₂. The solutions were cooled to 4 °C and NO gas was bubbled through them for 15-30 min, resulting in a solution of approximately 2.9 mM NO. This solution was diluted to the desired NO concentration with anaerobic buffer and transferred to a Hamilton gastight syringe. Both the protein- and gas-containing syringes were used to load the drive syringes of a HiTech SF61 DX2 stopped-flow instrument. Both syringes were allowed to equilibrate in a constant temperature bath for 15-30 min before recording data. Two detection systems were used. A HiTech UV-vis diode array spectrophotometer collected data over a wide range of wavelengths. A photomultiplier tube and monochromator were used to collect data at single wavelengths.

To examine the effects of methane substrate, the NO containing buffer was further treated. An anaerobic methane stock solution was prepared by bubbling argon followed by methane through a septum sealed vial of 25 mM MOPS pH 7.0. An aliquot of this solution was mixed in a 1:1 ratio with NO-saturated buffer before being loaded into the stopped-flow syringe.

Rapid Freeze-quench Mössbauer Sample Preparation. All freeze-quench samples were made as described in detail elsewhere (32). Rapid freeze-quench samples were performed with an Update instruments Model 705A computer and syringe-ram apparatus. Protein solutions were 1.1 mM in H_{red}. NO solutions were prepared by purging a 25 mM MOPS buffer sample with argon and allowing it to come to equilibrium in a chamber filled with 1 atm of NO gas at room temperature. The final NO concentration was approximately 1.9 mM. The reactants were loaded into RFQ syringes and allowed to cool to 4 °C in an ice/water bath. The protein and gas solutions were mixed rapidly, allowed to react for various fixed time periods governed by the length of tubing between the

mixing chamber and the nozzle, and then sprayed into isopentane at $-140\text{ }^{\circ}\text{C}$. The resulting snow was packed into Delrin[®] Mössbauer sample holders.

Rapid Freeze-quench EPR Sample Preparation. Rapid freeze-quench samples were prepared by using an Update Instruments Model 715 syringe-ram apparatus. Solutions of proteins and NO gas were prepared in a manner similar to that described above for the stopped-flow procedures. H_{red} concentrations were approximately $300\text{ }\mu\text{M}$. The reactants were loaded into gas tight syringes and cooled to $4\text{ }^{\circ}\text{C}$. The solutions were mixed rapidly, allowed to react for fixed time periods (28 ms - 60 s) in the aging tubing, and then sprayed into isopentane at approximately $-140\text{ }^{\circ}\text{C}$. The resulting snow was packed into quartz EPR tubes.

EPR Measurements. X-band EPR spectra were measured on a Bruker ESP 300 spectrometer equipped with an Oxford EPR 900 liquid helium cryostat. Spectra were recorded under the following conditions: temperature, 4.2 - 8.0 K; microwave frequency, 9.41 - 9.65 GHz; microwave power, $10\text{ }\mu\text{W}$ - 158 mW; modulation frequency, 100 kHz; modulation amplitude, 6.64 Gauss. Specific conditions are reported on the individual spectra. EPR quantitation was performed by double integration under nonsaturating conditions using 0.960 mM CuSO_4 , 1 M NaClO_4 as a standard. Quantitations were corrected for g-value anisotropy and spin. EPR power saturation data were collected by measuring signal intensity as a function of the applied microwave power over a range of four orders of magnitude.

Mössbauer Measurements. Mössbauer spectra were collected by using either a weak-field spectrometer equipped with a Janis 8DT variable-temperature cryostat or a strong-field spectrometer outfitted with a Janis 12 CNDT/SC SuperVaritemp cryostat encasing an 8 T superconducting magnet. Both spectrometers were operated in a constant acceleration mode in a transmission

geometry. The centroid of a room temperature iron foil spectrum was used as the zero velocity reference point.

Nitrous Oxide Detection by Gas Chromatography. Solutions of H_{red} both with and without 2 equiv of protein B were prepared in 1 mL septum-sealed vials. These samples were $\sim 300 \mu\text{M}$ in H_{red} and 300 μL in volume. A saturated 2.9 mM NO buffer sample was prepared at 4 °C as described above. A 100 μL aliquot of the NO buffer was added to the protein sample. At 5 min and 30 min intervals after NO addition, 50 μL headspace aliquots were removed and injected on a Hewlett-Packard 5890 gas chromatograph equipped with a 6 ft. packed Haysept column and a thermal conductivity detection system. The column He gas flow rate was 21-23 mL/min at 35 °C. Under these conditions, retention times for various gases were determined to be ~ 1.3 min for N_2 and NO and 5.1-5.2 min for N_2O . N_2O standards were prepared by assembling mock reaction vials with BSA at w/v concentrations equivalent to the hydroxylase in 25 mM MOPS buffer. Known amounts of N_2O were injected into these vials and they were subjected to the same 5 min and 30 min 50 μL headspace analysis as the $H_{red}+\text{NO}$ samples. Several N_2O vials were analyzed and a standard curve was constructed.

Results

Preparation of NO complexes of H_{red} and $H_{red}+2B$. Addition of NO gas to samples of H_{red} and H_{red} with two equiv of protein B ($H_{red}+2B$) immediately afforded greenish brown solutions, henceforth designated $H_{red}+\text{NO}$ and $H_{red}+2B+\text{NO}$, respectively. The NO addition method was varied and included direct addition of excess NO gas, direct addition of limited quantities of NO gas by a gas-tight Hamilton syringe, addition of NO via a NONOate precursor and addition of NO by NO-saturated buffer. No appreciable difference was observed

in the resulting optical or EPR spectral results for samples generated by these different methods.

Optical Absorption Spectra. The optical spectrum of the $H_{\text{red}}+\text{NO}$ adduct is shown in Figure 1, with maxima at 450 nm and 620 nm. The extinction coefficient at 450 nm was determined to be $\sim 740 \text{ M}^{-1} \text{ cm}^{-1}$. The spectrum of the $H_{\text{red}}+2\text{B}+\text{NO}$ complex was nearly identical, the only difference being a small decrease in ϵ to approximately $\sim 700 \text{ M}^{-1} \text{ cm}^{-1}$.

These spectra are quite similar to those of the dinitrosyl adduct of $[\text{Fe}_2(\mu\text{-XDK})(\mu\text{-O}_2\text{CPh})(\text{ImH})_2(\text{O}_2\text{CPh})(\text{MeOH})]$ (33, 34), also shown in Figure 1. This compound has a ligand composition identical to that of H_{red} and displays similar reactivity toward dioxygen. Colored intermediates with characteristic peroxo-to-iron charge transfer bands form rapidly upon reaction with dioxygen. This compound forms a dinitrosyl adduct upon reaction with NO, as established by Mössbauer and EXAFS spectroscopy (34).

Mössbauer Analysis of $H_{\text{red}}+\text{NO}$ and $H_{\text{red}}+2\text{B}+\text{NO}$ Samples. Figure 2 shows the zero-field Mössbauer spectra recorded at 4.2 K of samples of H_{red} and H_{red} with 2 equiv. of protein B that has been allowed to react with NO for approximately 45 min. Several species can be identified, the relative proportions of which are summarized in Table 2. Both unreacted H_{red} and H_{ox} can be identified in the spectra according to their previously identified characteristics (11, 28). Species consistent with mononuclear $\{\text{Fe}(\text{NO})\}^7$ and mononuclear Fe(III) were identified on the basis of their isomer shift and high field Mössbauer properties. A diamagnetic species with Mössbauer parameters consistent with the dinitrosyl adduct of H_{red} , termed $H_{\text{dinitrosyl}}$, was detected. Finally, an unknown diamagnetic species with a very low isomer shift, 0.2 mm/s, was identified. This low isomer shift is consistent with an Fe(IV)-containing compound, such as species containing an $\text{Fe}(\text{NO})_2$ unit.

EPR Analysis of $H_{red}+NO$ and $H_{red}+2B+NO$ Samples. Figure 3 shows the X-band EPR spectra of the $H_{red}+NO$ and $H_{red}+2B+NO$ adducts at 4-5 K. The major signal in the $H_{red}+NO$ spectra has $g = 4.08, 4.02$ and 2.00 and arises from an $S = 3/2$ species consistent with mononuclear $\{Fe(NO)\}^7$ as observed in the Mössbauer spectra described above. Determination of the spin concentration of this signal from several independent samples showed that it represents 20-30% of the total iron in the sample. The half-saturation value, $P_{1/2}$, for this $\{Fe(NO)\}^7$ center was determined to be ~ 7 mW. Interestingly, this signal splits into at least three species with slightly different rhombicities ($g = 4.08, 4.02$; $g = 4.15, 3.95$; and $g = 4.22, 3.86$) upon addition of protein B. This splitting was obtained by addition of protein B either before or after NO exposure. Mononuclear Fe(III) associated with exogenous iron impurities is present, also consistent with the Mössbauer samples, exhibiting a $g = 4.3$ high spin ferric signal. Spin quantitation of this signal reveals that it represents 2-6% of total iron in the sample.

Stopped-flow Analysis of the $H_{red}+NO$ and $H_{red}+2B+NO$ Reaction. Stopped-flow optical spectrophotometry was used to analyze the kinetics of formation and decay of species formed in the reaction of NO with the reduced diiron center of the hydroxylase. As shown in Figure 4, an optical signal with maxima at 450 nm and 620 nm builds up rapidly upon mixing, maximizing at ~ 150 ms. After 150 ms, the signal decays slowly until all visible changes stop, approximately 20-30 min after NO addition. At that time, the signal had approximately half of its 150 ms maximum intensity. The buildup was best fit by a biphasic $A \rightarrow B \rightarrow C$ model that, at $4^\circ C$, had rate constants $k_1 = 78 \pm 6 \text{ s}^{-1}$ and $k_2 = 18 \pm 2.7 \text{ s}^{-1}$. Global analysis of the stopped-flow data revealed that the spectra of species B and C in the two phase model were nearly identical, the only difference being a 1-2% decrease in extinction coefficient for B. The decay of the optical signal could not be fit well to any specific model, indicating that it is a complex process

comprising various component reactions. First-order fits approximating the decay at 4 °C produced a rate constant of $0.06 \pm 0.02 \text{ s}^{-1}$. Variation of the NO concentration over a 10-fold range did not appreciably change the observed rate constants. All stopped-flow experiments subsequently reported here were conducted with at least a 20-fold excess of NO. The temperature dependence of the rate constants for buildup of the optical species was measured. Eyring plots of these data, shown in Figure 5, yielded the activation parameters shown in Table 3. A simulation of the time-dependent growth and decay of species formed in the $\text{H}_{\text{red}}+\text{NO}$ reaction, obtained by using the rate constants obtained from stopped-flow data, is presented in Figure 6.

The reaction of NO with the reduced hydroxylase and two equiv of protein B was also examined by stopped-flow spectroscopy. The optical signals detected were essentially identical to those in the $\text{H}_{\text{red}}+\text{NO}$ reactions, the major difference being a small diminution in observed extinction coefficient as described above. The buildup of this species could, in contrast with the $\text{H}_{\text{red}}+\text{NO}$ reactions, be fit well by a single exponential buildup. At 4 °C, the rate constant was determined to be $k = 26 \pm 0.8 \text{ s}^{-1}$. The decay, as in the $\text{H}_{\text{red}}+\text{NO}$ case, was too complex to be fit satisfactorily by a simple model. First order approximation of the decay yielded a rate of $0.05 \pm 0.02 \text{ s}^{-1}$, within error the same value as for the $\text{H}_{\text{red}}+\text{NO}$ reaction. Temperature-dependent studies of this reaction produced activation parameters listed in Table 3, with the Eyring plots of these data shown in Figure 5.

The kinetics of the $\text{H}_{\text{red}}+\text{NO}$ and $\text{H}_{\text{red}}+2\text{B}+\text{NO}$ reactions were also examined in the presence of methane. The optical bands that appeared were identical to those formed without methane present. The rates for both reactions could be fit well by first order equations.

Rapid Freeze-Quench EPR Characterization of $H_{red}+NO$ Reaction Species.

Freeze-quench samples of the $H_{red}+NO$ reaction were collected at 28 ms, 158 ms, 1 s and 60 s. Spectra taken from those samples are shown in Figure 7. The signal corresponding to the $S = 3/2$ $\{Fe(NO)\}^7$ species can be seen growing in at 28 ms, achieving its maximal value in the 158 ms sample. Fits of these data indicate that the first order rate constant for the buildup of this signal is $10-20\text{ s}^{-1}$ at $4\text{ }^\circ\text{C}$. Its concentration, 27% of the total amount of iron centers in the sample, does not change within the error limits of the experiment after this time point (see inset, Figure 7). The signal at $g = 1.97$ is due to free NO in solution, and can be observed to decrease in intensity during the time course. In the 60 s sample, a signal at $g = 2.04$ has appeared. This signal is most likely due to a small amount of some $S = 1/2$, $Fe(NO)_2$ species. It accounts for $<2\%$ of total iron in the sample.

Mössbauer Characterization of $H_{red}+NO$ Reaction Species. The protein concentration used in these experiments was much higher than in other $H_{red}+NO$ work, in order to optimize the signal-to-noise ratio obtainable with Mössbauer spectroscopy. A consequence of this limitation is that the NO concentration ($\sim 1.9\text{ mM}$) is substoichiometric with respect to the amount of iron ($\sim 3.9\text{ mM}$). As a result, more than 50% of the hydroxylase remains in the reduced state. In addition, the rates of the NO reactions cannot be directly compared with those obtained in the stopped-flow and EPR freeze-quench experiments, because those data were obtained under pseudo-first-order conditions where NO was in great excess.

Figure 8 shows the Mossbauer spectra of the reaction of H_{red} with NO at three different times after mixing, and Table 4 contains the Mössbauer parameters used for the fits to the data. Reactions were quenched at 61 ms, 126 ms, and 440 ms. The major component of all the spectra is a quadrupole doublet attributable to unreacted H_{red} . A $\sim 10\%$ amount of H_{ox} can be seen in all samples

that cannot be reduced, as previously observed for the *M. capsulatus* (Bath) hydroxylase (11). These two species can be identified in the spectra according to their previously identified characteristics (11, 28). A species corresponding to mononuclear $\{\text{Fe}(\text{NO})\}^7$ develops very quickly, reaching its maximal concentration before 61 ms. It does not decay after 440 ms, in accord with the freeze-quench EPR data. A species with Mössbauer parameters characteristic of $\text{H}_{\text{dinitrosyl}}$ also forms very quickly, consistent with the stopped-flow evidence. This species decays to approximately 80% of its maximal value at the 440 ms time point. This rate of decay is slightly faster than that observed in the stopped-flow experiments. Such a difference might arise if the “unidentified” decay product of $\text{H}_{\text{dinitrosyl}}$ has optical properties similar to that of other iron nitrosyl species, a likely possibility. Thus the measured decay rate of $\text{H}_{\text{dinitrosyl}}$ as observed by optical stopped-flow spectroscopy may be inaccurate owing to the buildup of other colored components. The Mössbauer parameters of a decay product from the $\text{H}_{\text{red}}+\text{NO}$ reaction at the 440 ms time point suggest that it may be some $\text{Fe}(\text{NO})_2$ containing species.

The Mössbauer freeze-quench work serves to identify $\text{H}_{\text{dinitrosyl}}$ species as the diamagnetic reaction component that forms and decays slowly in the stopped-flow experiment (Figure 6). It also supports the rapid freeze-quench EPR data indicating that a mononuclear $\{\text{Fe}(\text{NO})\}^7$ species develops very quickly upon reaction of NO with H_{red} and does not decay.

Decay of $\text{H}_{\text{dinitrosyl}}$ to N_2O . The dinitrosyl adduct of the diiron center in the R2 subunit of ribonucleotide reductase decays slowly with a first order rate constant of $\sim 0.013 \text{ min}^{-1}$ to R2_{met} and N_2O (27). To determine whether the sMMO dinitrosyl adduct undergoes similar chemistry, the headspace of a $\text{H}_{\text{red}}+\text{NO}$ sample was analyzed for N_2O by gas chromatography. Samples taken at both 5 and 30 min after exposure to NO contained 0.06-0.12 equiv of N_2O per

hydroxylase diiron center. Similar samples taken of the $H_{\text{red}}+2B+\text{NO}$ reaction contained 0.10-0.16 equiv of N_2O per hydroxylase diiron center. One of the decay pathways of the $H_{\text{dinitrosyl}}$ species is reductive elimination of N_2O , most likely affording H_{ox} as a product.

Discussion

Reaction of Reduced Hydroxylase with NO to Form a Diiron Dinitrosyl Species.

Nitric oxide reacts with the reduced diiron center in the sMMO hydroxylase to afford a diiron dinitrosyl species referred to as $H_{\text{dinitrosyl}}$. As indicated in Figure 9, this EPR-silent $[\{\text{Fe}(\text{NO})\}^7]_2$ unit accounts for a majority of the iron, the remainder being mononuclear (vide infra). The $H_{\text{dinitrosyl}}$ intermediate models H_{peroxo} in the sMMO reaction cycle. Its two $\{\text{Fe}(\text{NO})\}^7$ centers antiferromagnetically couple to afford a diamagnetic ground state.

The spectroscopic properties of $H_{\text{dinitrosyl}}$ were revealed by stopped-flow, RFQ EPR and RFQ Mössbauer experiments. When H_{red} is allowed to react with NO, an optical spectrum rapidly grows in, maximizes after approximately 150 ms, and subsequently decays. The optical spectrum closely resembles those of diiron dinitrosyl model complexes (34) and a similar dinitrosyl adduct of the ribonucleotide reductase R2 protein (27). The optical data are therefore consistent with formation of a diiron dinitrosyl unit, but alone are insufficient to prove that assignment.

Rapid freeze-quench Mössbauer data indicate that only two species containing iron-nitrosyl moieties form within the first 500 ms of reaction. The isomer shifts and quadrupole splitting parameters are consistent with the formation of $H_{\text{dinitrosyl}}$ and a mononuclear $\{\text{Fe}(\text{NO})\}^7$ center. Rapid-freeze-quench EPR as well as Mössbauer spectroscopy establish that the mononuclear $\{\text{Fe}(\text{NO})\}^7$

unit forms in the first 100 ms after NO addition and does not decay even after 60 s of reaction. The RFQ Mössbauer data reveal that the species assigned as $H_{\text{dinitrosyl}}$ decays after 150 ms. Since the stopped-flow experiments indicate that the optical bands at 450 and 620 nm bands also decay after 150 ms of reaction, it can be concluded that $H_{\text{dinitrosyl}}$ contributes significantly to the observed optical signals.

Although it is possible that the mononuclear $\{\text{Fe}(\text{NO})\}^7$ species also absorbs at 450 and 620 nm, its contribution is likely to be minimal. The EPR spectra reveal that most of the iron is diamagnetic. Moreover, both the $H_{\text{dinitrosyl}}$ and mononuclear $\{\text{Fe}(\text{NO})\}^7$ species appear, from all available data, to build up during the first 200 ms of reaction. If the contribution from a mononuclear $\{\text{Fe}(\text{NO})\}^7$ species were similar to that of $H_{\text{dinitrosyl}}$, one would expect to be able to distinguish the two formation rates kinetically. Instead, the stopped flow data could be fit well to simple $A \rightarrow B$ ($H_{\text{red}}+2B+\text{NO}$) and $A \rightarrow B \rightarrow C$ ($H_{\text{red}}+\text{NO}$) models (vide infra). Fits to $A \rightarrow B$, $A \rightarrow C$ buildup kinetics could not account for the data. It is therefore likely that only one major optical species forms in the $H_{\text{red}}+\text{NO}$ reaction. Since $H_{\text{dinitrosyl}}$ is a significant contributor to the optical signals seen in the stopped-flow spectroscopic experiments (vide supra), we conclude that $H_{\text{dinitrosyl}}$ is the major component.

A Mononuclear $\{\text{Fe}(\text{NO})\}^7$ Minority Species in the $H_{\text{red}}+\text{NO}$ Reaction.

Approximately 15-30% of the protein active sites react with NO to afford a paramagnetic, $S = 3/2$ $\{\text{Fe}(\text{NO})\}^7$ unit. This species probably forms in the active site of the hydroxylase, because its EPR characteristics are affected by the presence of protein B (vide infra). We considered the possibility that the $\{\text{Fe}(\text{NO})\}^7$ EPR signal might arise by reaction of the active sites to eject one iron atom, leaving the second to react with NO to form a mononuclear species. Such a mechanism is unlikely, however, since the iron atoms are well coordinated by

protein ligands and not expected to be extruded from the active site simply by addition of nitric oxide. Moreover, the iron content of the hydroxylase was determined both before and following NO treatment, and no metal was lost as a result of the reaction (data not shown). The sMMO hydroxylase as currently isolated from *M. capsulatus* (Bath) has 3.4-3.7 iron atoms per molecule, fewer than the expected number of 4 if all sites were fully occupied. The absence of one iron atom from 20% of the active sites would amount to a 10% deficiency of total iron, consistent with the measured amount of iron in the protein. We therefore attribute the $\{Fe(NO)\}^7$ signal to mononuclear species resulting from iron-depleted enzyme. Heterogeneity in the sMMO hydroxylase as isolated has previously been noted in kinetics and spectroscopic experiments (11).

Effects of Protein B on the Mononuclear $\{Fe(NO)\}^7$ Species. The presence of protein B causes the $S = 3/2$ EPR signal of the $\{Fe(NO)\}^7$ species to split into three signals arising from three species with slightly different rhombicities. This phenomenon can be explained by the following model. The species with the least rhombic character ($g = 4.08, 4.02$) is assigned to hydroxylase having no bound protein B. When protein B binds to this enzyme, the active site environment is altered, and the $\{Fe(NO)\}^7$ unit assumes a slightly more rhombic coordination environment. This species is assigned to the $g = 4.15, 3.95$ signal. When a second molecule of protein B is bound, the iron site rhombicity is shifted even further, resulting in the observation of yet a third signal. Although interesting, this information is of limited value, for it is impossible to assign specific structures to the EPR observed species, and it is unlikely that the hydroxylase sites housing the $\{Fe(NO)\}^7$ centers have the native conformation.

Comparison Between the Reactions of the sMMO Hydroxylase with NO and O₂. The reaction of reduced hydroxylase with dioxygen in the absence of protein B has not been investigated in detail. Under these conditions, the consumption of

electrons and dioxygen is completely uncoupled from substrate hydroxylation (14), although the hydroxylase does become oxidized. Intermediates H_{peroxo} and Q do not accumulate. By contrast, the reaction of H_{red} and two equiv of protein B with O_2 has been well characterized (7, 11). The first step is the formation of the H_{peroxo} intermediate, which is most likely a (μ -1,2-peroxo)diiron(III) species. Further reaction produces intermediate Q, which oxidizes substrate. There are clear differences between the reactions with and without the presence of protein B.

The reaction of H_{red} with NO to form the H_{peroxo} analogue $H_{\text{dinitrosyl}}$, however, occurs whether or not protein B is present. There are two possible models to explain this difference. If the binding of protein B to the hydroxylase modulates the iron-iron distance, in the absence of this component the iron atoms may not have the correct separation to accommodate a peroxide-bridged structure. If dioxygen were to bind under such circumstances, it might be reduced to the superoxo level but not react further without being released from iron. The binding of protein B might bring the iron atoms to the proper distance to support 1,2-peroxo bridge formation. With NO as the reactant, the iron-iron distance should not be an issue, and a dinitrosyl species should form whether or not protein B is present. In the second model, protein B adjusts the relative orientations of the available coordination sites in H_{red} . Without protein B present, the coordination sites may be positioned such that peroxide cannot bridge. Binding of protein B may cause a shift of the ligands such that the available coordination sites are oriented to facilitate formation of a peroxide bridge. Such shifting would not be required for NO binding to the two iron atoms. These two models are not mutually exclusive.

The available crystallographic data for reduced sMMO hydroxylase (35) are consistent with aspects of both models, as illustrated in Figure 10. The iron-

iron distance in the diiron(II) center is 3.28 Å, shorter than the 4.0 Å distance in a crystallographically characterized μ -1,2-peroxodiiron(III) model complex having the same Mössbauer parameters as H_{peroxo} (8). Moreover, there are two sites in the reduced diiron center structure that are occupied by very weakly bound water molecules, and are therefore available for exogenous ligand binding. These sites are approximately 80°, or gauche, to one another when viewed down the iron-iron axis, as illustrated in Figure 10. Binding of protein B may shift the coordination environment so as to bring these open coordination sites into a more eclipsed conformation and possibly also to alter the iron-iron distance. In Figure 11, this model is elaborated by hypothesizing that Glu243 undergoes a carboxylate shift, bridging the two iron atoms in a μ -1,2 fashion, as previously hypothesized (35). The resulting diiron environment is very much like that in the ribonucleotide reductase $R2_{\text{red}}$ structure (36), where the available coordination sites are adjacent to one another. Details of this model may be altered when information about the structure of the complex between the hydroxylase and protein becomes available.

Buildup of $H_{\text{dinitrosyl}}$. The formation of $H_{\text{dinitrosyl}}$ from the reaction of H_{red} with NO in the absence of protein B and methane is clearly biphasic. There are several possible interpretations of this result. The first is that the initial intermediate formed is a mononitrosyl species, with an NO molecule bound to one of the iron atoms. Reaction with a second NO would lead to formation of $H_{\text{dinitrosyl}}$. This hypothesis is not consistent with the available data, however. Such a mononitrosyl species would be expected to have spectroscopic properties very similar to those of the hemerythrin nitrosyl adduct. The ferrous iron and resulting $\{\text{Fe}(\text{NO})\}^7$ center would couple antiferromagnetically, forming an $S = 1/2$ paramagnetic species that would be clearly visible by EPR spectroscopy in rapid freeze quench samples. No such signal was apparent. Moreover, the optical

spectrum of the intermediate revealed by global analysis of the stopped flow data closely resembles that of $H_{\text{dinitrosyl}}$. A mononitrosyl species would be expected to have a much smaller extinction coefficient.

The preferred explanation is that the initial reaction of the reduced diiron center with NO affords a dinitrosyl intermediate, designated $[H_{\text{dinitrosyl}}]^*$, which spontaneously rearranges to the final, $H_{\text{dinitrosyl}}$ form. Since the spectra of both species are nearly identical, they most likely have similar structures. It may be that the $[H_{\text{dinitrosyl}}]^*$ to $H_{\text{dinitrosyl}}$ transition is the result of a shift in the relative positions of the NO ligands, such as that drawn in Figure 11. Another possibility is that the iron ligand environments are largely unchanged, but that formation of the initial $[H_{\text{dinitrosyl}}]^*$ species triggers a conformational change in the hydroxylase, producing $H_{\text{dinitrosyl}}$, which can be resolved kinetically.

The absence of an mononitrosyl intermediate in the reaction of NO with the reduced hydroxylase suggests a mechanism for the dioxygen reaction. This observation means that there is a readily available coordination site on each iron in the diiron active site that can quickly react with NO, resulting in the formation of the diiron dinitrosyl species without formation of a diiron mononitrosyl intermediate. This implies that the dioxygen reaction will proceed similarly, with near-simultaneous reaction of both oxygen atoms with the two iron atoms, respectively. This rules out a hemerythrin-type mechanism, where dioxygen binds to just one iron and is reduced to peroxide without coordination to the second iron.

When the $H_{\text{red}} + \text{NO}$ reaction is performed in the presence of protein B the kinetics of buildup become monophasic; no $[H_{\text{dinitrosyl}}]^*$ intermediate is observed. This observation can be interpreted in terms of the ligand rearrangement model (Figure 11). If the $[H_{\text{dinitrosyl}}]^*$ to $H_{\text{dinitrosyl}}$ transition as observed in reactions without protein B is due to a shift in NO ligands from gauche to eclipsed

conformations, the shift to monophasic kinetics upon addition of protein B is a reasonable consequence of that model.

The pseudo-first-order rate constant for reaction of NO with $H_{\text{red}}+2B$ to form $H_{\text{dinitrosyl}}$ at 4 °C is $\sim 26 \text{ s}^{-1}$. This value is nearly identical to the rate constant for reaction of O_2 with $H_{\text{red}}+2B$ to form H_{peroxo} at 4 °C, $\sim 25 \text{ s}^{-1}$ (6). The rate constants for the initial reaction with NO and O_2 with H_{red} alone cannot be compared, since no value is available for the latter reaction. The rate constant for initial reaction with NO ($\sim 78 \text{ s}^{-1}$) is much larger than with protein B present, however, which suggests that the corresponding reaction with dioxygen would also be much faster.

An investigation of the $H_{\text{red}}+\text{NO}$ reaction without protein B, but in the presence of methane, revealed monophasic buildup kinetic behavior, similar to that as observed in the presence of protein B. This result suggests that protein B and methane gas might be able to modify the sMMO hydroxylase structure in a similar way. For example, it may be that both protein B and methane serve to extrude weakly bound water from the diiron center, clearing the way for dioxygen and nitric oxide exogenous ligand binding. One of the two steps observed kinetically in the $H_{\text{red}}+\text{NO}$ stopped-flow experiments might therefore be loss of bound water. Addition of methane or protein B would facilitate this reaction, resulting in first-order kinetics. A similar effect is well known in the cytochromes P-450 (37), where substrate binding to the protein facilitates loss of a water ligand from the heme cofactor. This explanation is also consistent with the activation parameters determined for the reactions of $H_{\text{red}}+\text{NO}$ and $H_{\text{red}}+2B+\text{NO}$, as reported in Table 3. For the reaction of NO with H_{red} in the presence of protein B, a ΔS^\ddagger value of $-24.9 \text{ cal mol}^{-1} \text{ K}^{-1}$ was calculated. This result is consistent with binding of two NO molecules to the iron center in the transition state. The corresponding reaction of NO with H_{red} without protein B

has a much less negative ΔS^\ddagger value of $-1.1 \text{ cal mol}^{-1} \text{ K}^{-1}$. This value must reflect a compensating entropic gain in the transition state during the $H_{\text{dinitrosyl}}$ formation, such as loss of water. These results support the hypothesis that protein B serves to organize the diiron cluster for optimal reaction with dioxygen, as shown in Figure 11. The substrate methane appears to share aspects of this organizational capacity.

Decay of $H_{\text{dinitrosyl}}$. The decay of the dinitrosyl species is complex and stopped-flow data for this process could not be fit well to any single model. The final mixture of products, as observed by Mössbauer spectroscopy, is heterogeneous (data not shown). In one decay pathway, nitrous oxide is eliminated from $H_{\text{dinitrosyl}}$ to afford H_{ox} . This reaction is supported by gas chromatographic detection of N_2O in the headspace above the reaction mixture. The ability of protein B to increase the amount of N_2O formed is consistent with the hypothesis that, in $H_{\text{dinitrosyl}}$, the two NO molecules are oriented in positions unfavorable for N–N bond formation. Addition of protein B could reposition the two NO coordinated molecules towards one another, as depicted in Figure 11, to promote ligand migration and subsequent N–N bond formation. Reductive coupling between two metal-bound NO molecules to form N_2O is well precedented in the literature. The dinitrosyl adduct of the ribonucleotide reductase R2 subunit reacts in this manner (vide supra) (27). N_2O formation has also been observed in dicopper(I) complexes (38).

A second decay pathway is suggested by the presence of the “unidentified” species in the Mössbauer spectra of $H_{\text{red}}+\text{NO}$ reaction mixtures. A product with a low isomer shift appears following decay of $H_{\text{dinitrosyl}}$ in the freeze-quench Mössbauer data. This product is diamagnetic, has Mössbauer properties consistent with a high-valent Fe(IV) species, and may contain the $\text{Fe}(\text{NO})_2$ fragment. The data are consistent with an active site having two such

{Fe(NO)₂} centers, antiferromagnetically coupled. Formation of such a species might result from further reaction of NO with the diiron center, displacing water or protein side chain ligands.

Comparison with the NO Reactions of the Reduced Ribonucleotide Reductase R2 Subunit and Hemerythrin. There are many similarities between the reactions of the reduced sMMO hydroxylase and R2_{red} with NO. The major products formed by each enzyme are [{Fe(NO)}⁷]₂ dinitrosyl species that model aspects of peroxo intermediates in the two systems. These dinitrosyl intermediates are metastable. In the R2 system, decay is slow and apparently consists only of reductive coupling to afford R2_{met} and N₂O. The H_{dinitrosyl} adduct decays more rapidly, forming a more complex mixture of products. A reductive coupling pathway to form N₂O is apparently present, but does not account for all of the H_{dinitrosyl} decay.

The minor products formed in both reactions are also similar and include mononuclear {Fe(NO)}⁷ centers and unidentified diamagnetic species having Mössbauer parameters consistent with [{Fe(NO)₂}]₂. This species appears to be a byproduct of H_{dinitrosyl} decay in the sMMO system. The similarities emphasize the close relationship between the structures and functions of these two enzymes, which is to perform chemistry by using dioxygen as a reactant. The NO chemistry contrasts with that of hemerythrin, which forms a relatively homogenous and stable NO adduct. The function of hemerythrin is to bind dioxygen reversibly, which is consistent with its reaction with NO.

The present results have been useful in suggesting specific roles for the action of protein B in the sMMO system. Examination of the NO chemistry of related proteins, including stearoyl Δ-9 desaturase (39, 40), toluene-4-monooxygenase (41) and phenol hydroxylase (42), would be useful in

elucidating the similarities and differences in the reactivities of this class of proteins.

References

1. Valentine, A. M., and Lippard, S. J. (1997) *J. Chem. Soc., Dalton Trans.* 21, 3925-3931.
2. Kurtz, D. M. (1997) *JBIC* 2, 159-167.
3. Wallar, B. J., and Lipscomb, J. D. (1996) *Chem. Rev.* 96, 2625-2657.
4. Liu, K. E., and Lippard, S. J. (1995) in *Adv. Inorg. Chem.* (Sykes, A. G., Ed.) pp 263-289, Academic Press, San Diego.
5. Lipscomb, J. D. (1994) *Annu. Rev. Microbiol.* 48, 371-399.
6. Liu, K. E., Valentine, A. M., Qiu, D., Edmondson, D. E., Appelman, E. H., Spiro, T. G., and Lippard, S. J. (1995) *J. Am. Chem. Soc.* 117, 4997-4998.
7. Lee, S.-K., Nesheim, J. C., and Lipscomb, J. D. (1993) *J. Biol. Chem.* 268, 21569-21577.
8. Kim, K., and Lippard, S. J. (1996) *J. Am. Chem. Soc.* 118, 4914-4915.
9. Dong, Y., Yan, S., Young, V. G., and Que, L. (1996) *Agnew. Chem. Int. Ed. Engl.* 35, 618-620.
10. Ookubo, T., Sugimoto, H., Nagayama, T., Masuda, H., Sato, T., Tanaka, K., Maeda, Y., Okawa, H., Hayashi, Y., Uehara, A., and Suzuki, M. (1996) *J. Am. Chem. Soc.* 118, 701-702.
11. Liu, K. E., Valentine, A. M., Wang, D., Huynh, B. H., Edmondson, D. E., Salifoglou, A., and Lippard, S. J. (1995) *J. Am. Chem. Soc.* 117, 10174-10185.
12. Shu, L., Nesheim, J. C., Kauffmann, K., Münck, E., Lipscomb, J. D., and Que, L. (1997) *Science* 275, 515-517.
13. Green, J., and Dalton, H. (1985) *J. Biol. Chem.* 260, 15795-15801.
14. Gassner, G., and Lippard, S. J. (1998) *manuscript in preparation.*
15. Hendrich, M. P., Münck, E., Fox, B. G., and Lipscomb, J. D. (1990) *J. Am. Chem. Soc.* 112, 5861-5865.

16. Pulver, S., Froland, W. A., Fox, B. G., Lipscomb, J. D., and Solomon, E. I. (1993) *J. Am. Chem. Soc.* 115, 12409-12422.
17. Pulver, S. C., Froland, W. A., Lipscomb, J. D., and Solomon, E. I. (1997) *J. Am. Chem. Soc.* 119, 387-395.
18. Richter-Addo, G. B., and Legzdins, P. (1992) *Metal Nitrosyls*, Oxford Univeristy Press, New York.
19. Zhang, Y., Pavlosky, M. A., Brown, C. A., Westre, T. E., Hedman, B., Hodgson, K. O., and Solomon, E. I. (1992) *J. Am. Chem. Soc.* 114, 9189-9191.
20. Brown, C. A., Pavlosky, M. A., Westre, T. E., Zhang, Y., Hedman, B., Hodgson, K. O., and Solomon, E. I. (1995) *J. Am. Chem. Soc.* 117, 715-732.
21. Enemark, J. H., and Feltham, R. D. (1974) *Coord. Chem. Rev.* 13, 339-406.
22. Nelson, M. J. (1987) *J. Biol. Chem.* 262, 12137-12142.
23. Arciero, D. M., Lipscomb, J. D., Huynh, B. H., Kent, T. A., and Münck, E. (1983) *J. Biol. Chem.* 258, 14981-14991.
24. Arciero, D. M., Orville, A. M., and Lipscomb, J. D. (1985) *J. Biol. Chem.* 260, 14035-14044.
25. Nocek, J. M., Kurtz, D. M., Sage, J. T., Debrunner, P. G., Maroney, M. J., and Que, L. (1985) *J. Am. Chem. Soc.* 107, 3382-3384.
26. Nocek, J. M., Donald M. Kurtz, J., Sage, J. T., Xia, Y.-M., Debrunner, P., Shiemke, A. K., Sanders-Loehr, J., and Loehr, T. M. (1988) *Biochemistry* 27, 1014-1024.
27. Haskin, C. J., Ravi, N., Lynch, J. B., Münck, E., and Lawrence Que, J. (1995) *Biochemistry* 34, 11090-11098.
28. DeWitt, J. G., Bentsen, J. G., Rosenzweig, A. C., Hedman, B., Green, J., Pilkington, S., Papaefthymiou, G. C., Dalton, H., Hodgson, K. O., and Lippard, S. J. (1991) *J. Am. Chem. Soc.* 113, 9219-9235.

29. Liu, K. E., Johnson, C. C., Newcomb, M., and Lippard, S. J. (1993) *J. Am. Chem. Soc.* 115, 939-947.
30. Maragos, C. M., Morley, D., Wink, D. A., Dunams, T. M., Saavedra, J. E., Hoffman, A., Bove, A. A., Issac, L., Hrabie, J. A., and Keefer, L. K. (1991) *J. Med. Chem.* 34, 3242-3247.
31. Morley, D., and Keefer, L. K. (1993) *J. of Card. Pharm.* 22, S3-S9.
32. Ravi, N., Bollinger, J. M., Huynh, B. H., Edmundson, D., and Stubbe, J. (1994) *J. Am. Chem. Soc.* 116, 8007-8014.
33. Herold, S., and Lippard, S. J. (1997) *J. Am. Chem. Soc.* 119, 145-156.
34. Mizoguchi, T. J., DuBois, J. L., Bautista, M. T., Hedman, B., Hodgson, K. O., and Lippard, S. J. (1998) *manuscript in preperation.*
35. Rosenzweig, A. C., Nordlund, P., Takahara, P. M., Frederick, C. A., and Lippard, S. J. (1995) *Chemistry & Biology* 2, 409-418.
36. Åberg, A. (1993) , Stockholm University.
37. Sono, M., Roach, M. P., Coulter, E. D., and Dawson, J. H. (1996) *Chem. Rev.* 96.
38. Paul, P. P., and Karlin, K. D. (1991) *J. Am. Chem. Soc.* 113, 6331-6332.
39. Fox, B. G., Shanklin, J., Somerville, C., and Münck, E. (1993) *Proc. Natl. Acad. Sci. USA* 90, 2486-2490.
40. Fox, B. G., Shanklin, J., Ai, J., Loehr, T. M., and Sanders-Loehr, J. (1994) *Biochemistry* 33, 12776-12786.
41. Pikus, J. D., Studts, J. M., Achim, C., Kauffmann, K. E., Münck, E., Steffan, R. J., McClay, K., and Fox, B. G. (1996) *Biochemistry* 35, 9106-9119.
42. Nordlund, I., Powlowski, J., and Shingler, V. (1990) *J. Bact.* 172, 6826-6833.
43. Feig, A. L., Bautista, M. T., and Lippard, S. J. (1996) *Inorg. Chem.* 35, 6892-6898.
44. Kraulis, P. J. (1991) *J. Appl. Cryst.* 24, 946-950.

Table 1: Spectroscopic Properties of Non-Heme Carboxylate-Bridged Diiron Nitrosyl Complexes

Sample	Optical Properties:	Mössbauer Properties		Reference
	λ_{\max} [nm] (ϵ [$M^{-1} \text{ cm}^{-1}$])	δ (mm/s)	ΔE_Q (mm/s)	
$[\text{Fe}_2(\text{NO})_2(\text{Et-HPTB})(\text{OBz})]^{2+}$	520 (395), 620 (579)	0.67	1.44	49
<i>E. coli</i> Ribonucleotide Reductase R2 (dinitrosyl)	450 (760), 620 (220)	0.75	-2.13, -1.73	27
<i>P. gouldii</i> Hemerythrin (mononitrosyl)	408 (1200), 500 (700), 600 (500)	0.68 1.21 Fe(II)	0.61 2.65 Fe(II)	25, 26
Dinitrosyl Adduct of $[\text{Fe}_2(\mu\text{-XDK})(\mu\text{-O}_2\text{CPh})(\text{ImH})_2(\text{O}_2\text{CPh})(\text{MeOH})]$	450 (2100), 630 (670)	0.74	1.41	34

Table 2: Mössbauer Properties of Species Observed in Reactions of the Reduced sMMO Hydroxylase with Nitric Oxide

Species	% of $H_{\text{red}}+\text{NO}$ Reaction	% of $H_{\text{red}}+2\text{B}+\text{NO}$ Reaction	Mössbauer Properties	
			δ (mm/s)	ΔE_Q (mm/s)
mononuclear $\{\text{Fe}(\text{NO})\}^7$	36	10	0.7	-1.7
mononuclear Fe(III)	6	3	0.5	0.5
H_{red}	8	7	1.30	2.87
H_{ox}	6.5	38	0.49	1.12
$H_{\text{dinitrosyl}}$	6.5	23.1	0.75	1.30
“unidentified”	38	23.3	0.2	1.08

Table 3: Time-Dependent Changes in Rapid-Freeze-Quench Mössbauer Samples of the Reaction of Nitric Oxide with the Reduced sMMO Hydroxylase

Species	Percentage of Species after Mixing			Mössbauer Properties	
	61 ms	126 ms	440 ms	δ (mm/s)	ΔE_Q (mm/s)
H _{red}	54	57	53	1.30	2.87
H _{ox}	11	10	8	0.57	0.98
H _{dinitrosyl}	15	14	10	0.72	1.55
mononuclear {Fe(NO)} ⁷	20	19	20	0.7	-1.7
“unidentified”	-	-	9	0.19	0.63

Table 4: Activation Parameters from Eyring Plots of the Reaction of the Reduced Hydroxylase with Nitric Oxide

Reaction	ΔH^\ddagger (kcal mol ⁻¹)	ΔS^\ddagger (cal mol ⁻¹ K ⁻¹)
H _{red} +NO Reaction, Fast Phase	13.5 ± 5.6	-1.1 ± 4.5
H _{red} +NO Reaction, Slow Phase	15.8 ± 1.3	4.3 ± 3.0
H _{red} +2B+NO Reaction	7.3 ± 0.8	-24.9 ± 2.4

Figure 1: Optical spectra of the nitrosyl adduct of the reduced sMMO hydroxylase in 25 mM MOPS pH 7.0 (solid line) and the dinitrosyl adduct of $[\text{Fe}_2(\mu\text{-XDK})(\mu\text{-O}_2\text{CPh})(\text{ImH})_2(\text{O}_2\text{CPh})(\text{MeOH})]$ in THF (dashed line) (34).

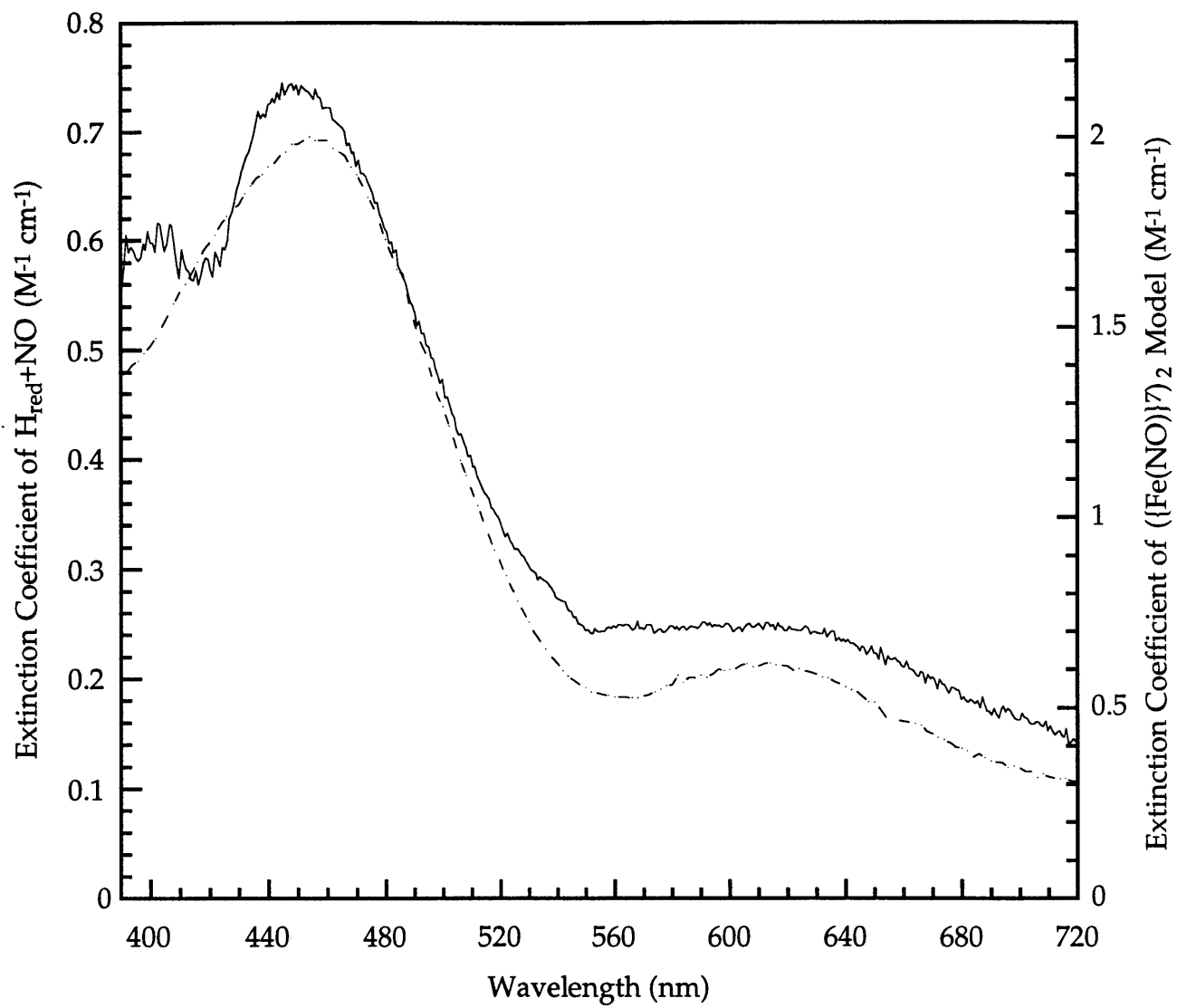


Figure 1

Figure 2: Mössbauer spectra of ^{57}Fe -enriched $\text{H}_{\text{red}}+\text{NO}$ and $\text{H}_{\text{red}}+2\text{B}+\text{NO}$.
Mössbauer spectra of ^{57}Fe -enriched H_{red} (a) and H_{red} in the presence of two equiv. of protein B (b) reacted with NO for 45 min at 4 K in zero applied field. The solid line drawn through the data represent a simulation of the species detailed in Table 2.

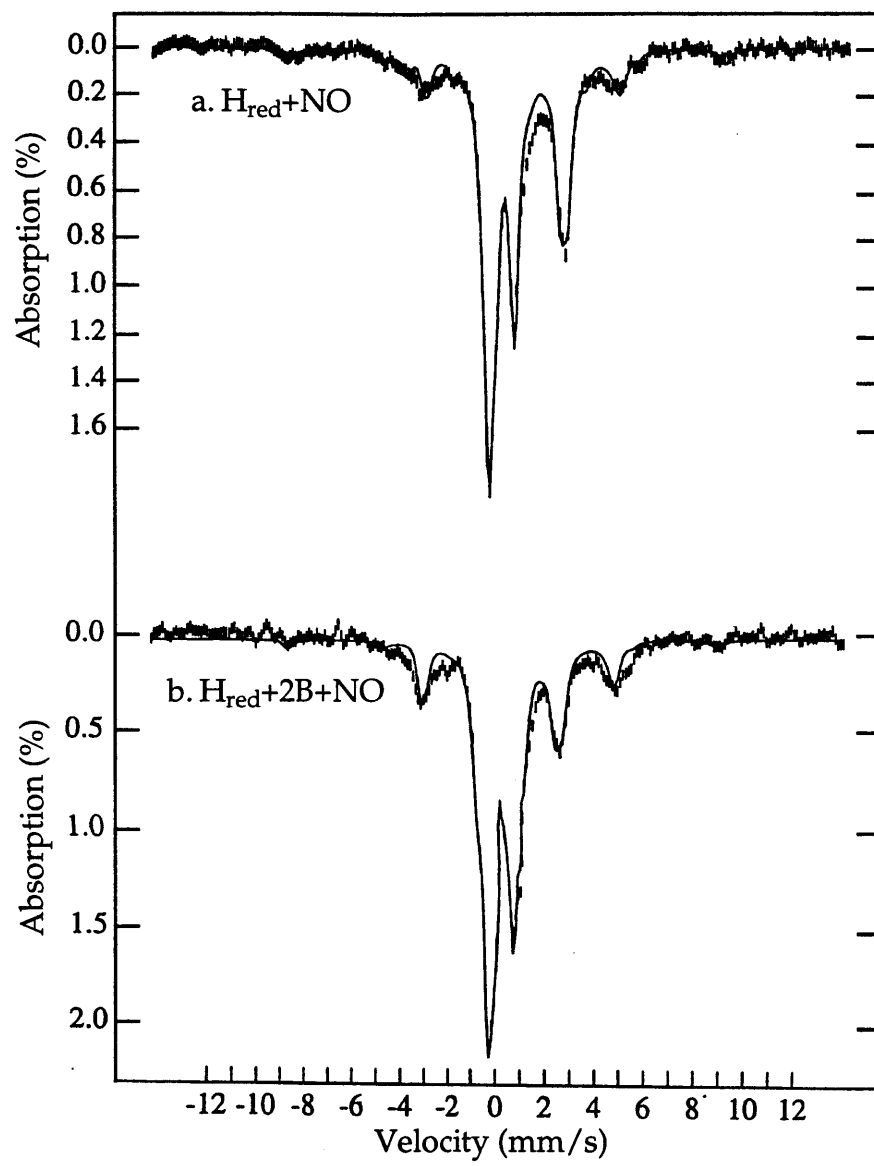


Figure 2

Figure 3: EPR spectra of H_{red} (a, b) and H_{red} in the presence of two equiv of protein B (c) exposed to NO for 45 min. Spectra were obtained at 4.3-4.8 K, 100 μ W and 9.41 GHz. The buffer was 25 mM MOPS, pH 7.0.

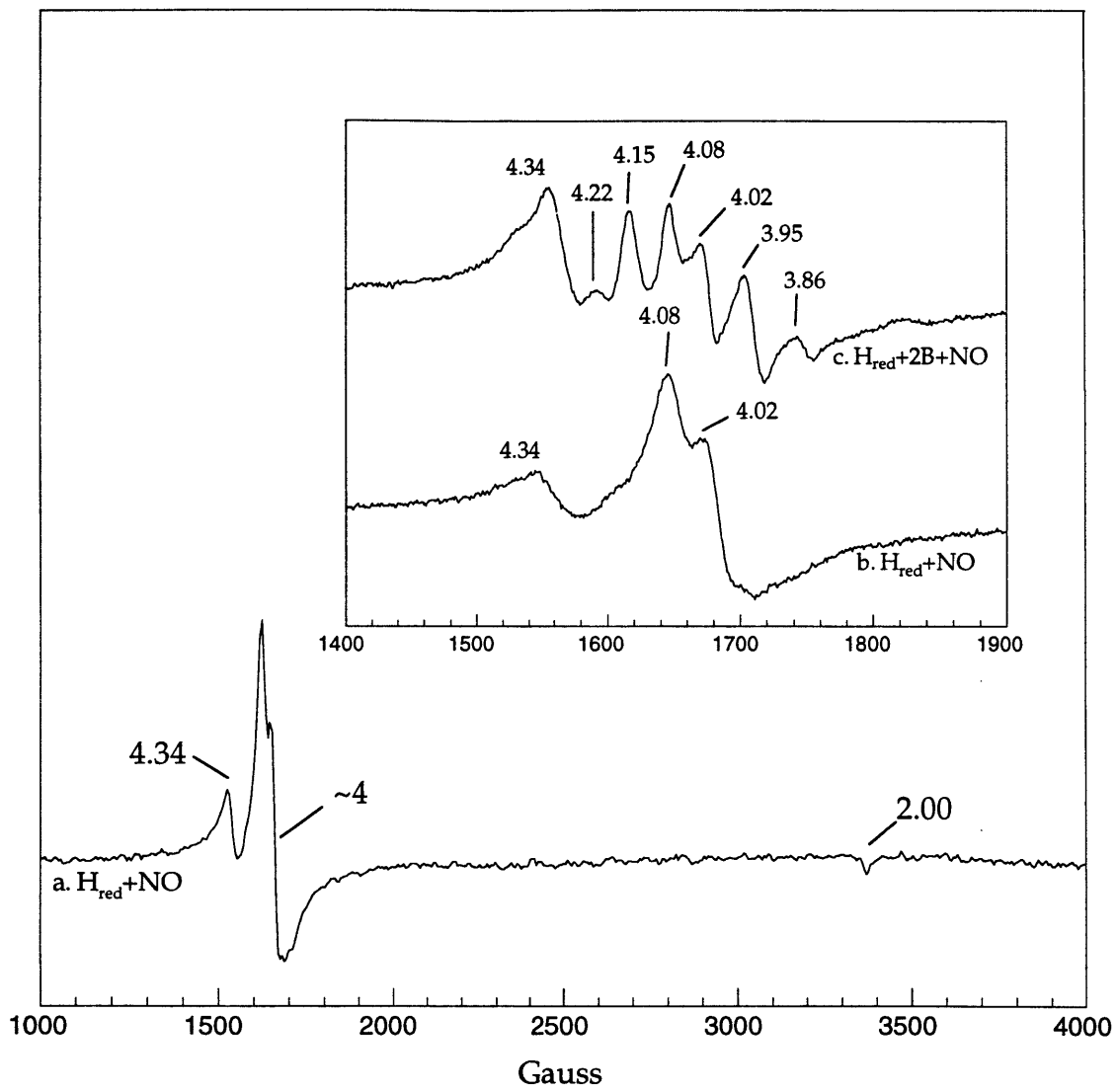


Figure 3

Figure 4: (a) Buildup of the optical species associated with reaction of NO with H_{red} as observed by using stopped-flow spectroscopy at 4 °C. (b) Two comparative fits of the stopped-flow data. The first graph is a fit of the data to an $A \rightarrow B$ buildup model and the second is a fit to an $A \rightarrow B \rightarrow C$ buildup.

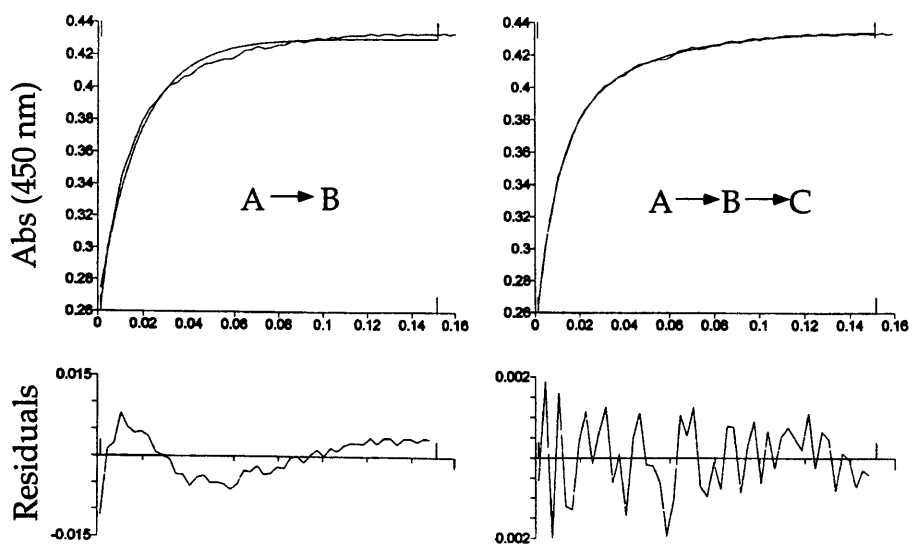
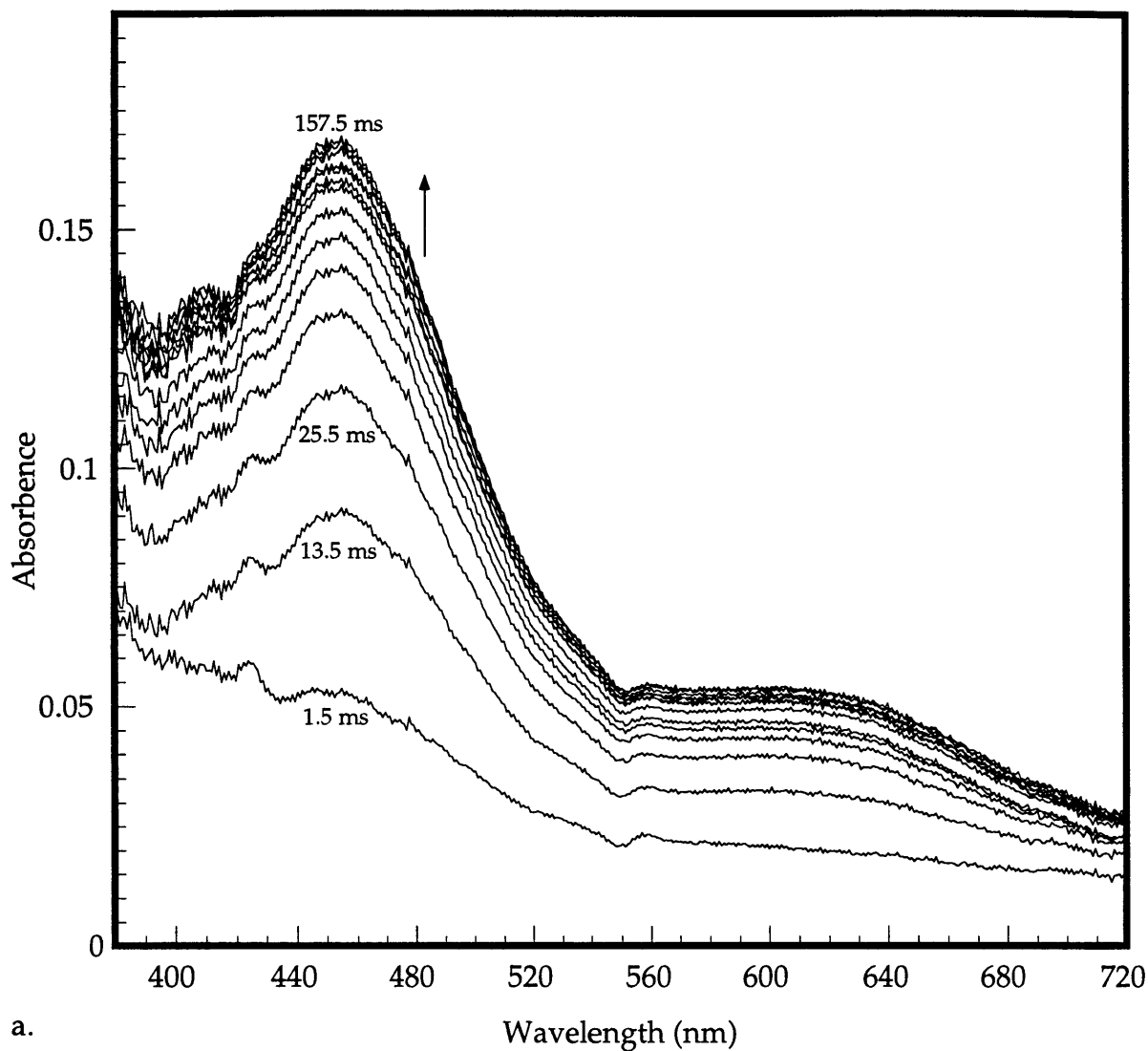


Figure 4

Figure 5: Eyring plots of the fast and slow reactions of the $H_{red}+NO \rightleftharpoons H_{dinitrosyl}$ buildup and of the $H_{red}+2B+NO \rightleftharpoons H_{dinitrosyl}$ buildup.

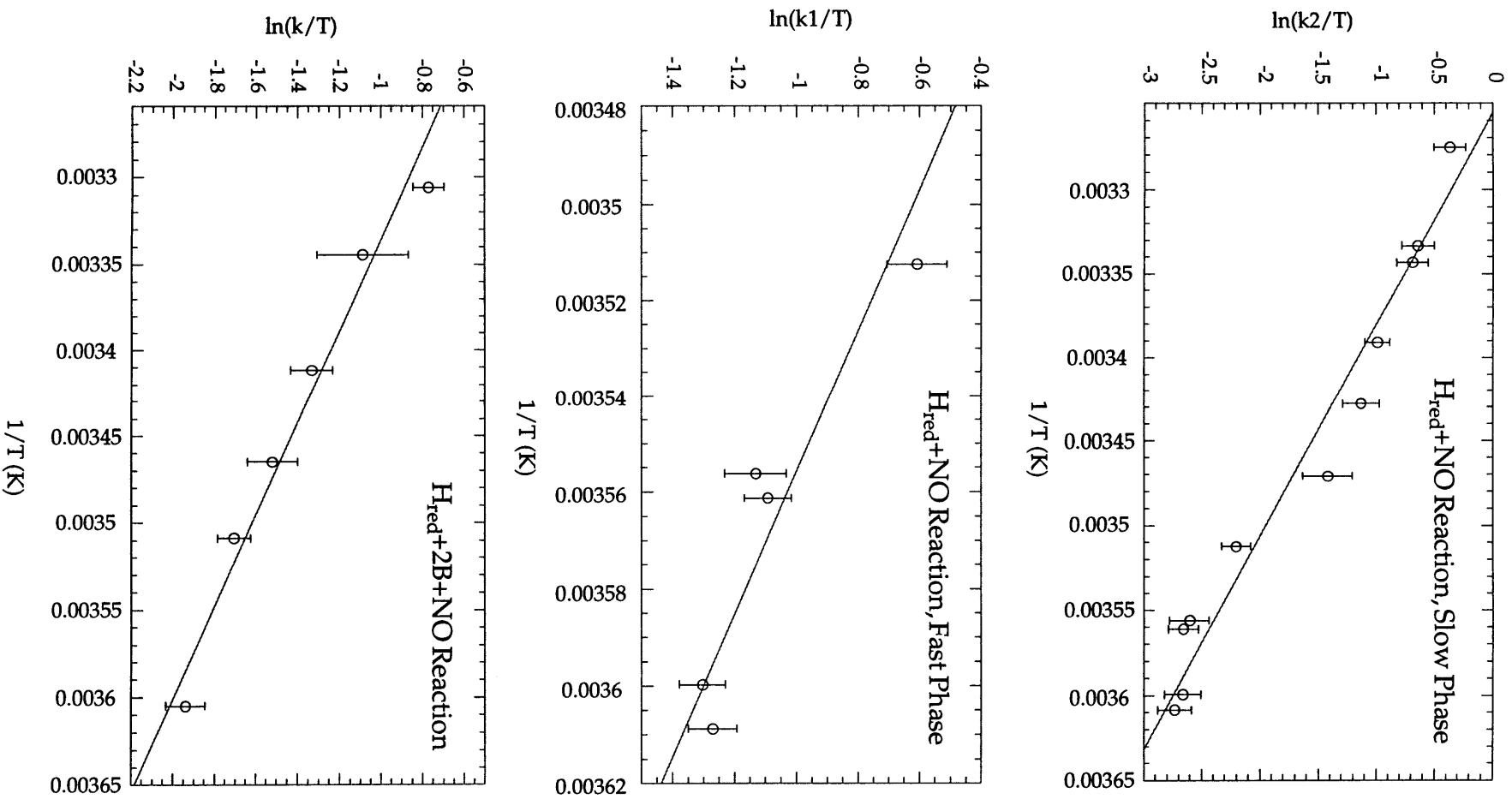


Figure 5

Figure 6: Simulation of the $H_{\text{dinitrosyl}}$ formation and decay reactions by using rate constants derived from stopped-flow data. (top) Simulation of the first 500 ms of reaction. Also plotted is the total of the two dinitrosyl species, which corresponds to a fit of the stopped-flow optical data. (bottom) Simulation of the reaction from 100 ms to 10 s.

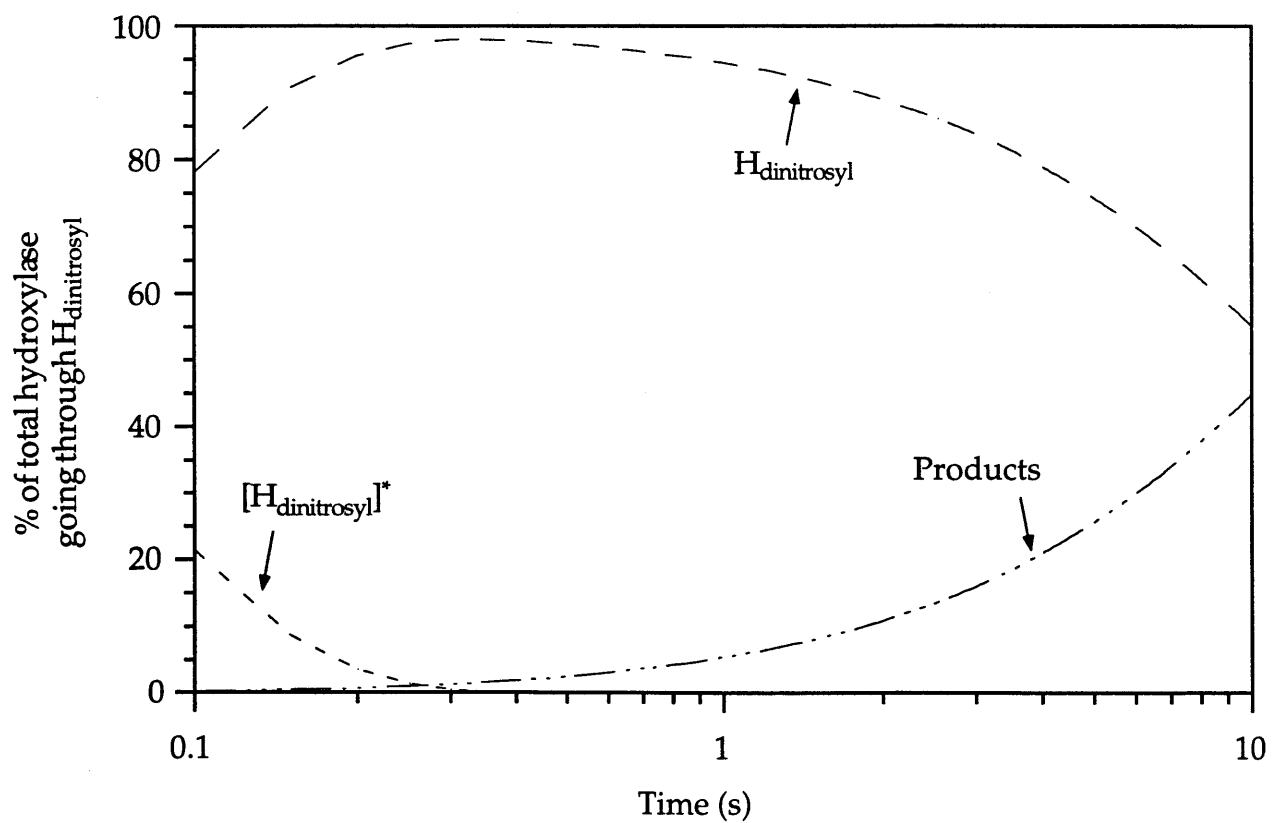
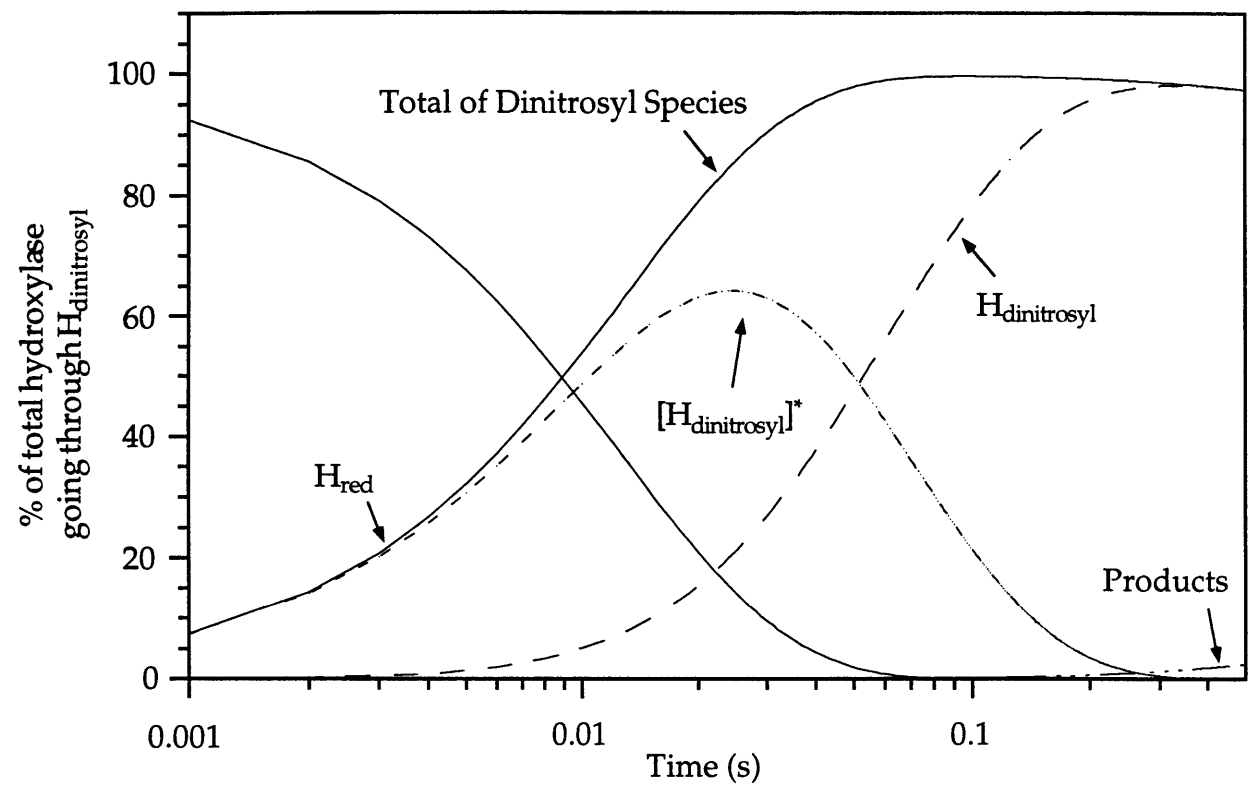


Figure 6

Figure 7: Time-dependent RFQ EPR spectra following the reaction of NO with the reduced sMMO hydroxylase at 4 °C. Spectra correspond to reaction times of 28 ms, 158 ms, 1 s and 30 s. Spectra were obtained at 4.5 K, 100 μ W and 9.41 GHz. The inset is a plot of the concentration of the mononuclear $\{Fe(NO)\}^7$ species as a function of time, with the solid line showing a monophasic fit of the data.

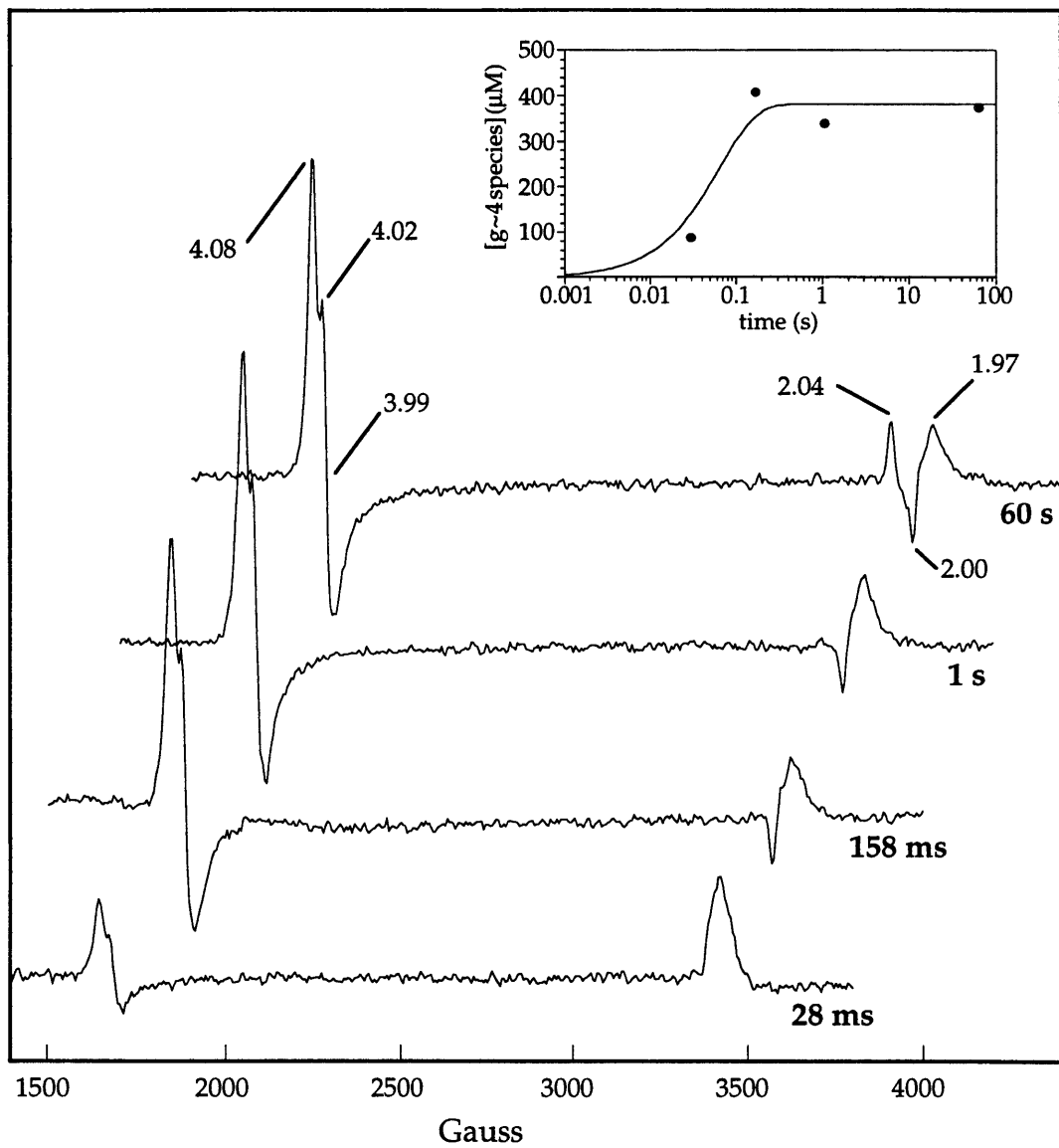


Figure 7

Figure 8: Time-dependent Mössbauer spectra following the reaction of H_{red} with NO at 4 °C. The H_{red} Mössbauer spectrum has been subtracted from all time points. The solid line through the data corresponds to simulations using parameters listed in Table 4.

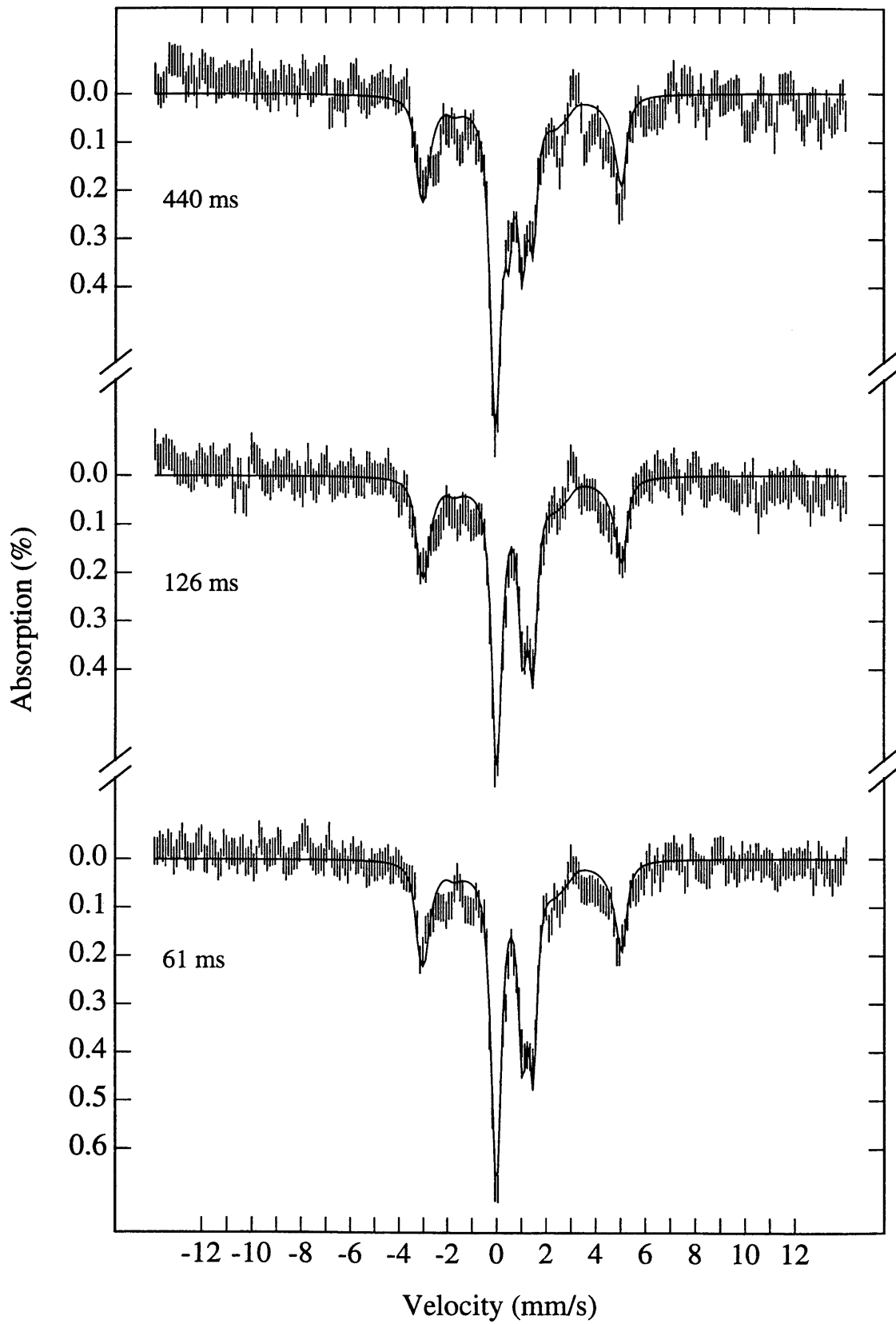


Figure 8

Figure 9: Proposed mechanism for the reactions of NO with H_{red} .

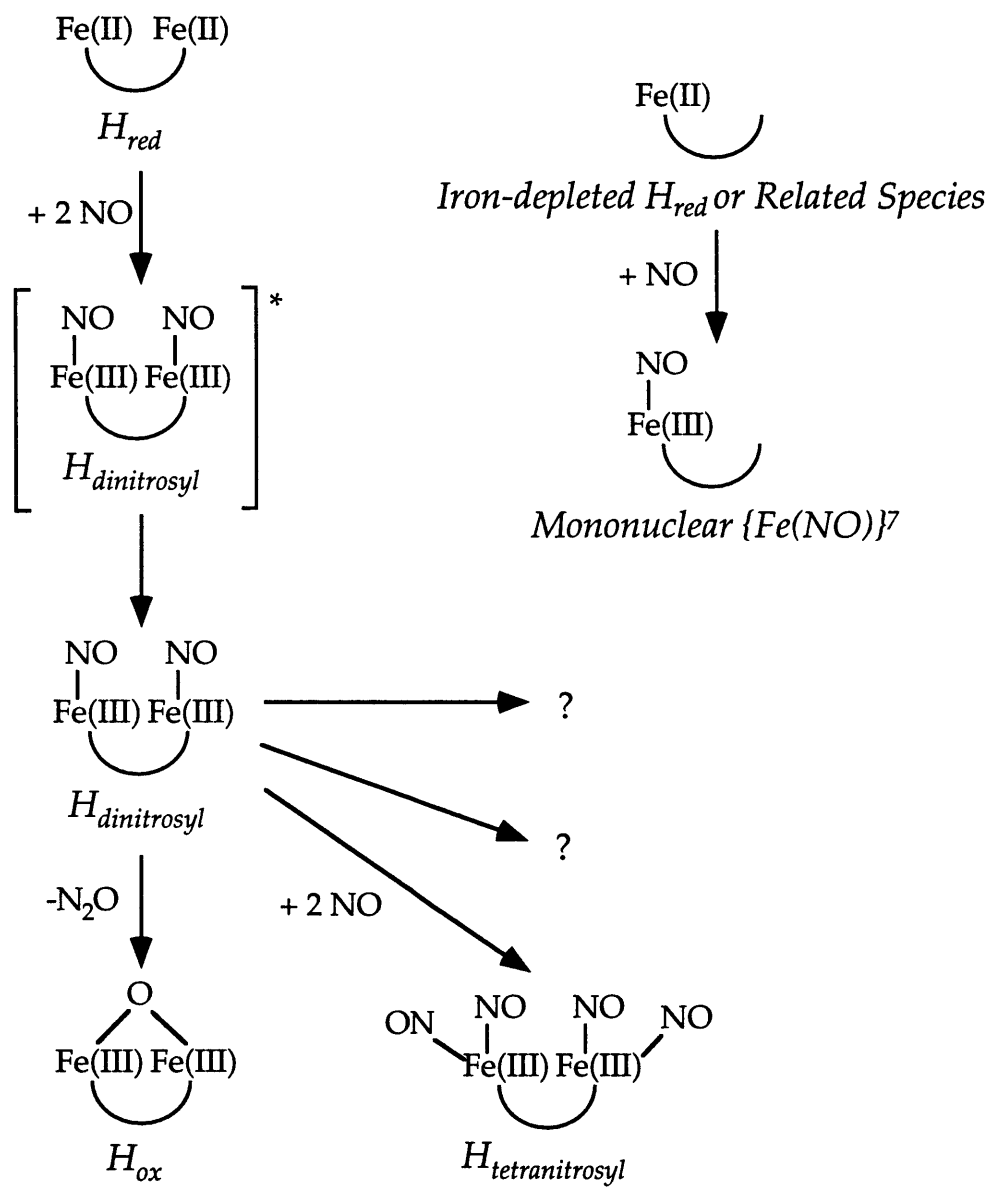


Figure 9

Figure 10: Active site structure of the reduced sMMO hydroxylase. a. Ligand arrangement around the iron site. Note that the open coordination sites on each iron, occupied by weakly bound water ligands. b. Newman projection viewed down the Fe-Fe axis in the H_{red} active site. The positions of the open coordination sites are shown. These figures were prepared with MolScript (44).

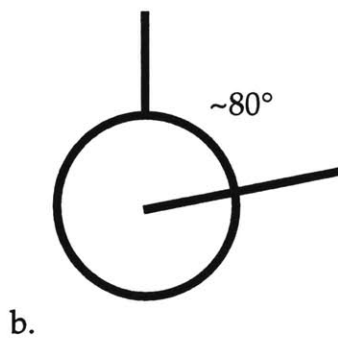
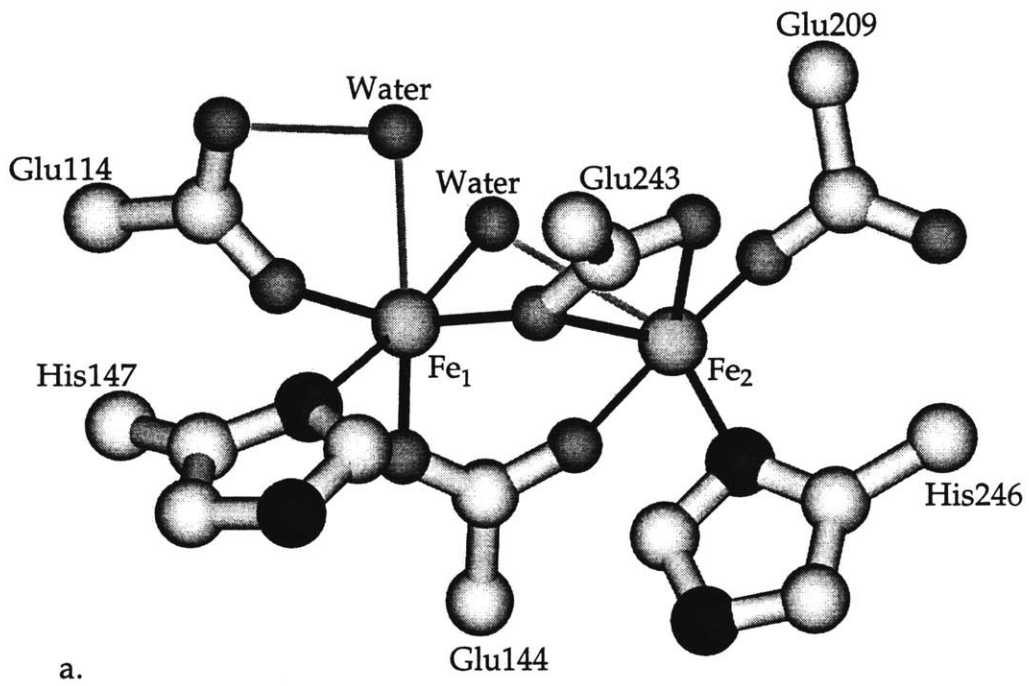


Figure 10

Figure 11: Proposal for ligand movements in the active site of the reduced sMMO hydroxylase induced by binding of protein B. The schematic for the H_{red} active site is taken from the crystal structure of the reduced sMMOH, and the $H_{\text{red}+2B}$ active site from the crystal structure of the reduced R2 subunit.

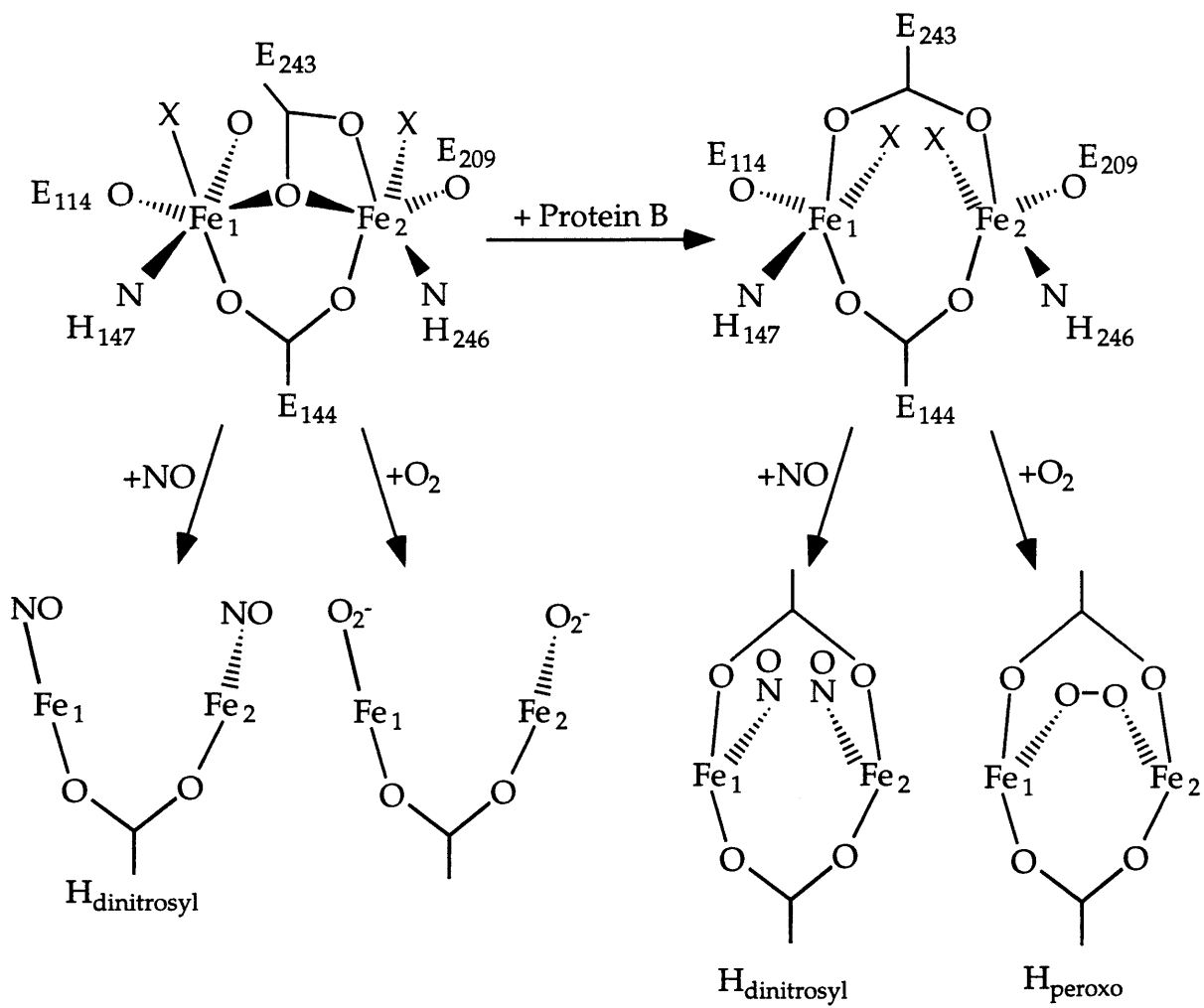
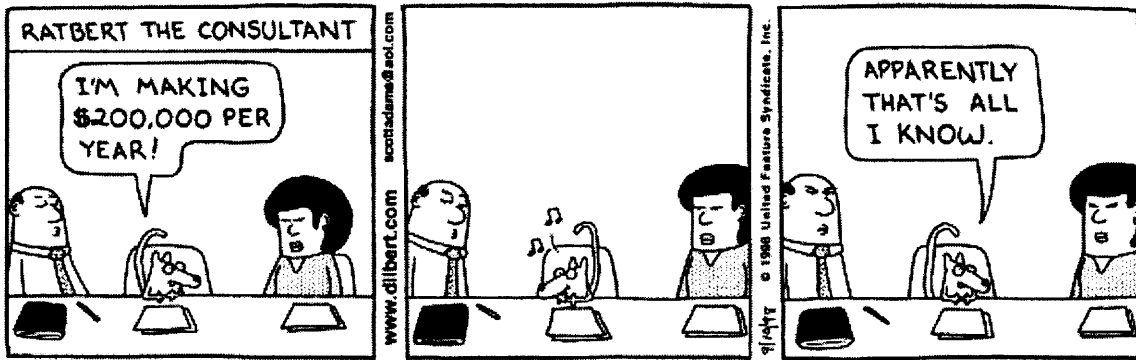


Figure 11

Biographical Note

David Ernest Coufal was born at Edwards Air Force Base in Lancaster, California on January 24, 1969, 177 days before the first moon landing, 441 days before the Beatles broke up and 4457 days before the first Space Shuttle landing at Edwards. He was raised in Colorado Springs, Colorado where he graduated from General William Mitchell High School in 1987. The California Institute of Technology (Pasadena, California) was his next stop, where he worked with both Dr. Daniel Diner in the robotics division at the Jet Propulsion Laboratory on 3-dimensional vision systems, and Prof. John Richard in the Caltech chemistry department on β -lactamase. After earning a B.Sc. in Chemical Biology in 1991, he went on to attend graduate school in the chemistry department at the Massachusetts Institute of Technology (Cambridge, Massachusetts), where his thesis advisor was Prof. Stephen J. Lippard. He earned a Ph.D. in Biological Chemistry in September of 1998. After graduation, he will join Tigris Microsystems (<http://www.tigris.com/>) in New York City as a consultant.



Copyright © 1998 United Feature Syndicate, Inc. DEI